THE UNIVERSITY
of EDINBURGH

Localization and Activation of the Fission Yeast γ-Tubulin Complex by Mto1/2

Eric Michael Lynch

Doctor of Philosophy

The University of Edinburgh

August 2012

Acknowledgements

First and foremost, I would like to thank my supervisor Ken Sawin for accepting me into his lab. Ken's knowledge, enthusiasm, and guidance have been invaluable to my PhD research, and also to my development as a scientist in general. Similarly, I am grateful to past and present members of the Sawin Lab: Hilary Snaith, Andreas Anders, Itaru Samejima, Lynda Groocock, Claudia Bicho, Vicky Miller, and Weronika Borek. Their helpful advice and discussion over the years has been critical to my research.

I would also like to thank David Kelly for his assistance and advice with all things microscopy-related. My research also benefited greatly from the advice and training provided by members of the Edinburgh Protein Production Facility (EPPF), in particular Martin Wear and Matt Nowicki.

Further, I would like to extend my gratitude to The Darwin Trust of Edinburgh and The Natural Sciences and Engineering Research Council of Canada (NSERC) for funding my studies. I am particularly grateful to The Darwin Trust, without whose support I would not have been able to undertake this research.

Thanks also to my friends and family for their support and encouragement over the years.

Declaration

This thesis and the research it represents are my own original work. Where other individuals have made contributions, this has been indicated within the text.

Eric M. Lynch

Abstract

Microtubules (MTs) are important components of the eukaryotic cytoskeleton, with critical functions in intracellular trafficking, establishing and maintaining cell morphology, and segregating chromosomes during mitosis. MTs are hollow, cylindrical polymers composed of αβ-tubulin heterodimers. The longitudinal assembly of αβ-tubulin subunits generates protofilaments, and multiple protofilaments (typically 13 *in vivo*) interact laterally to form the wall of the MT. *In vitro*, the polymerization of MTs proceeds in two steps: nucleation and elongation. During the nucleation phase, several αβ-tubulin subunits associate to form a seed, from which further MT elongation then occurs. However, at the relatively low αβ-tubulin concentrations found *in vivo*, the spontaneous assembly of MTs is not favoured, due largely to the slow kinetics of MT nucleation.

The nucleation of MTs *in vivo* requires the γ-tubulin complex (γ-TuC), a ring-like complex composed of γ-tubulin and γ-tubulin complex proteins (GCPs). Two copies of γ-tubulin associate with one copy each of GCP2 and GCP3 to produce the γ-tubulin small complex (γ-TuSC). Multiple γ-TuSCs, along with the additional GCPs 4,5, and 6, assemble to form the larger γ-tubulin ring complex (γ-TuRC). The γ-TuRC contains a ring of 13 γ-tubulins, which acts as a template for the nucleation of MTs. Typically, the γ-TuC nucleates MTs only when localized to specific subcellular sites, referred to as microtubule organizing centres (MTOCs). However, the precise mechanism by which the γ-TuC is activated at MTOCs remains unknown.

In fission yeast, the proteins Mto1 and Mto2 form a complex (Mto1/2) required for the nucleation and organization of cytoplasmic MTs. Mto1/2 determines sites of MT nucleation by recruiting the γ-TuC to several different MTOCs. Different sequences in the Mto1 C-terminus independently confer γ-TuC localization to spindle pole bodies, MTs, and

the cell equator. Here, I show that the Mto1 N-terminus is necessary for localization to the nuclear envelope (NE). By simultaneously removing the N- and C-terminal localization domains, I generated the "Mto1-bonsai" mutant, which fails to localize to any conventional MTOCs. In *mto1-bonsai* cells, MTs are still nucleated in the cytoplasm in an Mto1-dependent manner, but nucleation is spatially random. This reveals that targeting of the γ-TuC to conventional MTOCs is not necessary for MT nucleation, and suggests that Mto1/2 has a direct role in activating MT nucleation by the γ-TuC. Live-cell confocal microscopy allows us to detect individual MT nucleation events, in which newly nucleated MTs are associated with single γ-TuCs as well as Mto1/2-bonsai complexes. Fluorescence quantification reveals that these nucleating complexes contain approximately 13 molecules of both Mto1-bonsai and Mto2, matching the 13 copies of γ -tubulin anticipated for a single γ-TuC. We propose that Mto1/2 may contribute to γ-TuC activation by promoting γ-TuSC assembly and/or inducing conformational changes in the γ-TuC upon binding. I also expressed and purified recombinant Mto1/2-bonsai complex, using a baculovirus/insect cell system. This recombinant Mto1/2-bonsai self-assembles into higher-order complexes, comparable in size to the complexes analyzed *in vivo* by fluorescence microscopy.

Table of Contents

Acknowledgements ..... **ii**

Declaration ..... **iv**

Abstract ..... **vi**

List of Figures ..... **xii**

List of Tables ..... **xiv**

1. Introduction **1**

1.1 Microtubules are dynamic polymers with a variety of cellular functions 1

1.2 Microtubule polymerization 3

1.3 Microtubule organizing centres 6

1.4 The γ-tubulin complex 9

1.5 Localization and regulation of the γ-tubulin complex 16

1.6 Microtubule organization in fission yeast 19

1.7 The Mto1/2 complex and cytoplasmic MT organization 22

Project Aims **27**

2. Materials and Methods **29**

2.1 Growth of fission yeast strains 29

2.2 Genetic crosses 29

2.3 PCR amplification of DNA 30

2.4 Strain construction using the PCR-based method 32

2.5 Colony PCR 34

2.6 Fission yeast boiled extracts 35

2.7 SDS-PAGE, coomassie staining and Western blotting 36

2.8 Endogenously expressed *mto1* N-terminal truncations 37

2.9 DNA sequencing 38

2.10 Microscopy 39

2.11 Morphology assays 42

2.12 Cold-shock and MT regrowth 42

2.13 Measurement of nuclear positioning 43

2.14 Imaging of Mto1 in the presence of MBC 43

2.15 Growth of *E. coli* strains 43
2.16 Production of chemically competent *E. coli* 44
2.17 Transformation of *E. coli* 44
2.18 Isolation of plasmid DNA from *E. coli* 45
2.19 Restriction digestion, gel extraction and ligation of DNA 45
2.20 Insect cell culture 46
2.21 Construction of bacmids for Mto1/2 expression in insect cells 46
2.22 Generation of virus stocks 49
2.23 Characterization of V_2 virus stocks and expression of recombinant Mto1/2 50
2.24 Nickel purification of 6His-Mto1-bonsai, 6His-Mto2, and 6His-Mto1/2-bonsai complex 51
2.25 Gel filtration chromatography and SEC-MALS 52
3. Truncation of the Mto1 C-terminus reveals Mto1 localization to the nuclear envelope 59
3.1 Introduction 59
3.2 Results 61
3.2.1 Normal morphology is observed in *mto1* truncation mutants as small as *mto1(1-549)* 61
3.2.2 Mto1 C-terminal truncations localize to the nuclear envelope 64
3.2.3 Mto1(1-549) promotes increased MT nucleation from the NE 73
3.3 Discussion 77
4. The Mto1/2-bonsai complex activates MT nucleation by the γ-TuC 79
4.1 Introduction 79
4.2 Results 80
4.2.1 Over-expressed N-terminal truncations of Mto1 promote MT nucleation away from the NE 80
4.2.2 The Mto1 N-terminus mediates localization to the NE 83
4.2.3 Mto1-bonsai promotes spatially random MT nucleation 90
4.2.4 Mto1/2-bonsai activates MT nucleation by the γ-TuC 96
4.3 Discussion 101
5. Mto2 multimerizes Mto1 into higher-order complexes that activate the γ-TuC 105
5.1 Introduction 105

5.2 Results 106
5.2.1 Higher-order multimerization of Mto1/2 is required for γ-TuC activation 106
5.2.2 Mto2 shows limited multimerization in the absence of Mto1 110
5.2.3 MT nucleation from the NE has a minor role in nuclear positioning 112
5.2.4 *mto1-NE-GFP* and *mto1-bonsai-GFP* nucleate MTs in the absence of γ-TuRC-specific proteins 114
5.3 Discussion 116
6. Recombinant Mto1/2-bonsai complex self-assembles into large multimers ...119
6.1 Introduction 119
6.2 Results 120
6.2.1 Mto1/2-NE and Mto1/2-bonsai are expressed at higher levels in insect cells than full-length Mto1/2 120
6.2.2 6His-Mto1/2-bonsai has a particularly high-affinity for nickel 122
6.2.3 Recombinant Mto1/2-bonsai forms a range of complexes roughly 75-800 kDa in size 125
6.2.4 The Mto1/2-bonsai complex is in a dynamic equilibrium 127
6.2.5 Mto2 multimerizes and is in a dynamic equilibrium, while Mto1-bonsai is likely monodisperse 130
6.3 Discussion 134
7. Conclusions and Future Work 137
References 147

List of Figures

Figure 1.1: The current template model for MT nucleation by the γ-TuC.

Figure 1.2: Fission yeast MT organization varies throughout the cell cycle.

Figure 2.1: No significant photobleaching was observed in the movies used for fluorescence quantification of Mto1/2-bonsai and γ-TuC nucleating puncta.

Figure 2.2: Construction of bacmids for recombinant Mto1/2 expression.

Figure 3.1: Design of Mto1 C-terminal truncation mutants.

Figure 3.2: *mto1* truncations as small as *mto1(1-549)* have normal cell morphology.

Figure 3.3: Mto1 C-terminal truncation mutants localize to the NE.

Figure 3.4: The γ-TuC localizes to the NE in *mto1(1-549)* cells.

Figure 3.5: The γ-TuC is absent from the eMTOC and cytoplasmic face of the SPB in *mto1(1-549)* cells.

Figure 3.6: Mto1(1-549)-GFP does not localize to existing MT bundles.

Figure 3.7: Mto1(1-549) and the γ-TuC co-localize on the NE.

Figure 3.8: *mto1(1-549)-GFP* cells are capable of nucleating MTs.

Figure 3.9: *mto1(1-549)* cells show increased MT nucleation from the NE.

Figure 4.1: MT re-growth in *mto1* N-terminal truncation mutants occurs away from the NE.

Figure 4.2: Over-expressed Mto1 N-terminal truncations do not localize to the NE.

Figure 4.3: Endogenously-expressed Mto1 N-terminal truncations do not localize to the NE.

Figure 4.4: Localization of full-length Mto1 to the NE requires the Mto1 N-terminus.

Figure 4.5: Mto1 is dynamically partitioned between different MTOCs.

Figure 4.6: Mto1(131-549)-GFP does not decorate the MT lattice.

Figure 4.7: γ-TuC localization to the NE is virtually abolished in *mto1* N-terminal truncation mutants.

Figure 4.8: N-terminal truncations of Mto1 co-localize with the γ-TuC.

Figure 4.9: Extensive truncation of the Mto1 N-terminus impairs Mto1 function.

Figure 4.10: MT nucleation is spatially random in *mto1-bonsai*.

Figure 4.11: The various Mto1 truncations are expressed at different levels.

Figure 4.12: Discrete puncta containing Mto1/2-bonsai and the γ-TuC nucleate MTs.

Figure 4.13: The number of molecules in Mto1-bonsai, Mto2, Alp4, and Alp6 nucleating puncta was determined by comparison to known standards.

Figure 4.14: MTs are nucleated by complexes containing approximately 13 copies each of Mto1-bonsai and Mto2.

Figure 4.15: The intensity observed per GFP molecule is consistent across multiple experiments.

Figure 4.16: Multimers of Mto1/2-bonsai activate the γ-TuC.

Figure 5.1: Multimerization of Mto1-bonsai-GFP and Mto1-NE-GFP requires Mto2.

Figure 5.2: Mto2 is required for MT nucleation in *mto1-NE-GFP* and *mto1-bonsai-GFP*.

Figure 5.3: Faint Mto2-GFP puncta are observed in the absence of Mto1.

Figure 5.4: MT nucleation from the NE has a minor role in ensuring correct nuclear positioning.

Figure 5.5: *mto1-NE-GFP* and *mto1-bonsai-GFP* can nucleate MTs in the absence of Alp16.

Figure 6.1: Mto1-NE and Mto1-bonsai are expressed at higher levels than full-length Mto1.

Figure 6.2: 6His-Mto1/2-bonsai complex binds nickel even at high imidazole concentrations.

Figure 6.3: Mto1-bonsai and Mto2 were Nickel-purified separately or together as the Mto1/2-bonsai complex.

Figure 6.4: Mto1-bonsai and Mto2 co-fractionate with a 1:1 stoichiometry during gel filtration.

Figure 6.5: Recombinant Mto1/2-bonsai forms complexes ranging from ~75-800 kDa.

Figure 6.6: The Mto1/2-bonsai complex is in dynamic equilibrium.

Figure 6.7: Mto2 multimerizes and is in a dynamic equilibrium.

Figure 6.8: Mto1-bonsai is likely monodispersed.

Figure 6.9: Mto1-bonsai and Mto2 multimerize efficiently in vitro.

List of Tables

Table 1.1: γ-tubulin complex protein nomenclature in various species

Table 2.1: Oligonucleotides, plasmids and parent strains used to generate truncated and/or tagged mutants using the PCR-based method.

Table 2.2: Oligonucleotides used for construction of endogenously expressed Mto1 N-terminal truncation mutants.

Table 2.3 Conditions used for fluorescence microscopy.

Table 2.4: Mto1 and Mto2 PCR products generated for cloning into pFL acceptor plasmid.

Table 2.5: List of strains used in this study.

Table 2.6: List of plasmids used in this study.

Table 2.7: List of oligonucleotides used in this study.

1. Introduction

1.1 Microtubules are dynamic polymers with a variety of cellular functions

Microtubules (MTs) are vital components of the eukaryotic cytoskeleton and are essential for a variety of activities, including intracellular trafficking, maintenance of cell morphology, and segregation of chromosomes during cell division. MTs are hollow, cylindrical polymers composed of heterodimers of α-tubulin and β-tubulin, two proteins with significant primary sequence conservation and nearly identical 3-dimenstional structures (Burns, 1991; Lowe et al., 2001; Nogales et al., 1998). MTs polymerize with a specific polarity, with β-tubulin exposed at the growing (so-called plus) end and α-tubulin exposed at the opposite (so-called minus) end. Importantly, MTs are found to switch between periods of slow growth and rapid disassembly, a feature referred to as dynamic instability (Mitchison and Kirschner, 1984a; Mitchison and Kirschner, 1984b). The dynamic and polar properties of MTs are essential to their cellular functions: cell division and differentiation rely on dynamic re-modelling of the MT cytoskeleton, while features such as cell shape, polarity, and organization are largely defined by the polarity of microtubules. A variety of proteins interact with MTs. These proteins, generally referred to as microtubule associated proteins (MAPs), have roles in regulating the assembly and organization of MTs, and also in mediating MT functions within the cell.

MTs are perhaps most recognizable for their role in cell division. In proliferating animal cells, interphase MTs are generally arranged as a radial array with minus-ends anchored at the centrosome and plus-ends extending towards the cell periphery. As cells

enter mitosis, interphase MTs disassemble and give rise to the mitotic spindle, the bipolar MT array that segregates duplicated chromosomes into daughter cells prior to cell division. This process relies on a particular arrangement of MTs, with minus-ends focused at spindle poles and plus-ends available for the capture of chromosomes. This focusing of minus-ends requires MTs to be cross-linked and aligned, a process regulated by the activity of motor proteins, such as the plus-end directed kinesin Eg5 and minus-end directed dynein (Gaglio et al., 1996; Sawin et al., 1992). MTs within the mitotic spindle are highly dynamic, a feature which may increase the frequency with which MTs encounter and bind chromosomes. Work in *Xenopus laevis* egg extracts has revealed that the high turnover of spindle MTs may arise from the antagonistic activities of XMAP215 and XKCM1, MAPs which promote MT polymerization and depolymerization, respectively (Tournebize et al., 2000). Other factors, including the Ndc80 complex, mediate attachment of MT plus-ends to kinetochore sites on chromosomes (DeLuca and Musacchio, 2012). MTs become stabilized upon association with kinetochores (Zhai et al., 1995), thereby allowing chromosomes to be pulled towards the spindle poles in a process thought to involve both motor proteins and MT depolymerization (Mitchison, 2005). This coordinated activity of MTs, MAPs, and motor proteins is characteristic of the manner in which MTs are employed within the cell.

MTs also provide the tracks along which motor proteins transport vesicles and organelles in an ATP-dependent manner, a process first directly observed in cytoplasm isolated from the squid giant axon (Vale et al., 1985a; Vale et al., 1985b). The correct positioning and morphology of the golgi complex, for example, depends on interaction with centrosomal MTs as well as MTs originating from the golgi membranes themselves (Miller et al., 2009). Membrane trafficking in exocytosis and endocytosis relies on MT-mediated transport by kinesins and the dynein-dynactin complex. Trafficking of membranes amongst

organelles, such as the endoplasmic reticulum and golgi complex, similarly involves MTs and associated motor proteins (Caviston and Holzbaur, 2006).

Other organelles, including the nucleus and mitochondria, are also positioned by MTs (Yaffe et al., 1996) . In fission yeast, MTs are organized with plus-ends oriented towards the cell tips, and minus ends on or near the nuclear envelope (NE). A balance of forces produced as MTs polymerize and push against the cell cortex is thought to position the nucleus in the centre of the cell (Tran et al., 2001). Nuclear positioning in animal cells likely occurs by a similar mechanism, but may also involve the activity of motor proteins (Morris, 2003; Reinsch and Gonczy, 1998).

Both the actin and MT cytoskeleton are important to the establishment and maintenance of cell polarity, a process involved in cell morphogenesis, differentiation, and division (Li and Gundersen, 2008). Regions of cell growth and protrusion are associated with dynamic changes in the actin cytoskeleton, as observed in the focal adhesions of migrating cells (Small and Kaverina, 2003) and axonal growth cones of neurons (Kalil and Dent, 2004). In processes mediated by various proteins that associate with MT plus-ends, MTs are linked to the cell cortex, where they appear to be involved in regulating the actin cytoskeleton. In fission yeast, for example, the MT plus-end proteins Tea1p and Tea4p are required for the recruitment of the formin For3p, an activator of actin nucleation, to growing cell tips (Snaith and Sawin, 2005).

1.2 Microtubule polymerization

Heterodimers of $\alpha\beta$-tubulin assemble in a longitudinal, head-to-tail manner to generate MT protofilaments. Separate lateral interactions between parallel protofilaments

generate the cylindrical, polar structure of the microtubule. *In vivo*, MTs are typically composed of 13 protofilaments. MTs with 9-16 protofilaments have also been observed, although these more variable numbers of protofilaments are usually only observed when MTs are assembled *in vitro*. (Chretien and Wade, 1991; Evans et al., 1985; Tilney et al., 1973). In a 13-protofilament MT, individual protofilaments are effectively parallel to the axis of the MT itself. However, α- and β-tubulin monomers within the MT lattice follow a three-start, left-handed helix, meaning each turn around the helix axis corresponds to a rise of three monomers. As a consequence, MTs have a "seam" where lateral interaction between unlike α- and β-tubulin subunits occurs (Li et al., 2002; Mandelkow et al., 1986).

The polymerization of MTs *in vitro* was first demonstrated using tubulin partially purified from rat brains, and was found to require the presence of GTP, magnesium, and calcium chelators (Weisenberg, 1972). Early studies suggested that steady-state MTs undergo a process referred to as treadmilling, whereby the addition of tubulin subunits at one end of the polymer is balanced by tubulin loss at the other end (Margolis and Wilson, 1978). This interpretation, however, was based on the bulk analysis of populations of MTs *in vitro*. Subsequent analysis of the length distributions of individual, fixed MTs led to the "dynamic instability" model of MT dynamics, which remains generally accepted today (Mitchison and Kirschner, 1984a; Mitchison and Kirschner, 1984b). In essence, this model proposes that the plus-ends of individual MTs switch between states of slow assembly and rapid disassembly. MT minus ends can also polymerize and depolymerize. *In vivo*, however, MT minus ends are significantly more stable than MT plus ends. It was later determined that β-tubulin, rather than α-tubulin, was exposed at the more dynamic MT plus-end (Mitchison, 1993).

The dynamic instability of MTs is ultimately fuelled by hydrolysis of β-tubulin-bound GTP. Both α- and β-tubulin bind a single molecule of GTP, although only the GTP associated

with β-tubulin undergoes hydrolysis and exchange . As a new αβ-tubulin subunit is added to a MT, residues present on the newly-arrived α-tubulin catalyze hydrolysis of GTP on the receiving β-tubulin (Nogales et al., 1999). The resulting GDP is buried at the subunit interface, and can therefore no longer be exchanged. Importantly, though, MT polymerization can occur in the in the presence of the non-hydrolysable GTP analogue GMPCPP, revealing that GTP hydrolysis itself is not required for subunit addition (Hyman et al., 1992).

In fact, GMPCPP-microtubules are observed to be hyper-stable, thus implicating GTP hydrolysis in MT depolymerization. Indeed, hydrolysis of GTP in the MT lattice results in curving of protofilaments, which destabilizes the lattice and promotes MT depolymerization. Using electron microscopy (EM), these curved protofilaments have been directly observed at the ends of depolymerizing MTs (Arnal et al., 2000; Muller-Reichert et al., 1998). By contrast, GTP-bound protofilaments have a straight conformation and appear to grow as sheets which close to produce MTs with blunt-ends (Arnal et al., 2000; Chretien et al., 1995). In addition, GDP-tubulin is found to dissociate from MT plus-ends at a rate 2-3 orders of magnitude faster than GTP-tubulin (Mitchison and Kirschner, 1984a).

Taken together, these observations reveal an elegant model for the dynamic instability of MTs. As a MT polymerizes, GTP-bound subunits are added to the growing plus-end at a rate that exceeds GTP hydrolysis. As a result, the MT plus-end develops a "cap" of GTP-tubulin subunits (Mitchison and Kirschner, 1984a). The remainder of the MT, which may be composed mostly of GDP-tubulin, is protected from depolymerization by the GTP cap (Caplow and Shanks, 1996). However, the GTP cap can be lost if the rate of hydrolysis overtakes the rate of subunit addition due, for example, to a drop in the concentration of free GTP-tubulin. This results in a loss of GDP-tubulin from the MT end, curving of protofilaments, and ultimately MT disassembly, a process referred to as catastrophe. In

contrast, rescue events occur when GTP subunits are added to the end of a depolymerizing MT, resulting in a re-initiation of growth. These cycles of polymerization and depolymerization, fuelled by energy from GTP hydrolysis, allow MTs to do useful work within the cell.

In vitro, MT polymerization occurs in two steps, referred to as nucleation and elongation. During the nucleation stage, several αβ-tubulin subunits associate to form a seed from which further polymerization then occurs. At low tubulin concentrations (<10 μM), disassembly of these MT seeds is greatly favoured over assembly, resulting in limited MT polymerization (Kuchnir Fygenson et al., 1995; Mitchison and Kirschner, 1984b). However, once a sufficient number of tubulin subunits are assembled, polymerization becomes energetically favourable, and MT elongation proceeds rapidly. Most likely, this is because tubulin subunits within the MT lattice are stabilized, and have their conformation restricted, by both lateral and longitudinal interactions with one another (Gardner et al., 2011; Rice et al., 2008).

1.3 Microtubule organizing centres

In vivo, specialized sites referred to as microtubule organizing centres (MTOCs) allow cells to surmount the kinetic barrier imposed by MT nucleation. These sites contain factors, including γ-tubulin and its associated proteins (see below), which promote localized MT assembly. Therefore, by maintaining relatively low tubulin concentrations, at which spontaneous assembly of MTs is not favoured, cells can employ MTOCs to determine where and when MT polymerization occurs. As a result, MTOCs ensure that MTs are arranged and oriented in a manner that is useful to the cell. Generally, MT minus ends are

anchored at MTOCs, with plus-ends projecting outwards. MTOCs vary amongst species and throughout stages of cell division and differentiation, but can generally be categorized as either centrosomal or acentrosomal.

Purified centrosomes are capable of promoting MT nucleation at tubulin concentrations significantly lower than those required for spontaneous MT assembly *in vitro* (Mitchison and Kirschner, 1984b). In many animal cells, the centrosome acts as the principal MTOC, nucleating radial arrays of MTs during interphase, and the mitotic spindle during mitosis. The centrosome consists of a pair of centrioles, which are linked by fibrous proteins and surrounded by a matrix of proteins referred to as the pericentriolar material (PCM). The PCM is composed largely of coiled-coil proteins from the pericentrin and AKAP450 families and acts to anchor components required for MT nucleation, including γ-tubulin (Azimzadeh and Bornens, 2007; Bettencourt-Dias and Glover, 2007). Centrioles themselves are composed of an ordered, cylindrical array of 9 MT triplets but do not have a direct role in the nucleation of centrosomal MTs. Rather, centrioles appear to anchor the minus-ends of MTs nucleated from the PCM, in a process involving the protein ninein (Mogensen et al., 2000). In addition, centrioles can migrate to the plasma membrane, where they give rise to basal bodies which nucleate the axonemal MTs of cilia and flagella (Beisson and Wright, 2003). Animal cells in which the centrosomes have been destroyed by laser microsurgery retain the ability to assemble a mitotic spindle, revealing that centrosomes are not essential to MT nucleation or spindle assemble (Khodjakov et al., 2000).

In fact, centrioles and centrosomes are absent in both higher plants and fungi. However, fungi contain an analogous structure, the spindle pole body (SPB), which is embedded in the NE. EM in budding and fission yeast has revealed that the SPB consists of 3 primary layers, an outer layer which faces the cytoplasm, a central layer which spans the

NE, and an inner layer which faces the nucleoplasm (McIntosh and O'Toole, 1999; O'Toole et al., 1999). These layers are composed of structural proteins, including Spc42 and calmodulin/Cmd1, as well as proteins involved in SPB duplication, membrane insertion, and MT nucleation (Jaspersen and Winey, 2004). Cytoplasmic MTs are nucleated from the outer layer of the SPB, while the mitotic spindle is nucleated from inner layers following SPB duplication. In the budding yeast *Saccharomyces cerevisiae,* the SPB serves as the sole site of both interphase and spindle MT nucleation (Knop et al., 1999). In fission yeast, on the other hand, MTs are nucleated from SPBs as well as from additional sites on the NE, along existing MTs, and at the cell equator during cell division (Hagan, 1998; Sawin and Tran, 2006).

Acentrosomal (and non-SPB) MTOCs allow cells to generate a diversity of MT arrays, independent of a central organizing structure. In plants, for example, MTs are nucleated from sites on the NE and cell cortex, as well as from the sides of existing MTs (Ehrhardt and Shaw, 2006; Murata et al., 2005). Isolated plant nuclei are capable of promoting MT assembly, indicating that MT-nucleating material is directly associated with the NE (Seltzer et al., 2007; Stoppin et al., 1994). The NE also acts as a MTOC in myotubes, the multinucleate cells formed by myoblast fusion during skeletal muscle differentiation (Tassin et al., 1985). During this differentiation process, centrosomal proteins, including γ-tubulin, pericentrin, and ninein, are re-distributed to the nuclear surface, thereby re-defining sites of MT nucleation (Bugnard et al., 2005).

Other differentiated cells, such as neurons and epithelial cells, contain both centrosomal and acentrosomal MTOCs. In neuronal cells, MTs in the cell body are often associated with the centrosome, while MTs within dendrites and axons are organized in an acentrosomal fashion. MTs are critical for the development of axonal and dendritic extensions, and also facilitate the transport of cargo related to synaptic transmission

(Goldstein and Yang, 2000). As neuronal differentiation progresses, the centrosome loses its function as a MTOC, and acentrosomal MT assembly alone appears to be sufficient for promoting axon growth and regeneration (Stiess et al., 2010).

Polarized epithelial cells exhibit two fairly distinct acentrosomal MT arrays, in addition to the limited number of MTs generally associated with the centrosome. In the first type of acentrosomal array, MTs are arranged in parallel along the apico-basal axis, with minus ends anchored at the apical membrane (Waschke and Drenckhahn, 2000). The second array consists of a network of MTs that are associated with the basal cortex and exhibit mixed polarity (Reilein and Nelson, 2005). γ-tubulin has been observed at these acentrosomal MTOCs, although there remains no direct evidence for *de novo* MT nucleation from these sites (Reilein et al., 2005; Waschke and Drenckhahn, 2000). Rather, these MTs may be nucleated at the centrosome, released into the cytoplasm, and subsequently capture at cortical sites (Mogensen, 1999).

1.4 The γ-tubulin complex

It is evident that MT organization varies greatly across species and throughout stages of cell division and differentiation. Nonetheless, efficient MT nucleation at all MTOCs ultimately requires γ-tubulin. First discovered in *Aspergillus nidulas,* γ-tubulin is a homologue of αβ-tubulin that is conserved amongst eukaryotes (Oakley and Oakley, 1989; Stearns et al., 1991; Zheng et al., 1991). X-ray crystallography has revealed that the structure of γ-tubulin is very similar to the structures of α- and β-tubulin (Aldaz et al., 2005; Rice et al., 2008). Significantly, these structures also indicate that γ-tubulins associate with one another via lateral interactions, using the same surfaces involved in αβ-tubulin lateral

interactions in the MT lattice. Longitudinal interactions between γ-tubulin and aβ-tubulin could, therefore, stabilize lateral interactions between αβ-tubulin subunits and promote MT assembly.

Early work in *Drosophila* and *Xenopus* egg extracts demonstrated that γ-tubulin associates with a variety of evolutionarily conserved proteins, specifically the γ-tubulin complex proteins (GCPs) GCP2, GCP3, GCP4, GCP5, and GCP6 (Oegema et al., 1999; Zheng et al., 1995) [the GCP nomenclature is used throughout for convenience, but species-specific names for GCPs do exist (Table 1.1)]. Electron microscopy of these complexes revealed that they are ring-like structures, leading to the term "γ-tubulin ring complex" (γ-TuRC). These structures associate with the minus ends of MTs, and have a helical pitch and diameter approximately matching a MT (Moritz et al., 2000; Zheng et al., 1995). *In vitro*, γ-TuRCs are capable of nucleating MT assembly. However, under high-salt conditions, the γ-TuRC was found to disassemble into smaller complexes consisting of only γ-tubulin, GCP2, and GCP3. These smaller complexes, appropriately named γ-tubulin small complexes (γ-TuSCs), lacked the ability to promote MT polymerization (Oegema et al., 1999). Low-resolution 3-dimensional structures of the γ-TuRC, derived from EM tomography, appeared to consist of repeating V-shaped γ-TuSCs arranged around a "cap" structure, which was presumed to represent the additional GCPs (Moritz et al., 2000). Overall, these studies suggested a "template model" in which multiple γ-TuSCs are assembled to produce a γ-TuRC, thereby generating a ring of γ-tubulins that acts as a template for MT assembly.

Table 1.1: γ-tubulin complex protein nomenclature in various species.

Human	***D. melanogaster***	***Xenopus***	***A. thaliana***	***S.* cerevisiae**	***S.* pombe**	***A.* nidulans**
γ-tubulin	γ-tubulin	γ-tubulin	γ-tubulin	Tub4p	Tubg1/Gtb1	mipA
hGCP2	Dgrip84	Xgrip110	AtSpc97p	Spc97p	Alp4	AnGCP2
hGCP3	Dgrip91	Xgrip109	AtSpc98p	Spc98p	Alp6	AnGCP3
hGCP4	Dgrip75	Xgrip76	AtGCP4	-	Gfh1	AnGCP4§
hGCP5	Dgrip128	Xgrip133	AtGCP5	-	Mod21	AnGCP5
hGCP6	Dgrip163	Xgrip210	AtGCP6	-	Alp16	AnGCP6

Adapted from Wiese and Zheng, 2006

An alternative "protofilament model" for MT nucleation has also been proposed. In this model, the γ-TuRC unwinds to form a protofilament-like structure, with γ-tubulins associating in a longitudinal manner. These γ-tubulins interact laterally with αβ-tubulin dimers, stabilizing early protofilaments that can then facilitate further MT polymerization (Erickson, 2000; Erickson and Stoffler, 1996). The bulk of current structural data, however, strongly favours the template model.

Work in *S. cerevisiae*, which lacks homologues of GCPs 4, 5, and 6, has provided a great deal of insight into γ-TuSC structure and function. The budding yeast γ-TuSC is a stable complex consisting of 4 molecules: one copy of GCP2 (Spc97p in budding yeast), one copy of GCP3 (Spc98p in budding yeast), and two copies of γ-tubulin (Knop et al., 1997; Knop and Schiebel, 1997). Reconstituted γ-TuSCs, produced using baculovirus/insect cells, exhibit the same stoichiometry and sedimentation coefficient (11.6S) as endogenous γ-TuSCs (Vinh et al., 2002). These reconstituted complexes have the capacity to bind pre-formed MTs *in vitro*, but display only very weak nucleating activity. In budding yeast cells, γ-TuSCs promote MT nucleation only when localized to the SPB by the proteins Spc110 and Spc72, suggesting that these proteins may be necessary for γ-TuSC function (Knop and Schiebel, 1997; Knop and Schiebel, 1998). Reconstitution of γ-TuSCs in complex with Spc110, however, fails to promote γ-TuSC multimerization into larger complexes, and does not result in increased nucleating activity (Vinh et al., 2002). Interestingly, particular buffer conditions allow endogenous budding yeast γ-TuSC proteins to be isolated as a 22S complex, comparable in size to the 25-35S γ-TuRCs seen in higher eukaryotes (Vinh et al., 2002). This implies that additional non-GCP factors found *in vivo* may promote γ-TuSC multimerization and nucleating activity.

Following initial biochemical characterization, single particle EM was used to determine the structure of recombinant budding yeast γ-TuSC at 25-Å (Kollman et al.,

2008). The γ-TuSC was found to have a Y-shaped structure, with two "arms" roughly 100 Å in length each associated with a globular lobe approximately 50 Å in diameter. Gold-labelling and manually docking of the γ-tubulin crystal structure revealed that the lobes corresponded to γ-tubulin. Also, *in vivo* fluorescence resonance energy transfer (FRET), coupled with EM analysis of γ-TuSCs containing CFP and YFP-tagged components, was used to determine the relative orientations of proteins within the complex. The C-termini of both GCP2 and GCP3 were found to interact directly with γ-tubulin, while the N-termini of GCP2 and GCP3 overlapped and interacted with one another (Choy et al., 2009; Kollman et al., 2008). Importantly, the centre-to-centre spacing between γ-tubulins within the γ-TuSC was seen to vary from 70-85 Å, owing to flexibility in the GCP3 arm. This distance is significantly greater than the 53 Å spacing between adjacent protofilaments in the MT lattice, suggesting that conformational changes in the γ-TuSC may be necessary to generate an effective template for MT nucleation (Choy et al., 2009; Kollman et al., 2008).

Under specific low-salt buffer conditions, purified γ-TuSCs are capable of assembling into ring structures resembling Drosophila γ-TuRCs (Kollman et al., 2010). Remarkably, γ-TuSCs co-purified with truncated $Spc110^{1-220}$, and stabilized by the addition of glycerol, can polymerize into elongated filaments with a repeating helical structure. Due to the helical symmetry present in these filaments, it was possible to determine their EM structure to a high resolution of 8 Å (Kollman et al., 2010). Lateral associations between GCP2 and GCP3 of adjacent γ-TuSCs mediate the assembly of these elongated structures. Further, each turn of the helix corresponds to 13 γ-tubulins or 6 ½ γ-TuSCs, resulting in a half γ-TuSC overlap. The geometry of the filament therefore approximately matches that of a 13-protofilament MT, such that each rise of the helix could represent a template for MT assembly.

As predicted by the template model, γ-tubulins associate with GCP2 and GCP3 through their minus ends, leaving their plus ends available for longitudinal association with α-tubulin. However, the intra-γ-TuSC spacing of γ-tubulins in the filament structure does not match the lateral spacing of MT protofilaments, as observed with isolated γ-TuSCs. γ-Tubulins in adjacent γ-TuSCs, by contrast, appear to form lateral contacts that match those of the MT lattice. Thus, multimerization of γ-TuSCs appears to be insufficient for generating a potent MT-nucleating complex. Conformational changes would seem to be required to turn these γ-TuSC rings into effective MT nucleators. In fact, a 23^{o} rotation of GCP3 would be sufficient to generate a γ-tubulin template matching the MT lattice spacing (Kollman et al., 2010). Such a change could be induced by post-translational modifications or binding of additional proteins, although the exact mechanism of γ-tubulin complex (γ-TuC) activation remains unknown.

GCP4, 5, and 6 were previously thought to promote γ-TuRC assembly by acting as a scaffold for γ-TuSC multimerization. The absence of these proteins in budding yeast, as well as the findings described above, clearly reveal that GCP4, 5, and 6 are not required for the formation of γ-tubulin rings or MT nucleation. Further, deletion of the fission yeast genes encoding GCPs 4-6 results in only a minor reduction in the frequency of MT nucleation (Anders et al., 2006). In *D. melanogaster*, simultaneous RNAi depletion of GCPs 4-6 does not inhibit γ-TuSC localization to the centrosome, but does inhibit localization to the spindle. Cells retain the ability to nucleate interphase MTs as well as the mitotic spindle, although defects in MT organization are observed (Verollet et al., 2006). *Aspergillus nidulans* similarly does not require GCPs 4-6 for γ-TuSC localization to the SPB or for normal MT nucleation (Xiong and Oakley, 2009). These observations indicate that GCP4, 5, and 6 are not strictly required for MT nucleation by the γ-TuC, but may increase the efficiency of nucleation or promote γ-TuC localization to particular types of MTOCs.

Recently, the crystal structure of human GCP4 (hGCP4) was determined, which has helped to clarify the role of GCPs 4-6 in γ-TuC structure and function (Guillet et al., 2011). hGCP4 has an elongated structure, consisting of 5 successive helical bundles. This crystal structure fits extremely well into the cryo-EM structures of GCP2 and GCP3, suggesting a high degree of structural conservation amongst all GCPs. In addition, although hGCPs 2-6 vary significantly in length — with GCP4 being the shortest — all show significant primary sequence homology (Guillet et al., 2011). Previously, homology identified amongst GCPs was mostly limited to two particularly conserved sequences, referred to as gamma ring protein motifs (grip motifs) grip1 and grip2 (Gunawardane et al., 2000). The γ-TuSC structure revealed that the grip2 sequence, exposed near the C-terminus of GCP2 and GCP3, is likely involved in γ-tubulin binding (Kollman et al., 2010). grip1 is located towards the N-terminus of GCPs, and forms part of the surface involved in GCP lateral interactions. Portions of grip1 are also exposed on the outer surface of the γ-TuSC, suggesting grip1 may have an additional role in binding to γ-TuC-associated proteins (Kollman et al., 2011; Kollman et al., 2010). Significantly, the surfaces involved in GCP and γ-tubulin interaction are conserved in the GCP4 structure, and interaction between γ-tubulin and the GCP4 C-terminus has been confirmed by immunoprecipitation (Guillet et al., 2011).

Overall, these findings imply that all five GCPs share a similar structure and are able to bind to one another as well as to γ-tubulin. Therefore, it is possible that GCPs 4-6 associate with one another, GCP2, and GCP3 to form γ-TuSC-like structures that are incorporated into the γ-TuRC (Kollman et al., 2011) (Figure 1.1). γ-TuSC-like pairs of all GCPs can thus be imagined, although GCPs 4-6 appear to interact with one another (Anders et al., 2006; Xiong and Oakley, 2009). Biochemical analysis of purified, endogenous human γ-TuRCs shows that GCPs 4-6 are present only in limited copy number, with roughly 14 γ-tubulins associating with 12 copies of GCP2/3, 2-3 copies of GCP4, 1 copy of GCP5, and 0.5

copies of GCP6 (Choi et al., 2010). The observation of 0.5 copies of GCP6 suggests that γ-TuRCs may assembly with various stoichiometries of GCPs.

Given the ability of γ-TuSCs to form ring structures and nucleate MTs in vivo, the precise function of GCPs 4, 5, and 6 within the γ-TuRC is still unclear. However, biochemical studies of endogenous γ-TuCs indicate that GCPs 4-6 promote γ-TuRC stability (Verollet et al., 2006; Xiong and Oakley, 2009). It has also been proposed that GCPs 4-6 may act to initiate or terminate γ-TuRC assembly in a manner that limits rings to 13 γ-tubulins, although this remains to be demonstrated (Kollman et al., 2011).

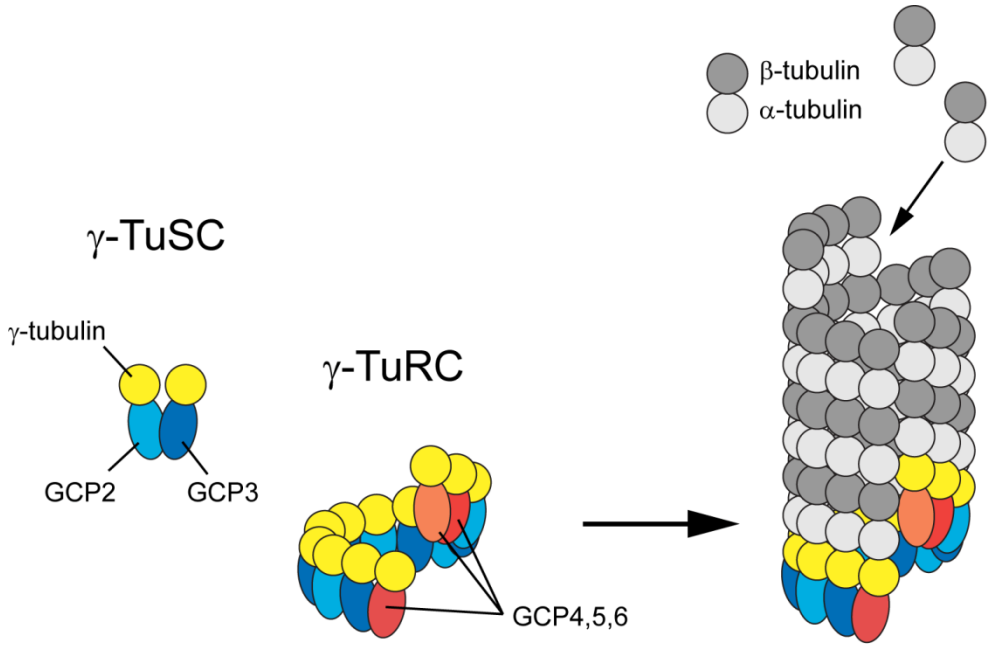

Figure 1.1: The current template model for MT nucleation by the γ-TuC. GCPs 2-6 all associate with γ-tubulin. One copy each of GCP2 and GCP3 associate to form the γ-TuSC, while multiple γ-TuSCs assembly into a γ-TuRC along with GCP4, 5, and 6. Within the γ-TuRC, γ-tubulins associate laterally to form a helical, ring-like structure. Longitudinal association between γ-tubulin and αβ-tubulin subunits allows this γ-tubulin ring to act as a template for MT polymerization. Note that the positions of GCPs 4, 5, and 6 within the γ-TuC structure are largely speculative, and remain to be confirmed experimentally.

1.5 Localization and regulation of the γ-tubulin complex

Fluorescence recovery after photobleaching (FRAP) experiments have demonstrated that centrosomal γ-tubulin exchanges with a pool of free, cytoplasmic γ-tubulin (Khodjakov and Rieder, 1999). Additional work in human lymphoblastic cells has shown that roughly 80% of γ-TuCs exist in this cytosolic form (Moudjou et al., 1996). However, ectopic MT nucleation is generally not observed, with γ-TuC activity being limited to specific MTOCs. This suggests that factors present at MTOCs activate the γ-TuC, perhaps by mediating the conformation changes necessary to generate an effective nucleator. A variety of proteins are involved in recruiting the γ-TuC to MTOCs, although the role of these proteins in activating the γ-TuC remains unclear.

The GCP-WD/NEDD1 family of proteins is involved in γ-TuC localization in plants and animals, but is absent in fungi (Gunawardane et al., 2003; Luders et al., 2006; Zeng et al., 2009). Despite lacking grip motifs, GCP-WD is generally considered to be a genuine γ-TuC component. Dgp71WD, the *Drosophila* GCP-WD homologue, associates with all 5 grip motif-containing GCPs, as well as γ-tubulin itself (Gunawardane et al., 2003). Association with γ-tubulin, as well as GCP-WD multimerization, is mediated by residues in the GCP-WD C-terminus (Manning et al., 2010). The GCP-WD N-terminus, on the other hand, is composed of WD40 repeats, which are predicted to form a β-propeller structure involved in protein interaction. It has thus been proposed that GCP-WD may act as a scaffold to promote γ-TuC assembly, although GCP-WD depletion has only a small effect on the formation of γ-TuRCs (Haren et al., 2006). Nonetheless, GCP-WD is critical for γ-TuC localization to both centrosomes and spindle MTs. Depletion of GCP-WD inhibits centrosomal and chromatin-mediated MT nucleation, thus preventing mitotic spindle formation (Haren et al., 2006; Luders et al., 2006). By contrast, γ-tubulin is not required for

GCP-WD localization to centrosomes, indicating that GCP-WD is a *bona fide* γ-TuC targeting factor (Haren et al., 2006).

Like GCP-WD, GCP8/MOZART2 lacks homology to GCPs 2-6 but appears to be a stable member of the γ-TuC (Hutchins et al., 2010; Teixido-Travesa et al., 2010). GCP8 is a small 16 kDa protein that is conserved almost exclusively amongst deuterostomes, and its study has been limited to human cells. Depletion of GCP8 by siRNA impairs γ-TuC localization to interphase centrosomes, and results in reduced centrosomal MT nucleation during interphase. Mitotic γ-TuC localization and MT nucleation, however, are unaffected by GCP8 depletion. Also, as seen with GCP-WD, γ-TuRC assembly does not depend on GCP8, perhaps suggesting a regulatory rather than structural role for GCP8 (Teixido-Travesa et al., 2010). MOZART1, a candidate γ-TuC component conserved amongst lower eukaryotes such as fission yeast, appears to have a role in spindle assembly and targeting of the γ-TuC to mitotic centrosomes (Hutchins et al., 2010).

The γ-TuC also associates with a variety of PCM components, many of which are large coiled-coil proteins. For example, γ-tubulin and pericentrin associate in an elaborate lattice structure at the centrosome that is associated with MTs. This lattice gradually increases in size as cells enter mitosis, and then rapidly disassembles (Dictenberg et al., 1998). Coimmunoprecipitation suggests that pericentrin may associate with the γ-TuRC via interactions with GCP2 and GCP3 (Zimmerman et al., 2004). The centrosomal proteins Kendrin and AKAP450 also form complexes with GCPs, and disruption of either protein interferes with MT nucleation (Takahashi et al., 2002). It is uncertain, however, whether or not these proteins interact directly with the γ-TuC to mediate centrosomal attachment. Instead, they may simply be involved in the overall assembly of the PCM.

In budding yeast, localization of γ-TuSC proteins to the nuclear and cytoplasmic face of the SPB is mediated by Spc110 and Spc72, respectively (Knop and Schiebel, 1997;

Knop and Schiebel, 1998). Both proteins are predicted to contain coiled-coils, as with many centrosomal proteins, and interact with the γ-TuSC via an N-terminal domain. As described above, a fragment of Spc110 is able to promote γ-TuSC multimerization *in vitro*, but fails to significantly enhance γ-TuSC nucleating activity (Kollman et al., 2010).

The centrosomal protein CDK5RAP2 is of particular interest, as it appears to have roles in both γ-TuC localization and activation. CDK5RAP2 is a relatively large (1893 amino acid) coiled-coil protein that contributes to centrosomal γ-TuC recruitment and MT nucleation, but does not appear to have a role in γ-TuRC assembly (Fong et al., 2008). Interaction between CDK5RAP2 and the γ-TuC is mediated by a short stretch of approximately 50 amino acids, referred to as centrosomin motif 1 (CM1). The CM1 region is conserved amongst animal and fungal cells, and is generally found towards the N-terminus of proteins predicted to contain coiled-coils. CM1 proteins, including *Drosophila* Centrosomin (Cnn), human Myomegalin and CDK5RAP2, as well as fission yeast Mto1 and Pcp1, have various roles in centrosome function, MT organization, and brain development (Bond et al., 2005; Flory et al., 2002; Fong et al., 2008; Megraw et al., 1999; Samejima et al., 2008; Sawin et al., 2004; Verde et al., 2001). *In vivo*, over-expression of the CDK5RAP2 CM1 fragment causes γ-tubulin to be de-localized from the centrosome, and promotes acentrosomal MT nucleation (Choi et al., 2010; Fong et al., 2008). Further, both full-length CDK5RAP2 and a CM1-containing fragment are capable of enhancing MT nucleation by purified γ-TuRCs *in vitro* (Choi et al., 2010). These findings suggest that CDK5RAP2 is a γ-TuRC activator, although the mechanism of activation remains to be determined.

1.6 Microtubule organization in fission yeast

Owing to its relatively simple arrangement of MTs, the fission yeast *Schizosaccharomyces pombe* is an attractive model for the study of MT dynamics and organization. Fission yeast exhibit a diversity of MTOCs, which vary throughout the cell cycle (Hagan, 1998; Sawin and Tran, 2006) (Figure 1.2A). During interphase, fission yeast cells contain roughly 3-5 MT bundles, which are arranged with plus ends oriented towards the cell tips and minus ends near the nucleus. These interphase MTs contribute to nuclear positioning, as well as the establishment of cell polarity, helping to define the characteristic rod shape of *S. pombe (Hagan and Hyams, 1988; Sawin and Snaith, 2004; Tran et al., 2001)*. Interphase MT nucleation occurs from the SPB and from interphase MTOCs (iMTOCs) on the NE and along existing MTs. Anti-parallel bundling and minus end-directed sliding of MTs helps to focus minus ends around the nuclear envelope. Bundling proteins such as Ase1 and Dis1, as well as the minus end-directed motor Klp2, facilitate this process (Carazo-Salas and Nurse, 2006; Roque et al., 2010).

As fission yeast cells enter mitosis, interphase MTs depolymerize. MTs are then nucleated form the nucleoplasmic face of the duplicated SPBs, ultimately giving rise to a mitotic spindle that spans the nucleus at metaphase. Fission yeast undergo a closed mitosis, such that NE breakdown does not occur. As anaphase proceeds, the spindle elongates to span the long axis of the cell, acting to segregate chromosomes and achieve nuclear separation (Hagan and Yanagida, 1997; Hagan and Hyams, 1988). Astral MTs, nucleated from the cytoplasmic face of the SPBs, are thought to align the mitotic spindle by pushing against the cell cortex (Oliferenko and Balasubramanian, 2002; Tolic-Norrelykke et al., 2004).

During late anaphase, MTs are nucleated from the equatorial MTOC (eMTOC), generating a post-anaphase array (PAA) of MTs at the site of septation/cytokinesis. Septum formation and cell division require the contractile actin-myosin ring, which is positioned at the centre of the cell in order to ensure accurate division into two identical daughter cells (Feierbach and Chang, 2001). The position of the contractile ring is defined by the pre-divisional nucleus, in a process whereby the protein Mid1 is released from the nucleus onto the adjacent cell cortex (Daga and Chang, 2005). The position of Mid1 defines the site for subsequent recruitment of myosin and other contractile ring components (Wu et al., 2003). The position of the eMTOC, in turn, is defined by the actin-myosin contractile ring. PAA MTs then ensure that the contractile ring remains positioned at the centre of the cell as cells progress through cytokinesis (Pardo and Nurse, 2003). The PAA may also have a role in re-positioning the nucleus towards the centre of the cell following cell division (Hagan and Yanagida, 1997).

The nucleation of spindle MTs in fission yeast is mediated by the essential protein Pcp1, which recruits the γ-TuC to the nucleoplasmic face of the SPB (Flory et al., 2002; Fong et al., 2010). Pcp1 is a coiled-coil protein containing the conserved γ-TuC-binding CM1 domain (Samejima et al., 2008). A temperature-sensitive *pcp1* mutant, which includes a point mutation within the CM1 region, inhibits γ-TuC localization to mitotic SPBs. This results in defective spindle formation and chromosome missegregation (Fong et al., 2010). A separate *pcp1* mutant, which also exhibits spindle defects, is deficient in polo kinase (Plo1) recruitment to SPBs. Given that Plo1 accumulation at SPBs is associated with mitotic entry and septum formation, this suggests an additional role for Pcp1 in cell-cycle regulation (Fong et al., 2010; Ohkura et al., 1995; Tanaka et al., 2001).

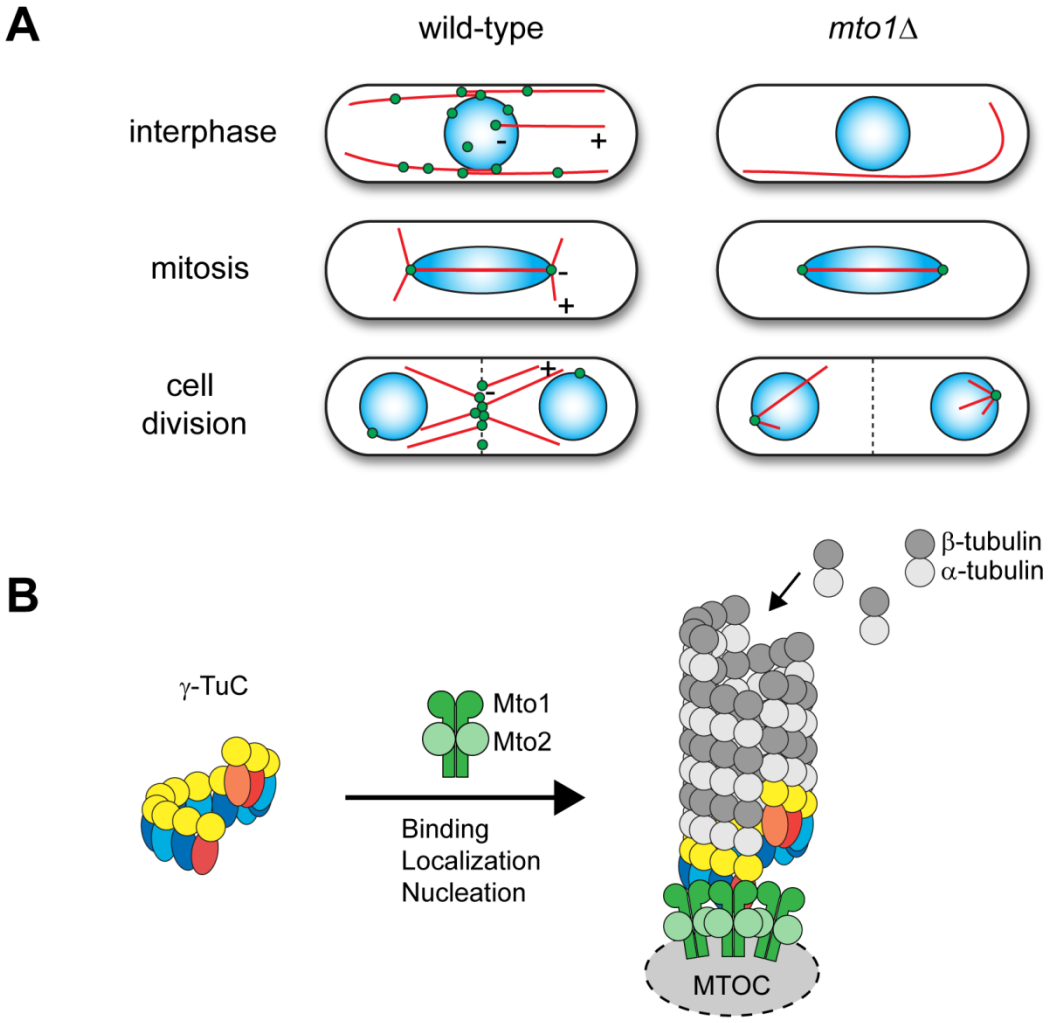

Figure 1.2: Fission yeast MT organization varies throughout the cell cycle. (A) During interphase, wild-type cells nucleate cytoplasmic MTs (red lines) from MTOCs (green circles) at the SPB, on the NE, and on the sides of existing MTs. As cells enter mitosis, intranuclear mitotic spindle and cytoplasmic astral MTs are nucleated from the duplicated SPBs. During cell division, MTs are nucleated from the eMTOC at the cell equator. Positions of plus (+) and minus (-) ends are indicated. In an *mto1*Δ background, cells retain the ability to nucleate the mitotic spindle. Remnants of the mitotic spindle often escape following cell division and persist as abnormal MT arrays during interphase. However, *mto1*Δ cells are completely deficient in *de novo* cytoplasmic MT nucleation. (B) The Mto1/2 complex binds the γ-TuC and recruits it to cytoplasmic MTOCs, where the γ-TuC actively nucleates MTs.

1.7 The Mto1/2 complex and cytoplasmic MT organization

In fission yeast, the proteins Mto1 and Mto2 are required for the assembly and organization of cytoplasmic MTs (Figure 1.2). Mto1 and Mto2 associate to form the Mto1/2 complex, which recruits the γ-TuC to iMTOCs, the eMTOC, and the cytoplasmic face of the SPB during both interphase and mitosis (Samejima et al., 2005; Sawin et al., 2004; Venkatram et al., 2005; Venkatram et al., 2004). Deletion of either *mto1* or *mto2* results in cells with abnormal interphase MT arrays, typically consisting of 1-2 long bundles which curve around the cell tips. This lack of proper MT organization results in defective nuclear positioning, as well as polarity defects which give cells a characteristic curved shape.

In wild-type cells, both Mto1 and Mto2 co-localize with the γ-TuC at cytoplasmic MTOCs. In *mto1Δ* cells, by contrast, localization of Mto2 and the γ-TuC to cytoplasmic MTOCs is abolished, although the γ-TuC is still localized to the nucleoplasmic face of the SPB in a process depending on Pcp1 (Flory et al., 2002; Samejima et al., 2005; Sawin et al., 2004; Venkatram et al., 2005; Venkatram et al., 2004). Live-cell imaging reveals that cells lacking Mto1 are completely deficient in *de novo* cytoplasmic MT nucleation, and therefore fail to assemble interphase, PAA, and astral MTs. In cold-shock experiments, in which cells are chilled to depolymerize MTs and subsequently warmed to allow MT re-growth, wild-type cells nucleate new MTs within 1 minute. *mto1Δ* cells, on the other hand, only exhibit cytoplasmic MTs after 10-15 minutes. These MTs likely originate from the nucleoplasmic face of the SPB and subsequently escape into the cytoplasm, thus accounting for the unusual interphase arrays observed in *mto1Δ* cells (Sawin et al., 2004; Venkatram et al., 2004).

In an *mto2Δ* background, cells lack iMTOCs on the NE and MTs, and interphase MTs are nucleated exclusively from the SPB. Cells lacking Mto2 also retain the ability to nucleate

astral and PAA MTs, although nucleation from the eMTOC is significantly impaired (Samejima et al., 2005; Venkatram et al., 2005). The γ-TuC localizes normally to SPBs in *mto2Δ* cells, but is absent from sites along MTs and only faintly detectable at the eMTOC (Samejima et al., 2005). Similarly, Mto1 localization to SPBs is unaffected in a *mto2Δ* background, although reduced levels of Mto1 are observed on MTs and at the eMTOC. Over-expression of Mto1 is sufficient to rescue Mto1 localization to cytoplasmic MTOCs in *mto2Δ* cells, and results in a decoration of MTs and the NE by Mto1. However, concurrent over-expression of Mto1 and Mto2 is required to achieve similar decoration of MTOCs by Mto2 (Samejima et al., 2005). Overall, these observations indicate that Mto2 function is mediated by Mto1. While Mto1 is the principle factor in determining γ-TuC localization, Mto2 appears to have a specific role in interphase MT nucleation from non-SPB sites.

Mto1 is a paralog of Pcp1, and contains a CM1 domain as well as a distinct Mto2-binding region, in addition to extensive predicted coiled-coils (Samejima et al., 2005; Samejima et al., 2008). Deletion of residues within the Mto2-binding region disrupts the Mto1-Mto2 interaction, and results in a phenotype that mimics *mto2Δ* with respect to Mto1 localization, γ-TuC localization, and MT nucleation (Samejima et al., 2008). Mutations in the CM1 domain, in which stretches of 9 amino acids are replaced with alanine, eliminate interaction between Mto1 and the γ-TuC. This does not affect Mto1 localization, but does abolish cytoplasmic MT nucleation, and results in a lack of γ-TuC localization to cytoplasmic MTOCs (Samejima et al., 2008). However, unlike the CDK5RAP2 CM1 region, the Mto1 CM1 domain alone is insufficient for association with the γ-TuC. In fact, both the CM1 domain and Mto2-binding regions must be present on the same Mto1 molecule in order for both Mto1 and Mto2 to associate with the γ-TuC, suggesting a cooperativity in binding (Samejima et al., 2008). Indeed, both Mto1 and Mto2 show little or no association with the γ-TuC in the absence of the other protein. In addition, the Mto1-Mto2 interaction

is preserved under high salt conditions that disrupt the Mto1/2-γ-TuC interaction. Coupled with the observation that Mto1 and Mto2 interact in *mto1* CM1 mutants, this suggests that Mto1 and Mto2 form a subcomplex that assembles independent of γ-TuC proteins (Samejima et al., 2008).

Mto1 also contains a conserved sequence of roughly 44 amino acids in its C-terminus, which is present in the C-terminus of a single protein in a variety of fungal species (Samejima et al., 2010). Like Mto1, many of these proteins contain a CM1 motif and are predicted to contain extensive regions of coiled-coil. Amongst these proteins, the most distantly related C-terminal motif is present in Spc72, which lacks a CM1 domain. However, given the analogous functions of Mto1 and Spc72 in mediating cytoplasmic MT nucleation from the SPB, this sequence is referred to as MASC (*M*to1 *a*nd *S*pc72 *C* terminus)(Samejima et al., 2010).

The Mto1 MASC region, as well as an adjacent stretch of ~20 amino acids, is required for targeting Mto1 to MTOCs, and thus regulates Mto1/2 complex and γ-TuC localization in the cytoplasm (Samejima et al., 2010). The MASC sequence is remarkably modular, containing distinct sequences that mediate localization to the eMTOC, interphase SPB (iSPB), and mitotic SPBs (mSPBs). However, expression of GFP-tagged Mto1 fragments reveals that the MASC sequence alone does not localize to prospective MTOCs. In order to localize effectively, MASC-containing fragments of Mto1 must be multimerized, either by inclusion of Mto1 coiled-coil sequence or by fusion with heterologous coiled-coil sequences (Samejima et al., 2010).

MASC-dependent localization of Mto1 to the eMTOC, and by extension PAA nucleation, depends on the non-essential type II myosin Myp2 (Samejima et al., 2010). Myp2 localizes to the contractile actin ring but is only required for cytokinesis under stress conditions, such as nutrient starvation or high salt (Bezanilla et al., 1997; Motegi et al.,

1997). Co-immunoprecipitation and yeast two-hybrid assays strongly suggest that Mto1 interacts directly with Myp2 (Samejima et al., 2010), and this interaction may account for the dependence of PAA nucleation on actin ring formation (Pardo and Nurse, 2003). Further, localization of Mto1 to mSPBs requires Sid4 and Cdc11, both of which are present at SPBs and involved in recruiting proteins related to septation (Samejima et al., 2010). Nonetheless, the receptors which directly mediate Mto1 attachment to SPBs remain to be determined.

Unlike Mto1, The fission yeast homologues of GCPs 4, 5, and 6 (Gfh1, Mod21, and Alp16) are dispensable for both interphase and mitotic MT nucleation. Individual or simultaneous deletion of all three proteins produces no qualitative change in MT organization, but does result in a quantitative reduction in the frequency of interphase MT nucleation and number of interphase MT bundles (Anders et al., 2006). Simultaneous deletion of GCPs 4-6 has no additive effect relative to single deletions, suggesting that these proteins have redundant roles in MT nucleation. GCPs 4-6 are also co-dependent for association with γ-TuSC proteins, which may account for the lack of an additive phenotype in the triple deletion mutant (Anders et al., 2006). These observations imply that γ-TuSCs, in association with Pcp1 or the Mto1/2 complex, may be sufficient for promoting MT assembly. Notably, γ-TuRC ring structures have not been directly identified in fission yeast, and sucrose gradient analysis indicates that the vast majority of fission yeast γ-TuCs are present as small complexes (Anders et al., 2006). However, GCPs 4-6 co-localize with γ-TuSC components at all MTOCs, suggesting that γ-TuRCs are indeed present in *S. pombe* (Anders and Sawin, 2011).

Project Aims

Overall, current evidence suggests that the γ-TuC alone is not sufficient for MT nucleation. Additional factors present at MTOCs may be necessary for activating MT nucleation by the γ-TuC. However, with the exception of CDK5RAP2, activators of the γ-TuC remain to be identified. In the present work, I seek to address whether or not the Mto1/2 complex contributes directly to γ-TuC activation.

We know that the Mto1/2 complex is required for localization of the γ-TuC to cytoplasmic MTOCs, and also for cytoplasmic MT nucleation. This allows us to envisage two general models for Mto1/2 function: Mto1/2 could be responsible only for localizing the γ-TuC to MTOCs, where the γ-TuC is then activated by other proteins. Alternatively, Mto1/2 could be responsible for both localizing and activating the γ-TuC. To address these possibilities, I aimed to generate a mutant of the Mto1/2 complex that failed to localize to conventional MTOCs — if a non-localizing version of Mto1/2 were still able to promote MT nucleation from the γ-TuC, this would provide evidence that Mto1/2 is a γ-TuC activator. To truly prove that Mto1/2 is a γ-TuC activator, however, will require *in vitro* reconstitution of a complex that is capable of robust MT nucleation. Towards this more long-term objective, I aimed to express, purify, and characterize recombinant Mto1/2 complex produced using a baculovirus expression system.

2. Materials and Methods

2.1 Growth of fission yeast strains

Fission yeast were grown in rich yeast extract medium (YE5S) or Edinburgh minimal medium (EMM) with the following compositions:

YE5S: 0.5% (w/v) Difco Yeast Extract, 3.0% (w/v) glucose, 250 mg/L each of adenine, histidine, leucine, lysine hydrochloride, and uracil.
EMM: 14.7 mM potassium hydrogen phthalate, 15.5 mM Na_2HPO_4, 2% glucose, 1X salts (50X salt stock solution: 52.5 g/L $MgCl_2 \bullet 6H_2O$, 0.735 mg/L $CaCl_2 \bullet 2H_2O$, 50 g/L KCl, 2 g/L Na_2SO_4), 1X vitamins (1000X vitamin stock: 1 g/L pantothenic acid, 10 g/L nicotinic acid, 10 mg/L biotin), 1X minerals (10,000X mineral stock: 5 g/L boric acid, 4 g/L $MnSO_4$, 4 g/L $ZnSO_4.7H_2O$, 2 g/L $FeCl_2.6H_2O$, 0.4 g/L molybdic acid, 1 g/L KI, 0.4 g/L $CuSO_4.5H_2O$, 10 g/L citric acid), and 2.2 g/L NH_4Cl or 3.75 g/L L-glutamic acid monosodium salt. Amino acid supplements are added as required (200 mg/L).

2% Difco Bacto agar was added for growth on solid plates. G418 (Geneticin), nourseothricin (ClonNat), and hygromycin were added at 100 μg/ml when required for selection. YE5S + 5 mg/L Phloxin B was used to check for dead and diploid cells, which take up Phloxin B more readily than living/haploid cells and thus show dark pink staining.

Strains were stored at -80°C in YE5S + 25% Glycerol.

2.2 Genetic crosses

Fission yeast mating was performed on SPA plates [2% Difco Bacto agar, 30 g/L glucose, 5 g/L KH_2PO_4, amino acid supplements and 1X vitamins (as for EMM)]. h- and h+ strains to be mated were streaked onto SPA, mixed with a small volume (eg. 10 μl) of distilled water, and placed at 25°C or 28°C for 2X overnight to form asci. Asci from the

mating plate were streaked onto YE5S and placed at 32^{o}C for approximately 30-60 minutes to allow for ascus wall breakdown. Spores from individual tetrads were then dissected using a Singer dissection microscope and placed at 32^{o}C to germinate and form colonies. Once colonies reached a suitable size (1-2 mm diameter, typically after 2-3 days), they were replica-plated to phloxin B plates and also to appropriate selective media in order to identify genotypes.

2.3 PCR amplification of DNA

Polymerase chain reaction (PCR) amplification of DNA was performed using a MJ Research Thermal Cycler. Reactions were performed using either Phusion High-Fidelity DNA Polymerase (Thermo Scientific) or a combination of Pwo and homemade Taq (HMT) polymerases. The following reaction and cycling conditions were used:

Pwo/HMT Polymerase PCR:

Component	Concentration
*Buffer IV	1X
Forward primer	0.2 μM
Reverser primer	0.2 μM
Template DNA	1 ng/μl
dNTPs (dATP, dTTP, dGTP, dCTP)	500 μM each
$MgCl_2$	3.5 mM
HMT polymerase	0.2 U/μl
Pwo polymerase	0.003 U/μl

*10X buffer IV contains 750 mM Tris-HCl pH 8.8, 200 mM (NH4)2SO4, 0.1% Tween 20.

When using Pwo/HMT polymerase, annealing temperature was first optimized by performing gradient PCR over a range of annealing temperatures. Subsequent amplification was then performed at the temperature giving optimal yield of the desired product.

Temperature cycle:

1. 95°C 2 min
2. 95°C 15 sec
3. 50-70°C 30 sec
4. 72°C 6 min
5. Repeat steps 2-4 for 30 cycles
6. 72°C 5 min
7. 20°C hold

Phusion Polymerase PCR:

Component	Concentration
HF Buffer	1X
Forward primer	0.5 μM
Reverser primer	0.5 μM
Template DNA (plasmid)	1 ng/μl
dNTPs (dATP, dTTP, dGTP, dCTP)	200 μM each
Phusion polymerase	0.02 U/μl

Temperature cycle:

1. 98°C 2 min
2. 98°C 15 sec
3. 60°C 30 sec
4. 72°C 3 min
5. Repeat steps 2-4 for 30-35 cycles
6. 72°C 10 min
7. 20 °C hold

Product yields were determined by subjecting samples to electrophoresis on 1% agarose gels in TAE buffer (40 mM Tris Base, 0.1% glacial acetic acid, 1 mM EDTA) with 0.5 μg/ml ethidium bromide. Samples were prepared in 1X orange G buffer (6X stock: 0.05% Orange

G, 5% Glycerol). Gels were run at ~100V and visualized by UV illumination. A 1kb or 100 bp ladder (New England Biolabs) was used for size standards.

2.4 Strain construction using the PCR-based method

Truncation and tagging of fission yeast genes was performed using the PCR-based methods described by Bahler *et al.,* 1998. Primers were designed with 5' ends containing about 80 nucleotides of homology targeted to the genomic sequence of interest. 3' ends of primers contained 20-22 nucleotides of homology to tagging cassettes, and were used to amplify sequences encoding antibiotic resistance (G418, hygromycin, nourseothricin), *nmt* promoters, and/or GFP tags. Homologous integration of these PCR products into fission yeast strains was used to generate N- and C-terminal truncation mutants with or without GFP tags. The same approach was used for tagging genes at their full-length C-termini. N-terminal truncations produced using this method were placed under control of the thiamine-repressible *nmt81* promoter.

DNA amplification for tagging/truncation was performed by PCR using Pwo/HMT or Phusion polymerase, as described above. Approximately 20-30 μg of DNA was produced for each transformation (1 mL PCR reactions routinely yielded 50-100 μg of the desired product). Prior to transformation, PCR products were cleaned-up using phenol/chloroform/isoamyl alcohol (PCI) extraction. An equal volume of PCI was added to PCR reactions, which were then vortexed and spun at max speed (13000 RPM) for 5 minutes in a microfuge. The supernatant was then recovered and transferred to a fresh tube. PCI extraction was then repeated, and the supernatant recovered again. Chloroform was then added to remove remaining PCI, and samples were vortexed and spun for 5 minutes. NaOAc (pH 5.2) was added to the supernatant at a final concentration of 0.3M, followed by 2 volumes of ethanol (to precipitate DNA). Samples were mixed at RT for ~5 minutes, and spun in a microfuge for 10 minutes at 4^{o}C. DNA pellets were washed with 70% ethanol, dried, and resuspended in 50 μl of TE buffer (10 mM Tris-HCl, 1 mM EDTA, pH 8.0). DNA recovery was verified by running a sample of the PCI-clean product on a 1% agarose gel.

PCI-clean DNA was then transformed into a fission yeast parent strain. Cells were grown overnight at 30°C in YE5S to an OD of approximately 0.8. 20 mL of cells was spun at 4000 RPM for 5 minutes, washed with an equal volume of dH_2O, spun again, and washed with 1 mL of 0.1M LiOAc/TE (pH 7.5). Cells were spun again and resuspended in LiOAc/TE to a final volume of 100 μl. PCI-clean DNA (20-30 μg) was added to the cell suspension and left to incubate for 10 minutes at RT. 260 μl of 40% PEG in LiOAc was then added with gentle mixing, and cells were incubated at 32°C for 45 minutes. 43 μL of DMSO was then added, and cells were heat-shocked at 42°C for 5 minutes. Cells were then washed with 1 mL of dH_2O, plated onto 2X YE5S plates, and placed at 32°C. The following day, cells were replica-plated to YE5S containing G418, hygromycin, or nourseothricin, as required for selection. After 2 more days at 32°C, cells were again replica-plated to selective media (YE5S with the appropriate antibiotic). On the following day, single colonies were then streaked onto YE5S, grown ON, and replica-plated to selective media to check for stably integrated transformants. Stable integrants were identified as isolates where every colony that formed on YE5S also grew on selective media. A combination of colony PCR, Western blotting, and fluorescence microscopy was used to confirm successful generation of the desired strain. Strains constructed using the PCR-based method are shown in table 2.1.

Table 2.1: Oligonucleotides, plasmids and parent strains used to generate truncated and/or tagged mutants using the PCR-based method.

Strain	Primers (Forward/reverse)	Plasmid	Parent strain
KS5207	OKS459 / OKS462	pKS112	KS516
KS5209	OKS1927 / OKS462	pKS112	KS516
KS5211	OKS1928 / OKS462	pKS112	KS516
KS5213	OKS1929 / OKS462	pKS112	KS516
KS5215	OKS1930 / OKS462	pKS112	KS516
KS5217	OKS1931 / OKS462	pKS112	KS516
KS5381	OKS444 / OKS449	pKS706	KS820
KS5385	OKS444 / OKS449	pKS706	KS5209
KS5517	OKS444 / OKS1981	pKS706	KS5209
KS5520	OKS444 / OKS1983	pKS706	KS5209
KS5607	OKS2034 / OKS462	pKS108	KS515
KS5647	OKS444 / OKS345	pKS706	KS5209
KS5749	OKS1927 / OKS462	pKS112	KS2007
KS5817	OKS2077 / OKS2088	pKS131	KS516
KS5826	OKS460 / OKS2055	pKS112	KS516
KS5922	OKS1927 / OKS2055	pKS112	KS5851
KS5924	OKS1927 / OKS2055	pKS112	KS5853
KS5926	OKS1927 / OKS2055	pKS112	KS5855
KS5940	OKS2106 / OKS2055	pKS112	KS5851
KS6626	OKS2034 / OKS462	pKS108	KS5851
KS6682	OKS2286 / OKS2287	pKS112	KS516
KS6684	OKS2284 / OKS2285	pKS112	KS516

2.5 Colony PCR

Colony PCR was used to verify integration of transformed DNA at the correct locus. Amplification was performed using a primer with homology to the integrated antibiotic marker coupled with a primer homologous to sequence upstream of the target gene (for N-terminal tagging/truncation) or downstream of the gene (for C-terminal tagging/truncation). The generation of a PCR product of the correct predicted size was taken as confirmation that integration had occurred. To produce template DNA, cells to be analyzed were grown overnight on YE5S plates. A small patch (1-2 mm) of cells was resuspended in 50 μl of 0.25% SDS in TE, vortexed, and boiled for 5 minutes. Boiled samples were spun for 1 min at 13000 RPM, and the supernatant containing template DNA was then recovered. PCR reaction mixtures and cycling conditions were as follows:

Colony PCR reaction mixtures

Component	Concentration
*Buffer IV	1X
Forward primer	0.5 μM
Reverser primer	0.5 μM
Template DNA	2 μl / 25 μl reaction
dNTPs (dATP, dTTP, dGTP, dCTP)	200 μM each
$MgCl_2$	1.5 mM
HMT polymerase	0.2 U/μl
Pwo polymerase	0.003 U/μl
Triton X-100	1%

Temperature cycle:

1. 95°C 2 min
2. 95°C 15 sec
3. 50°C 30 sec
4. 72°C 3 min
5. Repeat steps 2-4 for 35 cycles
6. 72°C 5 min
7. 20 °C hold

2.6 Fission yeast boiled extracts

Boiled extracts were used for Western blot analysis of fission yeast proteins, primarily to check expression levels of Mto1 truncation mutants. To produce boiled extracts, cells were grown overnight to an OD of ~0.8. Cells were typically grown in YE5S, but EMM supplemented with adenine, leucine, and uracil was used when expression from the *nmt81* promoter was required. 25 mL of cells was spun at 4000 RPM for 3 minutes, and the cell pellet was then resuspended in 1 mL of TBS (Tris-buffered saline; 50 mM Tris base, 150 mM NaCl, pH 7.6). Samples were then spun for 1 minute at 13000 RPM in a microfuge. The supernatant was poured off, and the pellet was resuspended in the small remaining volume by vortexing. The pellet was then boiled for 5 minutes to inactivate any proteases. 0.5 mm zirconium beads were added and the samples were beat in a Ribolyser (2 cycles of 30 seconds at maximum speed). The bottoms of the tubes were pierced and placed into a second tube, and lysates were recovered by briefly centrifuging at 1000 RPM. 200 μL of TBS and 200 μL of 2X Laemmli sample buffer (4% SDS, 20% glycerol, 120 mM Tris-HCl, pH 6.8) were added to the flow-through. Samples were then boiled for 5 minutes, spun at 13000 RPM for 15 minutes, and the supernatant (boiled extract) was recovered.

Protein concentration in boiled extracts was determined by Bicinchoninic acid (BCA) assay. Reaction mixture was prepared by combining BCA reagent A (containing Bicinchoninic acid) and BCA reagent B (containing 4% copper (II) sulphate) at a 50:1 ration. 5 μl of boiled extract was added to 1 mL of BCA reagent mixture, incubated at 65°C for 15 minutes, and then immediately placed on ice. OD (562 nm) was then determined using a

spectrophotometer. Protein concentration was calculated based on previous calibration (not shown), which revealed that 1 μg/mL of protein yields an OD (562 nm) of 0.04. Boiled extracts were stored at -80^{o}C. Prior to running on SDS-PAGE, bromophenol blue (~0.01%) and DTT (0.1M) or β-mercaptoethanol (2.5%) were added to samples.

2.7 SDS-PAGE, coomassie staining and Western blotting

All sodium dodecyl sulfate polyacrylamide gel electrophoresis (SDS-PAGE) was performed with 5% acrylamide stacking gels and 10% acrylamide resolving gels in Laemmli running buffer (25 mM Tris-base, 192 mM glycine, 0.1% SDS, pH 8.3). Gels were cast using the Mini-Protean (BioRad) or "low-wide" 10 x 20 cm (Helena Biosciences) system. Protein samples were prepared in Laemmli sample buffer (2% SDS, 10% glycerol, 60 mM Tris-HCl pH 6.8, 0.01% bromophenol blue, 0.1M DTT or 2.5% β-mercaptoethanol), boiled, allowed to cool, and spun briefly in a microfuge before loading onto gels. Mini gels and low-wide gels were run at 30 mA and 70 mA per gel, respectively.

For coomassie staining, gels were transferred to staining solution (25% isopropanol, 10% acetic acid, 0.05% Brilliant Blue R-250) immediately after electrophoresis. Gels in staining solution were heated briefly (~30 sec) in a microwave on high setting and placed on a shaker for 10-15 minutes. Staining solution was replaced with destaining solution (10% acetic acid) and the gel was again heated in the microwave. Gels were left in destaining solution until sufficiently clear, and destaining solution was replaced if necessary.

For anti-Mto1 and anti-Mto2 Western blotting, proteins were transferred to nitrocellulose membrane (BioRad) in 10 mM CAPS and 10% methanol using a wet blotting apparatus. Mini gels were transferred for 80 minutes at 80V, and low-wide gels were transferred for 150 minutes at 40V. Efficient transfer of proteins was confirmed by briefly staining with Ponceau S (0.2% Ponceau S, 3% trichloroacetic acid, 3% sulfosalicylic acid), followed by gentle destaining in 5% acetic acid. Ponceau stain was removed by washing in water followed by TBS. Membranes were then placed in blocking solution (2% non-fat dried milk, 0.2% Tween 20 in TBS) for 30 minutes. Incubation with primary antibodies was performed overnight in blocking solution. Anti-Mto1 (S897, polyclonal raised in sheep) and anti-Mto2 (S975, polyclonal raised in sheep) primary antibodies were used at 1:1000

dilutions of serum. Membranes were then washed (0.02% Tween 20 in TBS) and incubated with secondary monoclonal mouse anti-sheep IgG for 1 hour (Sigma-Aldrich; 1:10000 in blocking solution). Finally, membranes were washed again and incubated in tertiary anti-mouse IRDye800 fluorescent antibodies for 1 hour (Licor Bioscience; 1:5000 in blocking solution). For more highly expressed recombinant proteins from Sf9 cells, only primary anti-Mto1 or anti-Mto2 antibodies with secondary anti-goat IRDye800 fluorescent antibodies (Licor Bioscience; 1:5000 in blocking solution) were used. An Odyssey scanner and associated software (Licor Odyssey v3.0) was used to visualize and quantify bands. For quantification, a rectangular region was drawn around the band of interest, and the integrated fluorescence intensity within that region was determined. Background was subtracted as the integrated intensity of a band of equal size, taken from a representative region of the blot lacking bands.

2.8 Endogenously expressed *mto1* N-terminal truncations

A two-step gene replacement technique was used to generate Mto1 N-terminal truncations expressed from the endogenous *mto1* promoter. In the first step, *mto1* nucleotides 1-390 (amino acids 1-130) in KS516 were replaced with the *ura4+* sequence, using the techniques described in section 2.4. Selection was performed on EMM supplemented with adenine and leucine, but lacking uracil. Stable *mto1Δ(1-130)::ura4+* integrants were identified by colony PCR. In the second step, megaprimer PCR was used to produce 567 base pair fragments of *mto1,* where the *mto1* start codon was immediately adjacent to *mto1* nucleotide 391, 607, or 724 (corresponding to amino acids 131, 203, and 242). Transformation of megaprimer products into *mto1Δ(1-130)::ura4+* was thus used to produce *mto1(131-1115)*, *mto1(203-1115)*, and *mto1(242-1115)* strains. Transformants were counter-selected by plating onto 5-fluoroorotic acid (5-FOA) plates (EMM + Na glutamate, leucine, adenine, ¼ uracil, 0.1% FOA). 5-FOA is converted to the toxic product 5-fluorouracil by the *ura4* gene product orotidine 5'-phosphate decarboxylase, leading to killing of the *ura4+* parent strain. Successful construction of *mto1(131-1115)*, *mto1(203-1115)*, and *mto1(242-1115)* was confirmed by DNA sequencing. The standard Bähler cassette method

was subsequently used to produce endogenously-expressed *mto1(131-549)*, *mto1(131-549)-GFP*, *mto1(203-549)-GFP*, and *mto1(242-549)-GFP.*

Megaprimer PCR was itself a 2-step process. In the first step, pairs of PCR reactions were used to amplify regions of *mto1* sequence. One reaction amplified approximately 280 base pairs of *mto1* 5' upstream sequence, followed by about 15 base pairs of *mto1* coding sequence starting at the desired N-terminal truncation site. The second reaction amplified about 15 base pairs of *mto1* 5' upstream sequence, followed by about 280 base pairs of *mto1* coding sequence starting at the desired N-terminal truncation site. Therefore, the products of these two reactions contained an approximately 30 base pair overlap. These products were then gel purified, in order to remove primers. In the second step, the gel-purified products were amplified by overlap extension PCR (ie. the first step products acted as "megaprimers"). Products from the second step were cleaned-up by PCI extraction prior to transformation into *mto1Δ(1-130)::ura4+* (KS5817).

Table 2.2: Oligonucleotides used for construction of endogenously expressed Mto1 N-terminal truncation mutants. Mutants were produced by 2-step megaprimer PCR. pKS272 was the template in all step 1 reactions. Step 2 PCR products were transformed into the KS5817 *ura4+* parent strain.

Strain	Step 1		Step 2	
	Reaction	Oligonucleotides (fwd/rev)	Template	Oligonucleotides (fwd/rev)
KS5851	1	OKS2079 / OKS2080	Products of 1 and 2	OKS2079 / OKS2090
	2	OKS2081 / OKS2090		
KS5853	3	OKS2079 / OKS2083	Products of 3 and 4	OKS2079 / OKS2089
	4	OKS2084 / OKS2089		
KS5855	5	OKS2079 / OKS2085	Products of 5 and 6	OKS2079 / OKS2082
	6	OKS2086 / OKS2082		

2.9 DNA sequencing

For sequencing of fission yeast mutants, colony PCR followed by gel purification was first performed to generate template DNA containing the region of interest. Plasmid DNA was sequenced directly. Sequencing reactions were prepared as follows: 2 μl BigDye 3.1 terminator mix (Applied Biosystems), 2.5 μl 5X sequencing buffer (Applied Biosystems), 2 μl oligonucleotide primer (at 3 μM in TE buffer), and 6 μl template DNA (PCR product or plasmid). Reactions were amplified according to:

Temperature cycle:

1. 96°C 30 sec
2. 50°C 15 sec
3. 60°C 4 min
4. Repeat steps 1-3 for 25 cycles
5. 4°C hold

Reactions were then sequenced by the University of Edinburgh GenePool sequencing service, using ABI 3730 capillary sequencing instruments. Sequencing data was analyzed using LaserGene SeqMan software (DNASTAR).

2.10 Microscopy

Wide-field microscopy was performed using a Nikon TE300 inverted microscope with a Nikon 100x/1.40 NA Plan Apo or Nikon 20X/0.75 NA Plan Apo objective, attached to a Photometrics Coolsnap HQ CCD camera. Confocal microscopy was performed using a Nikon TE2000 inverted microscope with a Nikon 100x/1.45 NA Plan Apo objective, attached to a Yokogawa CSU-10 spinning disc confocal unit (Visitech) and an Andor iXon+ Du888 EMCCD camera. An Optosplit III image splitter (Cairn Research) with a T560LPXR dichroic filter (Chroma Technology) was used for simultaneous imaging of GFP- and RFP-tagged proteins. The Optosplit III was used in co-imaging GFP-tagged Mto1/2 and γ-TuC proteins with mCherry-α-tubulin, and also for imaging the colocalization of Mto1-GFP and Alp4-tDT. Where they are compared directly, all still and time-lapse images were acquired under identical conditions. Image processing was performed using Metamorph imaging software (Molecular Devices). Images were adjusted using linear contrast enhancement and are presented as maximum projections through the full cell volume, unless otherwise indicated. For live-cell microscopy, cells were grown 2-3 days overnight in EMM at 25°C. Cultures were diluted daily to maintain exponential growth. Before imaging, cells were pipetted onto pads (~50 μm thick) composed of EMM with 2% agarose. A coverslip was placed on top of the cells, and the coverslip edges were sealed with VALAP (33% Vaseline, 33% lanolin, 33%

paraffin). Imaging was performed at room temperature. The conditions used for fluorescence microscopy are shown in table 2.3.

Table 2.3 Conditions used for fluorescence microscopy.

Image type	Figures	Laser power (%), exposure time (ms)		Z series	Timelapse
		488 nm	561 nm		
Mto1-GFP	3.3A, 4.3, 5.1	70, 500	-	9 x 0.6μm	-
Mto1-GFP, mCh-α-tubulin	3.3B	70, 500	40, 500	9 x 0.6μm	-
GFP-α-tubulin, Alp4-tdT	3.4, 3.5, 4.7	20, 100	20, 2000	8 x 0.6μm	-
Mto1-GFP (endogenous and over-expressed), mCh-α-tubulin	3.6, 4.6	70, 500	40, 500	9 x 0.6μm	-
Mto1-GFP, Alp4-tdT *	3.7, 4.8	50, 2000	40, 2000	8 x 0.6μm	-
GFP-α-tubulin	3.9, 4.9, 4.10A, 5.2A, 5.2C, 5.5A	20, 100	-	9 x 0.5μm	100 x 5s
Over-expressed Mto1-GFP	4.2	80, 500	-	9 x 0.6μm	-
Mto1-GFP in MBC	4.4	70, 800	-	8 x 0.6μm	-
Nucleating puncta (GFP tag), mCh-α-tubulin *	4.12, 4.13A	70, 200	70, 200	8 x 0.6μm	80 x 1.63s
Rlc1-GFP nodes *	4.13B	70, 200	70, 200	12 x 0.6μm	-
Plo1-GFP *	4.13B	70, 200	70, 200	12 x 0.6μm	-
Mto2-GFP, mCh-α-tubulin *	5.3	70, 200	70, 200	8 x 0.6μm	40 x 1.63s

* Imaged with Optosplit III image splitter (simultaneous illumination by 488 nm and 561 nm lasers).

Fluorescence quantification of nucleating puncta:

Fluorescence quantification was used to determine the copy numbers of Mto1-bonsai-GFP, Mto2-GFP, Alp4-GFP, and Alp6-GFP in puncta associated with microtubule nucleation. The intensities of nucleating puncta were measured, and converted into copy numbers by comparison to a standard imaged under the same conditions. The average intensity of Rlc1-GFP nodes, which contain on average 41.3 ± 23 molecules of Rlc1 (Laporte et al., 2011), was determined and used as the calibration standard. Plo1-GFP at recently separated SPBs was imaged and quantified during each imaging session, in order to verify that consistent values of intensty/GFP molecule were observed. Each protein was tagged with the same version of GFP [GFP(S65T)], to allow for direct comparison of fluorescence

intensity. Identical illumination conditions were used to image nucleating puncta, Rlc1-GFP, and Plo1-GFP, although nucleating puncta were imaged by time-lapse with fewer Z-sections (Table 2.3). When imaging nucleating puncta, only a single movie was made per slide, in order to minimize photobleaching. Movies with significant photobleaching were discarded, and little or no bleaching was observed in the movies used for quantification (Figure 2.1)

Fluorescence intensity was measured using Metamorph imaging software. Nucleating puncta were quantified at the onset of microtubule nucleation. 2 Z-sections containing the punctum of interest were summed, and the total intensity in a 5x5 pixel circular region around the punctum was determined. The intensities of 3 adjacent regions of the same size were averaged to provide a background value, which was then subtracted to produce the final intensity measurement. The intensities of Rlc1-GFP nodes were determined in the same manner, except 4 adjacent regions were averaged to produce a background value. Plo1-GFP intensity at SPBs was quantified in sum projections of 8 Z-sections using a 10x10 pixel circular region. For Plo1-GFP, the intensity of a single adjacent region of equal size was subtracted as background.

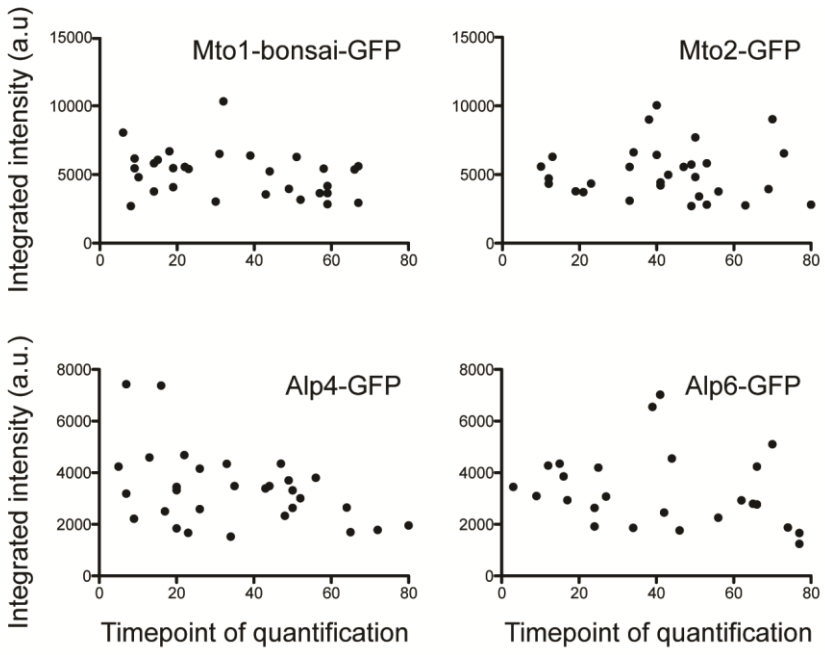

Figure 2.1: No significant photobleaching was observed in the movies used for fluorescence quantification of Mto1/2-bonsai and γ-TuC nucleating puncta. The intensities of Mto1-bonsai-GFP, Mto2-GFP, Alp4-GFP, and Alp6-GFP nucleating puncta were measured at various timepoints taken from time-lapse acquisitions. No significant reduction in intensity was observed for puncta quantified at later timepoints.

2.11 Morphology assays

To analyze cell morphology, cells were grown to stationary phase to cause partial depolarization, and then allowed to regrow in fresh YE5S to reveal any polarity phenotypes. Cells were patched uniformly onto YE5S plates, and allowed to grow for 2-3 days. Cells were then replica-plated to fresh YE5S and allowed to grow for 3 hours, after which they were washed from plates using PBS (Phosphate Buffered Saline; 1.5 mM KH_2PO_4, 5.1 mM Na_2HPO_4, 150 mM NaCl, pH 7.4) and fixed in 3.7% formalin for 30 minutes. Fixed cells were washed in PBS to remove excess formalin and imaged by wide-field DIC microscopy with a 20X objective.

2.12 Cold-shock and MT regrowth

Cells for cold-shock and MT regrowth experiments were grown in EMM at 30^{o}C to an OD of 0.8. MTs were depolymerized by chilling cells in flasks in an ice-water slurry for 30 minutes. MT regrowth was allowed to occur by returning flasks to a water bath at 25^{o}C. Cells were harvested by suction filtration and fixed in -80^{o}C methanol at various timepoints (Pre cold-shock and 0, 1, 3, and 10 minutes following return to 25^{o}C). Methanol-fixed cells were then processed for anti-tubulin immunofluorescence. Cells were pelleted and washed 2X in PEM buffer (100 mM NaPIPES pH 6.8, 1 mM $MgCl_2$, 1 mM EGTA), resuspended in PEMS (PEM + 1M sorbitol) containing 1 mg/mL zymolysase, and digested for 30 minutes at 37^{o}C. Following digestion, cells were washed 2X in PEMS and incubated in PEMS + 1% Triton X-100 for 30 seconds. Cells were again washed 2X in PEM before being resuspended in PEMBAL blocking solution (PEM + BSA, NaN_3, lysine monohydrochloride) for 3 hours. For anti-tubulin immunofluorescence, cells were then pelleted and resuspended in PEMBAL containing TAT1 anti-tubulin antibody (mouse monoclonal, used at 1:40 dilution) and incubated overnight. Following 3X 2 hour washes in PEMBAL, cells were incubated overnight in secondary antibodies. Alexa 568 labelled goat-anti-mouse IgG (Molecular Probes Europe BV) was used as the secondary antibody (1:100 dilution in PEMBAL). Finally, cells were washed 3X 2 hours in PEMBAL. For imaging by wide-field fluorescence microscopy, cells were spun onto coverslips pre-coated with poly-L-lysine (10 mg/mL).

2.13 Measurement of nuclear positioning

For staining of nuclei, cells were grown 3X overnight in EMM at 25°C. 0.5 mL of cells from an exponential culture was spun briefly in a microfuge at 5000 RPM, washed in dH_2O, and resuspended to a final volume of 10 μl in dH_2O. Cells were fixed by heat denaturation by pipetting them onto a coverslip on a 65°C heating block and allowing water to evaporate. 2.5 μl of mounting media containing Hoecsht DAPI stain was added to fixed cells. Bright-field images of whole cells and fluorescent images of stained nuclei were then obtained using a wide-field microscope. The distance from the centre of the nucleus to the nearest cell tip (S) and the furthest cell tip (L) was measured using ImageJ image analysis software. Nuclear eccentricity was reported as the ratio S/L (ie. where a perfectly centred nucleus would have an S/L = 1).

2.14 Imaging of Mto1 in the presence of MBC

Cells imaged in the presence of methyl benzimidazol-2-yl-carbamate (*carbendazim*, MBC) were initially grown under standard conditions (EMM, 25°C). A 5 mg/mL stock solution of MBC in DMSO was prepared, and MBC stock solution was added to aliquots of cells at a 1:100 dilution (giving 50 μg/ml MBC final). MBC was also added to EMM/agar pads used for imaging, at the same concentration. Cells were left to incubate in MBC for 10-15 minutes prior to imaging on a confocal microscope, and were imaged no later than 45 minutes after addition of MBC. As a control, the same strains were treated with DMSO alone and imaged under identical conditions.

2.15 Growth of *E. coli* strains

All *Escherichia coli* (*E. coli*) strains were grown at 37°C in liquid LB media (10 g/L Difco Bacto tryptone, 5 g/L Difco Bacto yeast extract, 5 g/L NaCl, pH 7.2) or on solid LB-agar plates (LB + 2% Difco Bacto agar). TOP10 (Invitrogen) or DH5α *E. coli* strains were used throughout for cloning and amplification of plasmids. Antibiotics were added to media as

required at the following concentrations: ampicillin (100 μg/mL), tetracycline (10 μg/mL), gentamicin (7 μg/mL), and kanamycin (50 μg/mL).

2.16 Production of chemically competent *E. coli*

Chemically competent *E. coli* cells were generated using the Rubidium Chloride method. A single *E. coli* colony was used to inoculate 5 mL of LB and grown overnight at 37°C. The culture was then diluted 1:200 into 100 mL of LB containing 20 mM $MgSO_4$ and allowed to grow at 37°C until an OD(600 nm) of approximately 0.5 was reached. Cells were then chilled on ice for 10 minutes, and pelleted by centrifugation for 5 minutes at 5000 RPM and 4°C. Media was decanted and cells were resuspended in 40 mL of cold TFB1 buffer (30 mM KAc, 100 mM $RbCl_2$, 10 mM $CaCl_2$, 50 mM $MnCl_2$, 15% glycerol, pH to 5.8 with HOAc, filter sterilized) and incubated on ice for 5 minutes. Cells were again pelleted at 4°C, then resuspended in 4 mL of TFB2 buffer (10 mM MOPS, 75 mM $CaCl_2$, 10 mM $RbCl_2$, 15% glycerol, pH 6.5 with KOH, filter sterilized) and incubated on ice for 15 minutes. 200 μL aliquots of competent cells were then transferred to -80°C for storage.

2.17 Transformation of *E. coli*

About 50-100 ng of DNA was typically used for transformation of ~50 μL of chemically competent *E. coli*. An aliquot of chemically competent cells was thawed on ice, DNA was added, and cells were left to incubate on ice for 30 minutes. Cells were then heat-shocked for 60 seconds at 42°C, returned to ice, and 450 mL of SOC media (20 g/L Difco Bacto tryptone, 5 g/L Difco Bacto yeast extract, 10 mM NaCl, 2.5 mM KCl, 10 mM $MgCl_2$, 10 mM $MgSO_4$, 20 mM glucose) was added. Cells were then allowed to recover in SOC at 37°C for 1 hour, before being plate to LB-agar (containing appropriate antibiotics for plasmid selection) and placed at 37°C for overnight to form colonies.

2.18 Isolation of plasmid DNA from *E. coli*

Plasmid DNA was extracted from *E. coli* using the Zyppy Plasmid Miniprep Kit (Zymo Research). *E. coli* cultures for plasmid miniprep were grown ON at 37°C in LB containing appropriate antibiotics. 100 μL of 7X Lysis Buffer was added to 600 μL of bacterial culture, and lysis was allowed to proceed for 1-2 minutes. 350 μL of cold Neutralization Buffer (containing 100 μg/mL RNase A) was then added with mixing. Cell debris was pelleted by centrifuging at 13000 RPM for 4 minutes, and the supernatant containing plasmid DNA was then transferred to a Zymo-Spin IIN column. The column was washed with 200 μL of Endo-Wash Buffer followed by 400 μL of Zyppy Wash Buffer. DNA was then eluted using 30-50 μL of Zyppy Elution Buffer. Where more plasmid DNA was required, minipreps were scaled-up appropriately.

2.19 Restriction digestion, gel extraction and ligation of DNA

DNA restriction digests were performed using enzymes from New England Biolabs (NEB). Digests were performed in compatible reaction buffers and at the appropriate temperatures and enzyme concentrations recommended by NEB. For cloning purposes, 1-5 μg of plasmid DNA was generally used in each digest. For analytical purposes (ie. to verify the presence of an insert), about 100 ng of plasmid DNA was used in each digest.

Products from restriction digests (and some PCR products) were purified by gel extraction using the QIAquick Gel Extraction Kit (Qiagen): Digests were subject to electrophoresis on 1% agarose gels containing ethidium bromide. Bands were visualized using a UV transilluminator and the desired band was excised from the gel using a clean razor blade. The agarose slice was weighed, and 300 μl of buffer QG was added for each 100 mg of gel. The gel slice was then dissolved by incubating at 50°C for 10-15 minutes, after which 1 gel volume of isopropanol was added. The sample was then added to a QIAquick silica column, and spun in a microfuge to bind DNA. Columns were then washed with buffer QG and buffer PE, before DNA was eluted into buffer EB (10 mM Tris, pH 8.5).

Ligation of both PCR products (blunt-end ligation) and restriction digest products (sticky-end ligation) into plasmids was performed using the Quick T4 Ligation Kit (NEB). 30 μl ligation reactions were generally performed, containing: 2 μl Quick T4 DNA ligase, 15 μl 2X Quick Ligase Buffer (132 mM Tris-HCl, 20 mM $MgCl_2$, 2 mM dithiothreitol, 2 mM ATP,

15% Polyethylene glycol, pH 7.6), 50-100 ng plasmid DNA, and 3-fold molar excess of insert DNA. Often, optimal vector:insert ratio was determined empirically. Ligation reactions were incubated at 25^{o}C for 1 hour, chilled briefly on ice, and then transformed into *E. coli*.

2.20 Insect cell culture

All baculovirus production and recombinant protein expression was carried out using Sf9 insect cells (a clonal isolate of the fall armyworm *Spodoptera frugiperda*). All Sf9 cell culture was performed at 27^{o}C and in Sf-900 II serum-free medium (Sf-900 II SFM; Gibco) supplemented with 50 units/mL penicillin and 50 μg/mL streptomycin (Gibco). Cells were maintained as adherent cultures in T-75 flasks and split 1:5 when ~90% confluent (every 5-6 days). Suspension cultures were initiated from T-75 flasks and grown in glass spinner flasks (Corning) on magnetic stir plates or in 2L plastic roller bottles (Corning) placed upright in a shaking incubator. A maximum of 500 mL of cell culture was grown in roller bottles, and spinner flasks were filled to no more than 50% of the indicated capacity. The side arm caps of spinner flasks and lids of roller bottles were closed loosely, to allow for aeration. Suspension cultures were maintained at cell densities between 0.6 x 10^{6}/mL and 3.0 x 10^{6}/mL. After being unthawed from frozen stocks, Sf9 cells were passaged for no longer than 6 months. For production of frozen cell stocks, a suspension culture was grown to a cell density of 1.5 x 10^{6}/mL. Cells were pelleted by spinning at 400 x g for 5 minutes, and resuspended in freezing medium (50% conditioned media, 50% fresh Sf-900 II SFM containing 7.5% DMSO) to a final density of 2.0 x 10^{6} cells/mL. 1.5 mL aliquots of cells were frozen slowly by placing them at -80^{o}C sealed in Styrofoam, and then left at -80^{o}C for storage.

2.21 Construction of bacmids for Mto1/2 expression in insect cells

Mto1 and Mto2 coding sequences were first cloned into the MultiBac acceptor plasmid pFL, and subsequently incorporated into the EMBacY bacmid via Tn7 transposition (Trowitzsch et al., 2010)(Figure 2.2). The plasmid pFL contains multiple cloning sites (MCS)

downstream of the p10 and polh (polyhedrin) promoters used for expression of recombinant proteins. Mto1 constructs were cloned into the p10 MCS using the NcoI and NsiI restriction sites, while Mto2 constructs were cloned into the polh MCS using the BamHI and SalI restriction sites. Mto2 inserts were designed with restriction sites for the BamHI-compatible enzyme BclI, as the Mto2 coding sequence contains BamHI sites. All Mto1 constructs included an N-terminal 6-histidine tag (6His) and TEV protease site (6His-TEV-Mto1, 6His-TEV-Mto1-NE, and 6His-TEV-Mto1-bonsai were constructed). Note that Mto1-NE and Mto1-bonsai are truncation mutants of Mto1 (described in chapters 3 and 4). For co-expression with Mto1, Mto2 was included with no tags. For individual purification of Mto2, Mto2 constructs also included an N-terminal 6His tag and TEV protease site.

MCS1 (p10 promoter)	MCS2 (polh promoter)
6His-TEV-Mto1	--
6His-TEV-Mto1-NE	--
6His-TEV-Mto1-bonsai	--
6His-TEV-Mto1	Mto2
6His-TEV-Mto1-NE	Mto2
6His-TEV-Mto1-bonsai	Mto2
--	6His-Mto2

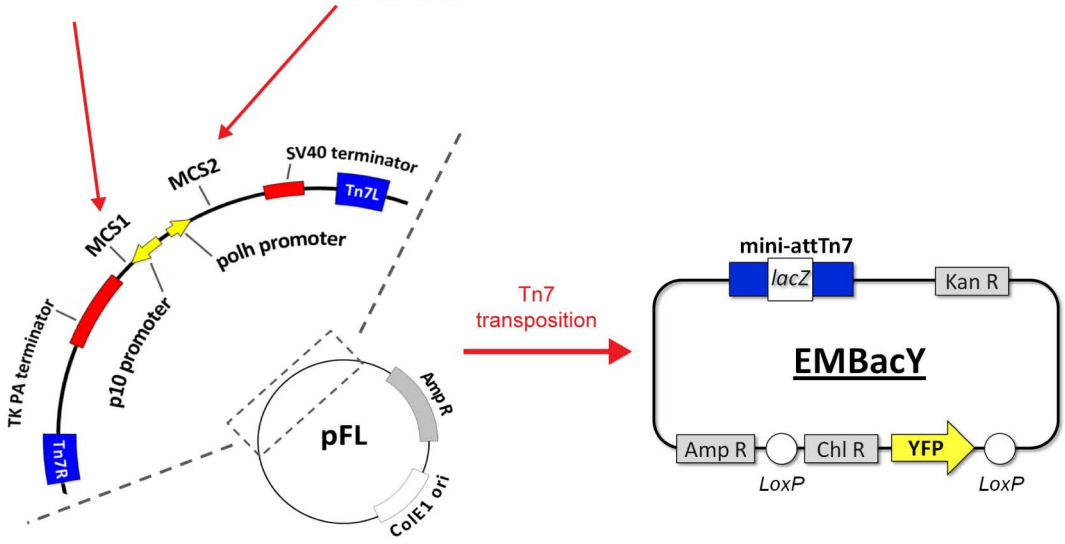

Figure 2.2: Construction of bacmids for recombinant Mto1/2 expression. Mto1 and Mto2 constructs were cloned into MCS1 and MCS2 of the plasmid pFL. This placed Mto1 and Mto2 expression under control of the baculovirus promoters p10 and polh, respectively. Various constructs were made, for the individual or co-expression of Mto1 and Mto2 (shown at top, dashes indicate no insert). The expression cassette from pFL was inserted into the EMBacY bacmid by Tn7 transposition in *E. coli*. Ultimately, the recombinant bacmids were transfected into insect cells to generate virus stocks and express recombinant Mto1, Mto2, and Mto1/2 complex.

PCR was used to amplify Mto1 and Mto2 sequences flanked with the appropriate restriction endonuclease sites, 6His tags, and TEV sites. The templates for PCR were pKS272 and pKS415, which contain the Mto1 and Mto2 coding sequences.

Table 2.4: Mto1 and Mto2 PCR products generated for cloning into pFL acceptor plasmid. Oligonucleotides and template DNA used to generate each product are shown.

Product	Oligonucleotides (forward/reverse)	Template
NcoI-6His-TEV-Mto1-NsiI	OKS2181 / OKS2183	pKS272
NcoI-6His-TEV-Mto1-NE-NsiI	OKS2181 / OKS2184	pKS272
NcoI-6His-TEV-Mto1-bonsai-NsiI	OKS2182 / OKS2184	pKS272
BclI-Mto2-SalI	OKS2185 / OKS2186	pKS415
BclI-6His-TEV-Mto2-SalI	OKS2320 / OKS2186	pKS415

PCR products were gel-purified, ligated into pJET1.2/blunt (Fermentas) by blunt-end cloning, and transformed into TOP10 cells for amplification. Plasmids were then isolated by miniprep and sequences of Mto1 and Mto2 constructs were verified by DNA sequencing. Standard restriction digest and ligation methods (section 2.19) were then used to isolate the Mto1 and Mto2 constructs from pJET1.2/blunt and clone them into pFL.

Recombinant bacmids were then generated via Tn7 transposition. The various pFL constructs containing Mto1 and Mto2 were transformed into DH10 EMBacY *E. coli* cells. DH10 EMBacY cells harbour the EMBacY bacmid (baculovirus genome) as well as a "helper" plasmid. This helper plasmid provides the Tn7 transposon complex required for transposition of the pFL expression cassette into EMBacY (Trowitzsch et al., 2010). Successful transposition disrupts the LacZ gene on EMBacY (Figure 2.2), such that positive clones can be selected for by blue/white screening. Following transformation with pFL constructs, DH10 EMBacY cells were therefore plated to LB containing kanamycin (50 μg/mL), tetracylcine (10 μg/mL), gentamicin (7 μg/mL), isopropyl β-D-1-thiogalactopyranoside (IPTG; 0.2 mM), and 5-bromo-3-indolyl-beta-galactoside (Bluo-Gal; 200 μg/mL). Kanamycin, gentamicin, and tetracycline resistance are conferred by EMBacY, pFL expression cassette, and Tn7 helper plasmid, respectively. White colonies were picked and streaked to plates (same composition as above) to verify a true white phenotype, indicating successful transposition.

Bacmid DNA was isolated from *E. coli* as follows: cells from white colonies were grown overnight at 37^{o}C in LB containing kanamycin (50 μg/mL), tetracylcine (10 μg/mL), and gentamicin (7 μg/mL). 1.5 mL of cell culture was used for each bacmid preparation.

Cells were spun for 1 minute in a microfuge (13000 RPM) and resuspended in 300 μL of buffer P1 (50 mM Tris-HCl pH 8.0, 10 mM EDTA, 100 μg/mL RNase A). 300 μL of lysis buffer P2 (200 mM NaOH, 1% SDS) was then added, and lysis was allowed to proceed for 5 minutes. 300 μL of neutralization buffer P3 (3.0M potassium acetate, pH 5.5) was added, and samples were placed on ice for 10 minutes. Samples were then spun for 15 minutes at 13000 RPM, after which supernatants were transferred to fresh tubes containing 800 μL of isopropanol and chilled on ice for 10 minutes. DNA was pelleted by spinning at 13000 RPM for 15 minutes, and then washed with 2X 0.5 mL 70% ethanol. DNA was again pelleted (13000 RPM, 5 minutes), air dried in a sterile hood, and gently resuspended in 40 μL TE.

2.22 Generation of virus stocks

Isolated bacmid DNA was transfected into Sf9 cells in order to produce an initial virus stock (V_0). Transfections were performed using Fugene HD transfection reagent (Roche). For each transfection, 20 μL of Fugene HD was added to 400 μL of Sf-900 II SFM and incubated for 5 minutes at room temperature. 40 μL of bacmid DNA was then added to the Fugene HD/SFM mix and incubated for 30 minutes at 27^{o}C. 100 μL of this mixture was then added to 1-2 x 10^6 cells in each of 4 wells in a 6 well plate. Approximately 48 hours later, media from each well was harvested and pooled as V_0. Fresh Sf-900 II SFM was then added to transfected cells, and protein expression was confirmed by Western blot following an additional 24-48 hours. V_0 was then used to scale up to higher volume, more infective V_1 virus stock. 3-5 mL of V_0 was added to a 50 mL suspension culture at 0.6 x 10^6 cells/mL. Cell counts were monitored and maintained below 1.0 10^6 /mL until proliferation arrest (typically 1-2 days). Cells were pelleted at 400 x g for 5 minutes and media harvested as V_1 48 hours after proliferation arrest. The same general process was then repeated to generate V_2 virus stocks from V_1 (500 mL suspension cultures were infected with 5 mL of V_1 stock). V_2 stocks were stored at 4^{o}C protected from light and used to infect Sf9 cells for protein expression and purification.

2.23 Characterization of V_2 virus stocks and expression of recombinant Mto1/2

V_2 virus stocks were characterized before protein expression was scaled up. The aim was to determine the volume of V_2 stock that resulted in essentially simultaneous infection of all cells in a culture and nearly immediate proliferation arrest, while generating optimal protein expression. Therefore, suspension cultures of Sf9 cells (at 0.8-1.0 x 10^6 cells/mL) were infected with various volumes of V_2. Cell counts were determined using a Countess Automated Cell Counter (Invitrogen), to check for proliferation arrest. For 4 days following infection, total and soluble protein expression was monitored by Western blot. On each day following infection, a 1.5 mL sample of cells was pelleted and resuspended in 300 μL of lysis buffer (1.5 mM KH_2PO_4, 5.1 mM Na_2HPO_4, 300 mM NaCl, 5% glycerol, 0.1% triton X-100, pH 8.0). Samples were then sonicated in a Bioruptor bath sonicator (Diagenode)(6 x 20 seconds on high setting). A sample of whole cell extract (WCE) was taken. Samples were then spun for 30 minutes at 13000 RPM and 4^{o}C, and a sample of the soluble lysate (SL) was taken. WCE and SL samples were added to 2X Laemmli sample buffer, and subjected to 10% SDS-PAGE followed by anti-Mto1 and anti-Mto2 Western blotting. For essentially all viruses tested, optimal soluble expression was observed after 3 days, using virus at 1:50-1:100 dilution in Sf9 suspension cultures at 0.8-1.0 x 10^6 cells/mL.

EMBacY also encodes yellow fluorescent protein (YFP) expressed form the polh promoter. YFP expression in cells was observed by fluorescence microscopy, as an indirect indicator of Mto1/2 expression. This allowed us to verify that all cells were infected and expressing protein, and also provided a qualitative measure of protein expression levels (ie. brighter cells corresponded to increased expression). Once V_2 stocks had been characterized by Western blot, YFP expression was monitored to confirm expression when generating Mto1/2 for purification.

2.24 Nickel purification of 6His-Mto1-bonsai, 6His-Mto2, and 6His-Mto1/2-bonsai complex

Sf9 suspension cultures were infected with an appropriate amount of V_2 (as described above) and harvested 3 days post-infection. For harvesting, cells were spun at 400 x g for 5 minutes, washed with PBS, and then spun again. Pellets (in 50 mL or 200 mL falcon tubes) were then flash-frozen in liquid nitrogen and stored at -80^{o}C. 6His-Mto1-bonsai, 6His-Mto2, and 6His-Mto1/2-bonsai complex were purified by essentially the same procedure. Pellets corresponding to 400 mL of Sf9 suspension culture were generally used for purification, to generate 1-3 mg of purified protein. Buffer A (1.5 mM KH_2PO_4, 5.1 mM Na_2HPO_4, 300 mM NaCl, 5% glycerol, pH 8.0) was used throughout all purification steps, with pH adjusted to 8.0 again after addition of imidazole. Cell pellets were thawed on ice and resuspended in lysis buffer (Buffer A + 0.1% triton X-100, 45 mM imidazole). Pellets were then incubated in lysis buffer on ice for 15 minutes, and dounced 20X in a glass Wheaton tissue grinder with a loose pestle. Nuclei and large cell debris were pelleted by centrifuging for 10 minutes at 400 x g and 4^{o}C in a tabletop Heraeus Megafuge 40R. Supernatants from this low-speed spin were then centrifuged for 5 minutes at 100000 RPM and 4^{o}C, using a TLA120.2 rotor in a Beckman Coulter tabletop ultracentrifuge. The resulting soluble lysate was added to nickel-charged His-bind Fractogel (Merck), which had been previously washed in buffer A containing 45 mM imidazole. Lysates were left to incubate with Fractogel beads for 20-30 minutes at 4^{o}C on a roller. Beads with bound protein were then added to a polypropylene column and washed extensively (~200 mL) with wash buffer (Buffer A + 90 mM imidazole). 6His-Mto1-bonsai and 6His-Mto1/2-bonsai complex were eluted with buffer A containing 300 or 600 mM imidazole. 6His-Mto2 required 600 mM imidazole to be eluted. Eluates were then concentrated to 0.5-1.0 mL by spinning for ~15 minutes (4000 x g and 4^{o}C) in a centrifugal filter unit with a 30 kDa molecular weight cutoff (Millipore).

2.25 Gel filtration chromatography and SEC-MALS

As a second purification step, Ni-purified 6His-Mto1-bonsai, 6His-Mto2, and 6His-Mto1/2-bonsai complex were fractionated by gel filtration on a Superose 6 10/300 GL column (GE Healthcare). Chromatography was performed using an ÅKTA fast protein liquid chromatography (FPLC) unit. Prior to running samples, the FPLC and Superose 6 column were washed with dH_2O and equilibrated with two column volumes (48 mL) of buffer A. 500 μL samples, typically containing 1-2 mg of protein, were injected onto the column. Samples were run at 0.5 mL/min and 1.2 MPa, with 36.0 mL of buffer A being passed over the column. 250 μL or 500 μL fractions were collected using an automated fraction collector. Samples of fractions were prepared in Laemmli sample buffer and analyzed by 10% SDS-PAGE followed by Coomassie staining or Western blotting. Size-exclusion chromatography with multi-angle light scattering (SEC-MALS) was performed using an ÅKTA FPLC and superose 6 10/300 GL column coupled with an on-line UV detector, 18-angle light scattering detector (Wyatt Dawn Heleos II), and refractive index detector (Wyatt Optilab rEX). Samples were run under the same conditions as described above for standard gel filtration chromatography. The 3 peak Mto1/2-bonsai fractions (750 μL total) from a Superose 6 run were pooled, concentrated to 250 μL, and analyzed by SEC-MALS.

Table 2.5: List of strains used in this study.

Strain number	Genotype	Source
KS515	*h+ ade6-M210 ura4-D18 leu1-32*	Sawin Lab
KS516	*h- ade6-M216 ura4-D18 leu1-32*	Sawin Lab
KS819	*h+ mto1-GFP::kanMX ura4-D18 leu1-32 ade6-M216*	Sawin Lab
KS1017	*h+ mto1Δ::kanMX6 ade6-M216 leu1-32 ura4-D18*	Sawin Lab
KS1407	*h– mto1-GFP:kanMX mto2Δ::kanMX6 ura4-D18 leu1-32 ade6-M216 mto2*	Sawin Lab
KS1999	*h- mto1(1-800)-GFP:kanMX6 ade6-210 leu1-32 ura4-D18*	Sawin Lab
KS2738	*h– mto1-GFP:kanMX6 kanMX6:nmt81:GFP-atb2 ade6-216 leu1-32 ura4-D18*	Sawin Lab
KS2802	*h+ hphMX6:nmt81:GFP-atb2 ade6-210 leu1-32 ura4-D18*	Sawin Lab
KS3887	*h+ kanMX6:nmt81:mto1-GFP:hphMX ura4-D18 leu1-32 ade6-M216*	Sawin Lab
KS5186	*h– mto1Δ::natMX6 hphMX6:nmt81:GFP-atb2 ade6-216 leu1-32 ura4-D18*	Sawin Lab
KS5207	*h- mto1(1-500)-GFP:kanMX6 ade6-210 leu1-32 ura4-D18*	This study
KS5209	*h- mto1(1-549)-GFP:kanMX6 ade6-210 leu1-32 ura4-D18*	This study
KS5211	*h- mto1(1-575)-GFP:kanMX6 ade6-210 leu1-32 ura4-D18*	This study
KS5213	*h- mto1(1-637)-GFP:kanMX6 ade6-210 leu1-32 ura4-D18*	This study
KS5215	*h- mto1(1-683)-GFP:kanMX6 ade6-210 leu1-32 ura4-D18*	This study
KS5217	*h- mto1(1-732)-GFP:kanMX6 ade6-210 leu1-32 ura4-D18*	This study
KS5349	*h+ mto1(1-549)-GFP:kanMX6 mto2Δ::kanMX6 ade6-M216 leu1-32 ura4-D18*	This study
KS5356	*h+ hphMX6:nmt81:GFP-atb2 alp4-tdT:natMX6 ade6-210 leu1-32 ura4-D18*	This study
KS5357	*h- mto1(1-549)-GFP:kanMX6 hphMX6:nmt81:GFP-atb2 alp4-tdT:natMX6 ade6-210 leu1-32 ura4-D18*	This study
KS5381	*h- natMX6:nmt81:mto1(131-1115)-GFP:kanMX ura4-D18 leu1-32*	This study
KS5385	*h- natMX6:nmt81:mto1(131-549)-GFP:kanMX ade6-210 ura4-D18 leu1-32*	This study
KS5491	*h- mto1(1-549)-GFP:kanMX6 hphMX6:nmt81:GFP-atb2 ade6-210 leu1-32 ura4-D18*	This study
KS5517	*h- natMX6:nmt81:mto1(203-549)-GFP:kanMX6 ade6-210 leu1-32 ura4-D18*	This study
KS5520	*h- natMX6:nmt81:mto1(242-549)-GFP:kanMX6 ade6-210 leu1-32 ura4-D18*	This study
KS5607	*h+ mto1(1-549)::kanMX6 ade6-M216 ura4-D18 leu1-32*	This study
KS5641	*h+ mto1(1-549):kanMX6 hphMX6:nmt81:GFP-atb2 alp4-tdT:natMX6 ade6-M216 ura4-D18 leu1-32*	This study
KS5645	*h- mto1(1-549)-GFP::kanMX6 alp16Δ::natMX6 hphMX6:nmt81:GFP-atb2 ade6-210 leu1-32 ura4-D18*	This study
KS5647	*h- natMX6:nmt81:mto1(1-549)-GFP:kanMX6 ade6-210 leu1-32 ura4-D18*	This study
KS5674	*h- mto1-GFP::kanMX alp4-tdT:natMX6 ura4-D18 leu1-32 ade6-M216*	This study
KS5678	*h+ mto1(1-549)-GFP:kanMX6 alp4-tdT:natMX6 ade6-210 leu1-32 ura4-D18*	This study
KS5749	*h+ mto1(1-9A1-549)-GFP ade6-216 leu1-32 ura4-D18*	This study
KS5817	*h- mto1Δ(aa1-130)::ura4+ ade6-M216 ura4-D18 leu1-32*	This study

KS5826	*h- mto1(1-800)-GFP:kanMX6 ade6-M210 ura4-D18 leu1-32*	This study
KS5851	*h- mto1(131-1115) ade6-M210 ura4-D18 leu1-32*	This study
KS5853	*h- mto1(203-1115) ade6-M210 ura4-D18 leu1-32*	This study
KS5855	*h- mto1(242-1115) ade6-M210 ura4-D18 leu1-32*	This study
KS5922	*h- mto1(131-549)-GFP:kanMX6 ade6-M210 ura4-D18 leu1-32*	This study
KS5924	*h- mto1(203-549)-GFP:kanMX6 ade6-M210 ura4-D18 leu1-32*	This study
KS5926	*h- mto1(242-549)-GFP:kanMX6 ade6-M210 ura4-D18 leu1-32*	This study
KS5929	*h+ mto1(131-549)-GFP:kanMX6 hphMX6:nmt81:GFP-atb2 ade6-M210 ura4-D18 leu1-32*	This study
KS5930	*h- mto1(203-549)-GFP:kanMX6 hphMX6:nmt81:GFP-atb2 ade6-M210 ura4-D18 leu1-32*	This study
KS5931	*h+ mto1(242-549)-GFP:kanMX6 hphMX6:nmt81:GFP-atb2 ade6-M210 ura4-D18 leu1-32*	This study
KS5933	*h+ mto1(131-549)-GFP:kanMX6 alp4-tdT:natMX6 ade6-M210 ura4-D18 leu1-32*	This study
KS5936	*h+ mto1(1-500)-GFP:kanMX6 hphMX6:nmt81:GFP-atb2 alp4-tdT:natMX6 ade6-M210 ura4-D18 leu1-32*	This study
KS5937	*h+ mto1(131-549)-GFP:kanMX6 hphMX6:nmt81:GFP-atb2 alp4-tdT:natMX6 ade6-M210 ura4-D18 leu1-32*	This study
KS5940	*h- mto1(131-1115)-GFP:kanMX6 ade6-M210 ura4-D18 leu1-32*	This study
KS5942	*h+ mto1(131-1115) hphMX6:nmt81:GFP-atb2 alp4-tdT:natMX6 ade6-210 leu1-32 ura4-D18*	This study
KS5944	*h- mto1(131-1115) hphMX6:nmt81:GFP-atb2 ade6-210 leu1-32 ura4-D18*	This study
KS6080	*h+ mto1(131-9A1-549)-GFP:kanMX6 ade6-216 leu1-32 ura4-D18*	This study
KS6086	*h- mto1(1-549):kanMX6 hphMX6:nmt81:GFP-atb2 ade6-M216 ura4-D18 leu1-32*	This study
KS6098	*h- mto1(131-9A1-549)-GFP:kanMX6 mto2Δ::kanMX6 ade6-M216 leu1-32 ura4-D18*	This study
KS6102	*h+ mto1(131-1115)-GFP:kanMX6 hphMX6:nmt81:GFP-atb2 ade6-M210 ura4-D18 leu1-32*	This study
KS6103	*h- mto1(131-1115)-GFP:kanMX6 alp4-tdT:natMX6 ade6-M210 ura4-D18 leu1-32*	This study
KS6315	*h+ mto1(131-549)-GFP:kanMX6 alp16Δ::natMX6 hphMX6:nmt81:GFP-atb2 ade6-M210 leu1-32 ura4-D18*	This study
KS6456	*h- mto1(131-549)-GFP:kanMX6 mto2Δ::kanMX6 ade6-? leu1-32 ura4-D18*	This study
KS6457	*h+ mto1(131-549)-GFP:kanMX6 mto2Δ::kanMX6 hphMX6:nmt81:GFP-atb2 ade6-? leu1-32 ura4-D18*	This study
KS6458	*h+ mto2Δ::kanMX6 hphMX6:nmt81:GFP-atb2 ade6-? leu1-32 ura4-D18*	This study
KS6459	*h+ mto1-GFP:kanMX mto2Δ::kanMX6 hphMX6:nmt81:GFP-atb2 ade6-? leu1-32 ura4-D18*	This study
KS6461	*h+ mto1(1-549)-GFP:kanMX6 mto2Δ::kanMX6 hphMX6:nmt81:GFP-atb2 ade6-? leu1-32 ura4-D18*	This study
KS6626	*h- mto1(131-549):kanMX6 ade6-M210 ura4-D18 leu1-32*	This study
KS6635	*h? mto1(131-549):kanMX6 hphMX6:nmt81:GFP-atb2 alp4-tdT:natMX6 ade6-210 leu1-32 ura4-D18*	This study
KS6637	*h? mto1(131-549):kanMX6 hphMX6:nmt81:GFP-atb2 ade6-210 leu1-32 ura4-D18*	This study
KS6672	*h- kanMX6:nmt81:mto1-GFP:hphMX Z:ADH15:mCherry-Atb2:natMX6 ade6 leu1-32 ura4-D18*	This study
KS6673	*h+ mto1-GFP::kanMX Z:ADH15:mCherry-Atb2:natMX6 ade6*	This study

	leu1-32 ura4-D18	
KS6675	*h+ mto1(1-9A1-549)-GFP:kanMX6 Z:ADH15:mCherry-Atb2:natMX6 ade6 leu1-32 ura4-D18*	This study
KS6676	*h+ mto1(131-9A1-549)-GFP:kanMX6 Z:ADH15:mCherry-Atb2:natMX6 ade6 leu1-32 ura4-D18*	This study
KS6677	*h+ mto1(1-549)-GFP:kanMX6 Z:ADH15:mCherry-Atb2:natMX6 ade6-M210 leu1-32 ura4-D18*	This study
KS6678	*h+ mto1(131-549)-GFP:kanMX6 Z:ADH15:mCherry-Atb2:natMX6 ade6-M210 leu1-32 ura4-D18*	This study
KS6679	*h+ natMX6:nmt81:mto1(1-549)-GFP:kanMX6 Z:ADH15:mCherry-Atb2:natMX6 ade6 leu1-32 ura4-D18*	This study
KS6680	*h+ natMX6:nmt81:mto1(131-549)-GFP:kanMX Z:ADH15:mCherry-Atb2:natMX6 ade6 leu1-32 ura4-D18*	This study
KS6682	*h- rlc1-GFP:kanMX6 ade6-M210 ura4-D18 leu1-32*	This study
KS6684	*h- plo1-GFP:kanMX6 ade6-M210 ura4-D18 leu1-32*	This study
KS6715	*h- natMX6:Z:ADH15:mCherry-Atb2 ade6 leu1-32 ura4-D18*	Sawin Lab
KS6776	*h+ alp4-GFP:hphMX6 natMX6:Z:ADH15:mCherry-Atb2 mto1(131-549):kanMX6 ade6-210 leu1-32 ura4-D18*	This study
KS6791	*h- mto2-GFP:kanMX6 mto1(131-549):kanMX6 natMX6:Z:ADH15:mCherry-Atb2 ade6-210 leu1-32 ura4-D18*	This study
KS6816	*h- mto1-GFP:kanMX alp16Δ::natMX kanMX6:nmt81:GFP-atb2 ade6-M216 leu1-32 ura4-D18*	This study
KS6898	*h+ alp6-GFP:kanMX6 natMX6:Z:ADH15:mCherry-Atb2 mto1(131-549):kanMX6 ade6-210 leu1-32 ura4-D18*	This study
KS7055	*h+ mto2-GFP:kanMX6 natMX6:Z:ADH15:mCherry-Atb2 ade6-216 leu1-32 ura4-D18*	This study
KS7056	*h- mto2-GFP:kanMX mto1Δ::kanMX6 natMX6:Z:ADH15:mCherry-Atb2 ade6-216 leu1-32 ura4-D18*	This study

Table 2.6: List of plasmids used in this study.

Plasmid number	Vector	Insert	Source
pKS108	pFA6a-kanMX6	none	Sawin Lab (Bahler et al., 1998)
pKS112	pFA6a-GFP(S65T)-kanMX6	none	Sawin Lab (Bahler et al., 1998)
pKS131	pHN159	ura4+	H. Ohkura
pKS272	pBS	mto1+	Sawin Lab
pKS415	pGEX-4T-2	mto2+	Sawin Lab
pKS706	pFA6a-natMX6-P81nmt1	none	Sawin Lab (Bahler et al., 1998)
pKS1215	pJET1.2/blunt	6His-TEV-mto1	This study
pKS1216	pJET1.2/blunt	6His-TEV-mto1(1-549)	This study
pKS1217	pJET1.2/blunt	6His-TEV-mto1(131-549)	This study
pKS1218	pJET1.2/blunt	mto2+	This study
pKS1219	pFL	none	Trowitzsch et al., 2010
pKS1220	pFL	6His-TEV-mto1	This study
pKS1221	pFL	6His-TEV-mto1(1-549)	This study
pKS1222	pFL	6His-TEV-mto1(131-549)	This study
pKS1223	pFL	6His-TEV-mto1, mto2+	This study
pKS1224	pFL	6His-TEV-mto1(1-549), mto2+	This study
pKS1225	pFL	6His-TEV-mto1(131-549), mto2+	This study
pKS1226	pFL	mto2+	This study
n/a	pFL	6His-TEV-mto2	This study
n/a	pJET1.2/blunt	6His-TEV-mto2	This study
n/a	pJET1.2/blunt	none	Fermentas

Table 2.7: List of oligonucleotides used in this study.

Oligonucleotide	Sequence
OKS345	TCCGTCAGCGAAAGACCAGCTAAATTATCCACTAGAACATTAAA GTTATTACTATCTAACTCACTGGAATTTTCTTCCATCATGATTTAA CAAAGCGACTATA
OKS444	ACTACATATATGCCATAGCGTATCAATAGGCATATCTTCGATCCC ATACTTTCTTTTAACAATTAACAATTTAAGAAAGAGAATTCGAGCT CGTTTAAAC
OKS449	CTATCTTCTTCATACTGCTCTTGGCTCTGAAACCCTTGATTAGCC GTAAGTACGGGAGAAAGCTGTTCATCATCAGTAGTCATGATTTA ACAAAGCGACTATA
OKS459	TGAATGCGATTGTAGAGGCAGAATCAAGCAAGAATGAATTGTGG GATTCTATGATGGTATCTAGAATGAAAACCCAAGAGCGGATCCC CGGGTTAATTAA
OKS460	ATTCTTTGCAGAATGCTATTATGGAAACATTTGATAAACAGGTCA CCCACTGCTCGGTTAACCATTTGGTACAACAGATACGGATCCCC GGGTTAATTAA
OKS462	TATAAATCTTGGAATTAGCTTATTTTGTCAATTAAATTCTCCAACT AAGTAGATATGTACTGGTGATTAAGAAAAGCTATGAATTCGAGCT CGTTTAAAC
OKS1927	TGATGAGAATGGAGCAACAATGGCGGGAAGATGTTGACCAACT CCAGGAATATGTCGAAGAGATTACCCAAGAACTCCAGCGGATCC CCGGGTTAATTAA
OKS1928	AGGATACCAAAGAGGTGCTGTCAAAGTCTTCAAAAGAGTCTGAT GATTACGAAGAAGTAGTAGGTAAACTTAGGACTGAACGGATCCC CGGGTTAATTAA
OKS1929	TGTCAGAACGTTATAACGATAAATGCCATGAATTTGACGAATTAC AAAAGCGGCTGCAAACTTTGGAAGAAGAAAATAATCGGATCCCC GGGTTAATTAA
OKS1930	CAGAAGCAGAAGTTGATTCTTTAAGGAAGGAAAATGAAGAAAAC AAGCAAGTAATTGCTTTGAAAGAAAGCGAGCTGGTGCGGATCCC CGGGTTAATTAA
OKS1931	TAAAAACTGAAATGGAAAGCGTTACAACGAGTAAAGAATCGTTA GCCGATTATCTTAGCAACTTGAAGGAAAGGCACAATCGGATCCC CGGGTTAATTAA
OKS1981	TAGGTCTTTCATAGCAGACGCCGGTATCAATATATCGGAGATCT TTTTGCTTAAAGCATTGGTAGTGGGGGCATCTTGAGACATGATTT AACAAAGCGACTATA
OKS1983	CAACCCAAACACTTCCTTTCTCAAATTATCAATCACGTTTGCTTG TTCCTTTAAAGTTAAGGAGGAGCCGGGCTGAGATTCCATGATTT AACAAAGCGACTATA
OKS2034	TTGATGAGAATGGAGCAACAATGGCGGGAAGATGTTGACCAACT CCAGGAATATGTCGAAGAGATTACCCAAGAACTCCAGTAACGGA TCCCCGGGTTAATTAA
OKS2055	TATAAATCTTGGAATTAGCTTATTTTGTCAATTAAATTCTCCAACT AAGTAGATATGTACTGGTGATTAAGAAAAGCTATGAATTCGAGCT CGTTTAAAC
OKS2077	ATCGCTCCTTTGAAATTGTTACAAGAGTCAATGCCTACTGCTTTG GATTTGCTTATGTCGAAGTTCGTTTTCTAATCAATTCGCCAGGGT TTTCCCAGTCACGAC
OKS2079	TAAACCTTCTAAAATTGTAAAGTCCGCAAT
OKS2080	TTCATCATCAGTAGTCATAATTGATTAGAAAACGAACTTCGACAT
OKS2081	TTCTAATCAATTATGACTACTGATGATGAACAGCTTTCTCCCGTA
OKS2082	CGGGCTGGGGGTGGAAAGGTTAAAAGACTG

OKS2083	GGGGGCATCTTGAGACATAATTGATTAGAAAACGAACTTCGACA T
OKS2084	TTCTAATCAATTATGTCTCAAGATGCCCCCACTACCAATGCTTTA
OKS2085	GCCGGGCTGAGATTCCATAATTGATTAGAAAACGAACTTCGACA T
OKS2086	TTCTAATCAATTATGGAATCTCAGCCCGGCTCCTCCTTAACTTTA
OKS2088	ACTATCTTCTTCATACTGCTCTTGGCTCTGAAACCCTTGATTAGC CGTAAGTACGGGAGAAAGCTGTTCATCATCAGTAGTAGCGGATA ACAATTTCACACAGGA
OKS2089	ATCGATGTTTTGCTTCATAATATCTTGAAC
OKS2090	AGACGCCGGTATCAATATATCGGAGATCTT
OKS2106	ACAGGAGTCTTTCAAGGCAAATAAAAACGGATAAAGAAAGCAAT TCTAGGTCTCCTTCTATATCATCACAAGAACATAAACGGATCCCC GGGTTAATTAA
OKS2181	GGGGCCATGGGACATCATCATCATCATCACGAAAATCTTTACTTT CAGGGTATGGAAGAAAATTCCAGTGAG
OKS2182	GGGGCCATGGGACATCATCATCATCATCACGAAAATCTTTACTTT CAGGGTACTACT GATGATGAACAGCTT
OKS2183	GGTCATGCATTTATTATTTATGTTCTTGTGATGA
OKS2184	GGTCATGCATTTATTACTGGAGTTCTTGGGTAAT
OKS2185	GGGGTGATCAATGTCTGAACATAATTACCAG
OKS2186	GGTCGTCGACTTACTAGGGGGAAGGAGTGTCTTG
OKS2284	GCATTTTCAGAAGACTTGAGATCTCGCTTAAAGTATATTCGCGAG ACGTTGGAATCGTGGGCGTCGAAAATGGAAGTGAGTCGGATCC CCGGGTTAATTAA
OKS2285	TGAATGGATGAATAGTACAAAAATGAGGATGTGAAATATGGAAA AATAGACAGCATAGTAACTTAACGCCCAAGTATAGATGAATTCGA GCTCGTTTAAAC
OKS2286	ATTTTACGCTCGTACACCAGTCATGGTGTATTCTATTACGAGAAA TTCGTTGATGCTATTGCTGGGTCAAAAGATAGCAATCGGATCCC CGGGTTAATTAA
OKS2287	ATTCGTCTAAGGGAAATGGCTCAGGTTAAAAAGATAAAGTATTAG AGGGAAGAATGTGAAACATATCTGGCTGCTCTTAACGAATTCGA GCTCGTTTAAAC
OKS2320	GGGGTGATCAATGCATCATCATCATCATCACGAAAATCTTTACTT TCAGGGTTCTGAACATAATTACCAGTCT

3. Truncation of the Mto1 C-terminus reveals Mto1 localization to the nuclear envelope

3.1 Introduction

Free γ-TuC is thought not to be active, suggesting that localization of the γ-TuC to MTOCs is necessary for MT nucleation. However, the mechanism of γ-TuC activation at MTOCs is unknown, making the identification of γ-TuC-activating proteins a topic of particular interest. Whether or not the proteins involved in localizing the γ-TuC are also involved in activating the γ-TuC remains unclear. CDK5RAP2 is a notable exception, as recent evidence suggests it is a γ-TuC activator (Choi et al., 2010). CDK5RAP2 contributes to γ-TuC localization to the centrosome, and both full-length CDK5RAP2 as well as a fragment containing its γ-TuC-binding CM1 domain promote MT nucleation from purified γ-TuRCs (Choi et al., 2010; Fong et al., 2008). The budding yeast γ-TuC targeting protein Spc110 fails to activate nucleation from purified γ-TuCs, but is capable of promoting the multimerization of γ-TuSCs into γ-TuRC-like structures (Kollman et al., 2010). According to the template model for MT nucleation, such multimerization is a requirement for generating an active γ-TuC.

Cytoplasmic MT nucleation in fission yeast invariably requires the γ-TuC localizing protein Mto1, thus making Mto1 a suspected γ-TuC activator. Like a variety of proteins involved in γ-TuC localization and/or activation, Mto1 is a relatively large (1115 amino acid) protein that contains extensive predicted coiled-coils as well as a CM1 domain (Samejima et al., 2008). Detailed characterization has revealed how various regions of Mto1 primary sequence are involved in specific Mto1 functions. Mutations within the Mto1 CM1 region eliminate interaction between the Mto1/2 complex and γ-TuC, resulting in a complete lack

of cytoplasmic MT nucleation (Samejima et al., 2008). Deletion of the Mto1 sequence required for Mto2-binding, on the other hand, limits Mto1 localization and MT nucleation almost exclusively to the SPB (Samejima et al., 2008).

An additional Mto1 sequence, referred to as MASC, mediates Mto1/2 localization to interphase and mitotic SPBs, as well as the eMTOC (Samejima et al., 2010). The MASC region is located near the Mto1 C-terminus, while the Mto2-binding and CM1 domains are located more centrally. Mto1 C-terminal truncation mutants lacking the MASC sequence, such as Mto1(1-1051)-GFP, retain localization to MTs and the NE, and are capable of promoting MT nucleation from non-SPB sites (Samejima et al., 2010).

In this chapter, my aim was to determine how much of the Mto1 C-terminus could be removed, while still preserving MT nucleation within the cytoplasm. By extension, I wished to determine whether or not a specific region of Mto1 contributed directly to activation of the γ-TuC. Therefore, a series of *mto1* mutants with increasingly large C-terminal deletions was constructed and analyzed with respect to morphology, Mto1/γ-TuC localization, and MT nucleation. I found that *mto1* mutants as small as *mto1(1-549)* retain the ability to nucleate cytoplasmic MTs. Mto1(1-549) fails to localize to MT bundles, and instead shows enhance localization to the NE. This leads to increased recruitment of the γ-TuC to the NE, resulting in increased MT nucleation from the nuclear surface.

3.2 Results

3.2.1 Normal morphology is observed in *mto1* truncation mutants as small as *mto1(1-549)*

PAIRCOIL2 software predicts that Mto1 contains regions of coiled-coils throughout much of its sequence, with the exception of the first 275 or so N-terminal residues (Figure 3.1A). Prediction of coiled-coils by the PAIRCOIL2 program is based on comparison of a target protein sequence to a database of two-stranded coiled-coil sequences (Berger et al., 1995; McDonnell et al., 2006). I used the PAIRCOIL2 analysis of Mto1 sequence as a rough guideline in generating *mto1* C-terminal truncation mutants. Truncations were targeted to sites between regions of predicted coiled-coil, in order to reduce the possibility of disrupting important structural features. The endogenous *mto1+* gene was simultaneously truncated and tagged with GFP to produce *mto1(1-800)-GFP*, *mto1(1-732)-GFP*, *mto1(1-683)-GFP*, *mto1(1-637)-GFP*, *mto1(1-575)-GFP*, *mto1(1-549)-GFP*, and *mto1(1-500)-GFP* mutants (Figure 3.1B).

As an initial test for *mto1* function, I analyzed the various truncations with respect to morphology. Previous work has revealed that both *mto1Δ* and *mto2Δ* cells exhibit a curved morphology, due to a lack of proper cytoplasmic MT nucleation and organization (Samejima et al., 2005; Sawin et al., 2004; Venkatram et al., 2005; Venkatram et al., 2004). This phenotype is most evident when cells are re-introduced to fresh media following growth to stationary phase. Wild-type and mutant *mto1* strains were therefore allowed to re-grow from stationary phase, fixed in formalin, and imaged by differential interference contrast (DIC) microscopy to assess cell shape (Figure 3.2).

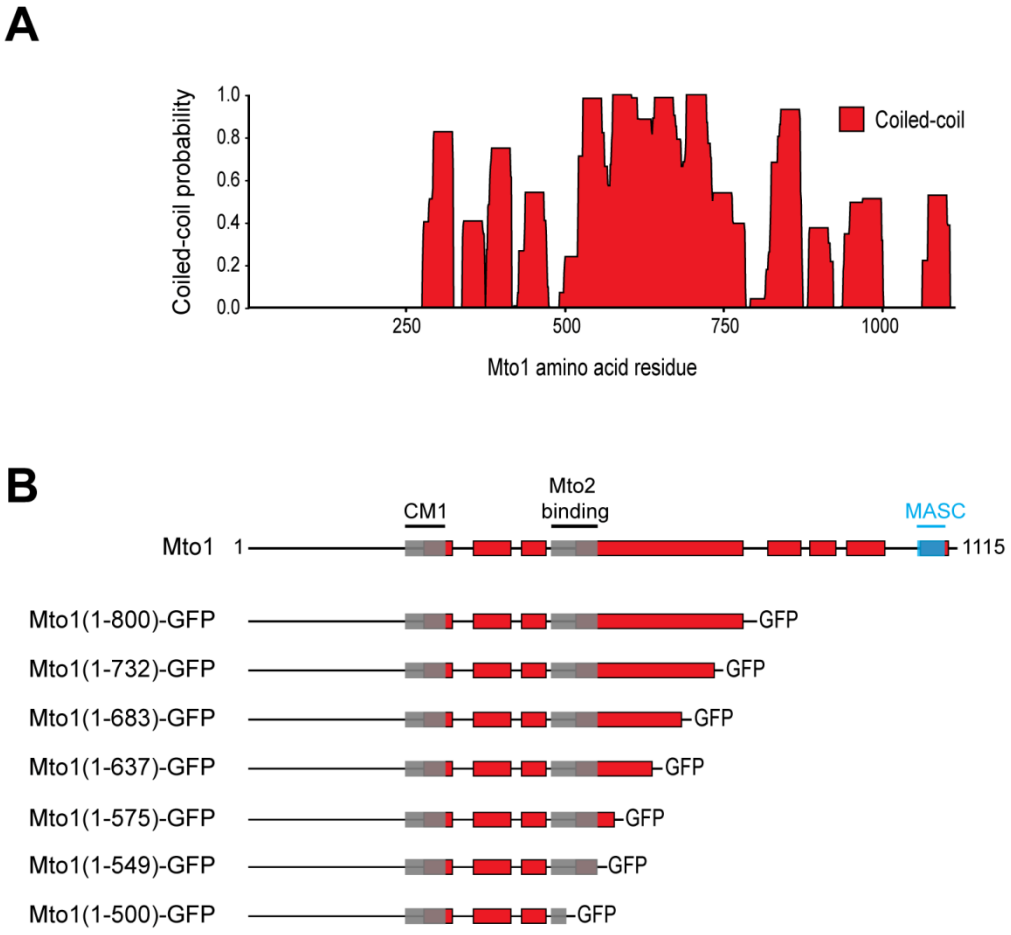

Figure 3.1: Design of Mto1 C-terminal truncation mutants. (A) PAIRCOIL2 software predicts that Mto1 contains extensive regions of coiled-coils, mostly in the C-terminal portion of the protein. (B) Top: schematic representation of wild-type Mto1 with predicted coiled-coils shown in red and CM1, Mto2-binding, and MASC regions indicated. Bottom: various Mto1 truncation mutants with C-terminal GFP tags. All C-terminal truncation mutants lacked the MASC region, and a portion of the Mto2-binding domain was deleted in Mto1(1-500)-GFP.

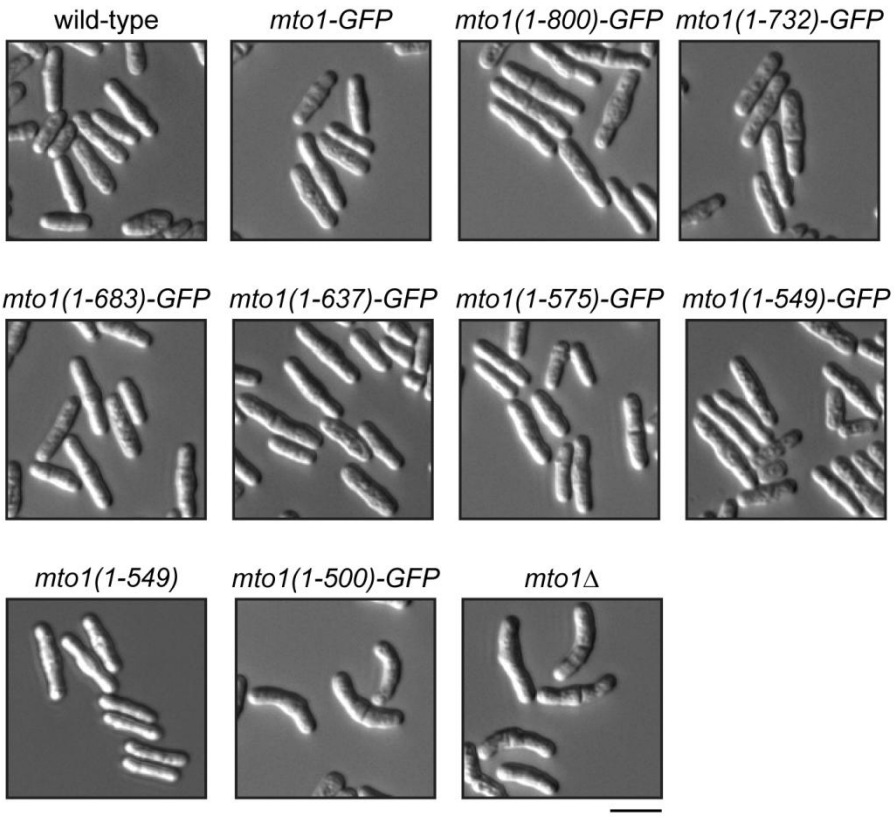

Figure 3.2: *mto1* truncations as small as *mto1(1-549)* have normal cell morphology. Cell morphology following growth to stationary phase and re-introduction to fresh medium. Wild-type and *mto1-GFP* strains showed normal, straight cell shape. Truncation of the Mto1 C-terminus up to amino acid 549 had no effect on morphology, while further truncation in *mto1(1-500)-GFP* results in the curved cell phenotype characteristic of *mto1*Δ. Bar, 5 μm. [Strains: KS515, KS1017, KS1999, KS819, KS5207, KS5209, KS5211, KS5213, KS5215, KS5217, KS5608]

As expected, wild-type (*mto1+*) and full-length *mto1-GFP* cells exhibited normal, straight morphology, while *mto1Δ* cells were clearly curved. Truncations as small as *mto1(1-549)-GFP* showed wild-type morphology, providing an initial indication that mto1 function was not abolished following extensive C-terminal truncation. Un-tagged *mto1(1-549)* was therefore also analyzed, to verify that capping of the truncated Mto1 C-terminus by GFP was not necessary to maintain Mto1 function and/or stability. Like *mto1(1-549)-GFP*, *mto1(1-549)* was found to have a wild-type cell shape. In contrast, *mto1(1-500)-GFP* was found to be curved, suggesting a decrease or lack of Mto1 function . This is consistent

with the finding that a central portion of Mto1, roughly encompassing amino acids 461-549, is required for interaction with Mto2 (Samejima et al., 2005; Samejima et al., 2008). Internal deletions within this region eliminate the Mto1-Mto2 interaction, resulting in a phenotype that mimics *mto2Δ*, including defects in cytoplasmic MT nucleation and curved morphology (Samejima et al., 2008).

3.2.2 Mto1 C-terminal truncations localize to the nuclear envelope

Localization of the GFP-tagged truncation mutants was analyzed, and compared to that of full-length Mto1-GFP. During interphase, full-length Mto1 localizes primarily to the SPB and sites along MTs, although occasional satellite particles of Mto1 can be detected on the NE (Figure 3.3A) (Sawin et al., 2004; Venkatram et al., 2004). In previous work, it was shown that Mto1 over-expression results in decoration of MTs and increased NE localization, with Mto1 appearing as a faint ring around the NE (Samejima et al., 2005). Here, all of the C-terminal truncations ranging in size from Mto1(1-800)-GFP to Mto1(1-549)-GFP were found to localize almost exclusively to the NE (Figure 3.3A). Unlike the "ring" of Mto1 seen on the NE upon over-expression, the C-terminal truncation mutants were visible as discrete puncta. Movies of Mto1(1-549)-GFP revealed that these puncta were dynamic, appearing to diffuse around the nuclear surface. Limited numbers of puncta were also observed in the cytoplasm away from the NE, where they exhibited rectilinear movements indicative of an association with MTs.

Mto1(1-500)-GFP showed no specific localization, instead producing only a diffuse signal throughout the cytoplasm (Figure 3.3A). Earlier studies have shown that full-length

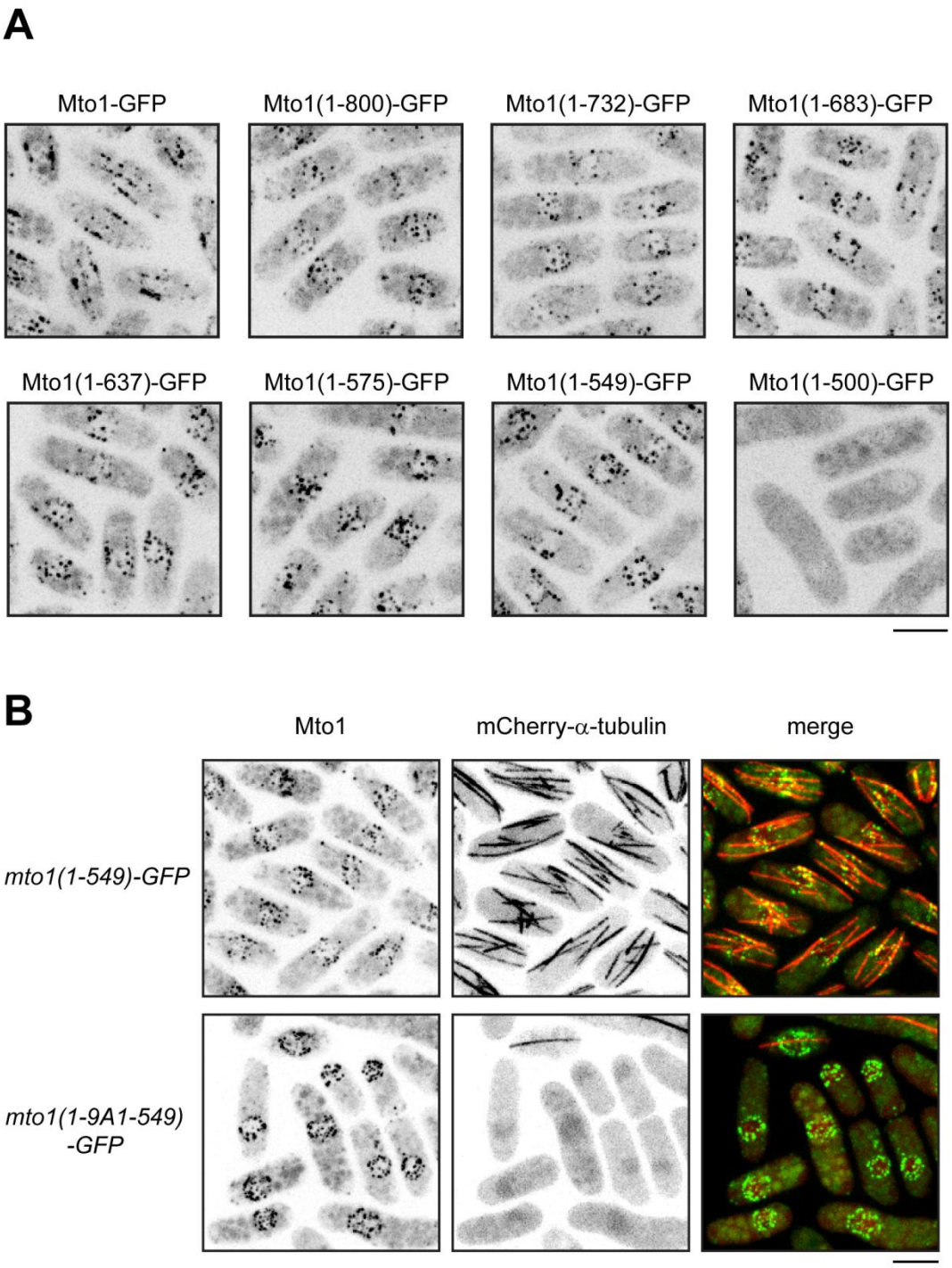

Figure 3.3: Mto1 C-terminal truncation mutants localize to the NE. (A) During interphase, Mto1-GFP is primarily visible along MTs and at the SPB. Various C-terminal truncations of Mto1, as small as Mto1(1-549)-GFP, localize to the NE. Mto1(1-500)-GFP shows no specific localization, and exhibits a diffuse signal throughout the cytoplasm. (B) Imaging with mCherry-α-tubulin reveals that Mto1(1-549)-GFP occasionally localizes to MTs, most often at the MT end. Mto1(1-9A1-549)-GFP fails to nucleate cytoplasmic MTs, and localizes to the NE in the absence of interaction with the γ-TuC. Bar, 5 μm. [Strains: KS5207, KS5209, KS5211, KS5213, KS5215, KS5217, KS819, KS5826, KS6677, KS6675]

Mto1 re-distributes to the NE upon cold-shock. Although the mechanism is unknown, this re-distribution of Mto1 to the NE does not occur in *mto2Δ* cells (Samejima et al., 2005). Therefore, Mto1(1-500)-GFP likely fails to localize to the NE owing to a lack of an intact Mto2-binding region. The findings presented here thus confirm that under physiological conditions and endogenous expression, Mto1 localizes to the NE in an Mto2-dependent manner.

We hypothesized that the γ-TuC itself could be re-distributed to the NE when not localized to conventional MTOCs by the Mto1 C-terminal truncations. If this were the case, the Mto1 C-terminal truncations could be recruited to the NE by the γ-TuC, rather than the γ-TuC being recruited to the NE by Mto1. To address this possibility, I generated a C-terminal truncation of the *mto1-9A1* mutant. In *mto1-9A1*, 9 residues within the CM1 region are mutated to alanine, leading to a lack of interaction between Mto1 and the γ-TuC (Samejima et al., 2008). Mto1(1-549)-GFP and Mto1(1-9A1-549)-GFP were imaged along with mCherry-α-tubulin (Figure 3.3B). The lack of normal cytoplasmic MT arrays in *mto1(1-9A1-549)-GFP* was taken as an indirect confirmation that Mto1(1-9A1-549)-GFP failed to interact with the γ-TuC, as with full length Mto1-9A1. Like Mto1(1-549)-GFP, Mto1(1-9A1-549)-GFP localized to the NE, indicating that interaction with the γ-TuC is not necessary for Mto1 NE localization (Figure 3.3B).

I also wanted to confirm that Mto1(1-549) was capable of recruiting the γ-TuC to the NE. Therefore, the γ-TuC protein Alp4-tdTomato (Alp4-tdT) was imaged along with GFP-α-tubulin (*nmt81:*GFP-Atb2) in wild-type, *mto1(1-549)*, and *mto1(1-549)-GFP* backgrounds. As expected, in a wild-type background Alp4-tdT was observed at the iSPB, mSPBs, NE and eMTOC, as well as along MTs (Figure 3.4, Figure 3.5). In *mto1(1-549)* and *mto1(1-549)-GFP* cells, on the other hand, Alp4-tDT localized mostly to the NE, but could also be observed at iSPBs and mSPBs (Figure 3.4, Figure 3.5). This SPB localization of the γ-TuC has been

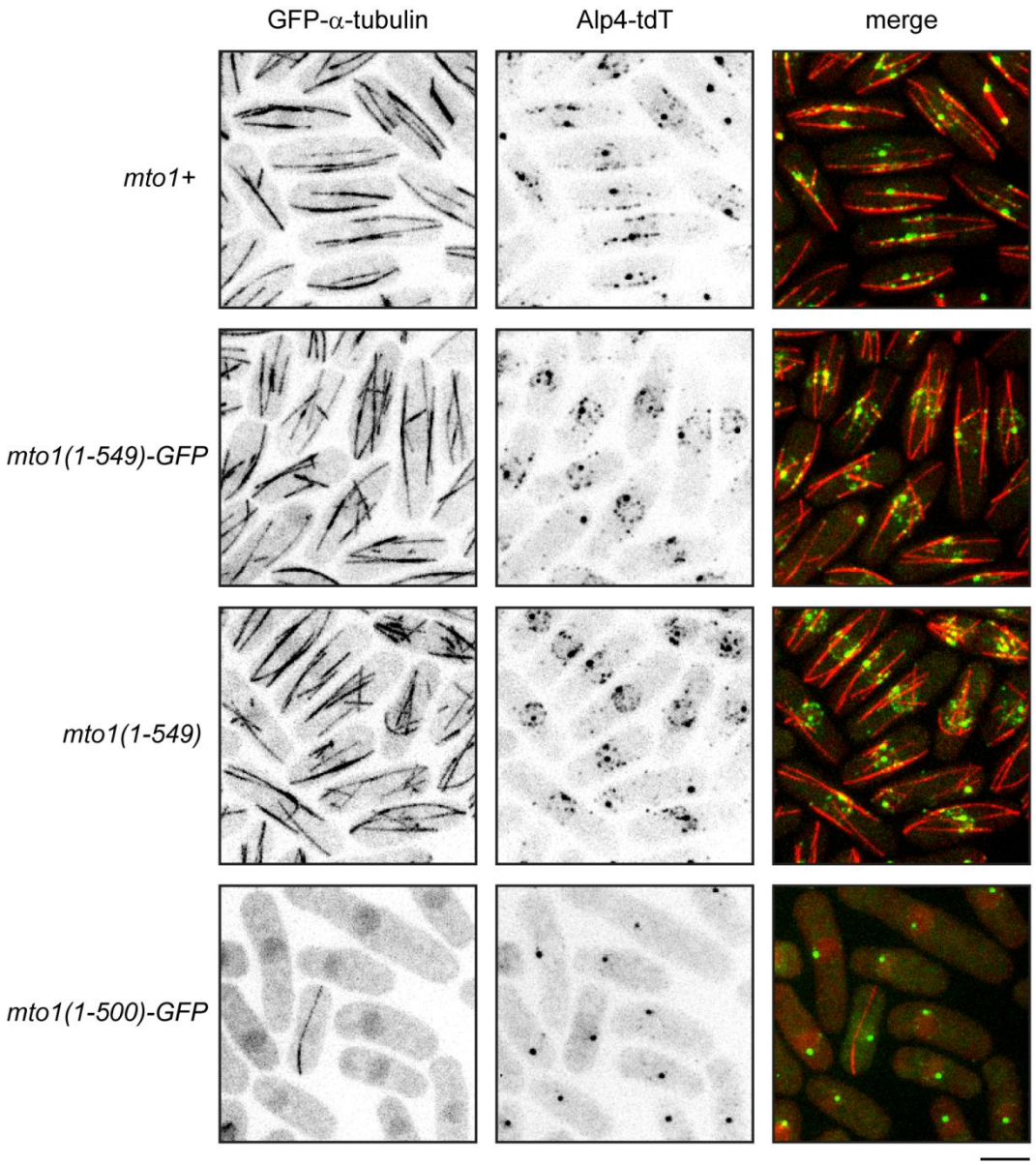

Figure 3.4: The γ-TuC localizes to the NE in *mto1(1-549)* cells. Interphase MTs (red) and Alp4-tdT (γ-TuC; green) localization in *mto1+* and *mto1* C-terminal truncation strains. In *mto1+* cells, the γ-TuC is seen at the SPB, along MTs, and to a lesser extent on the NE. In *mto1(1-549)* and *mto1(1-549)-GFP*, the γ-TuC localizes primarily to the NE, but also shows limited association with MTs, often at MT ends. In *mto1(1-500)-GFP*, cells fail to nucleate cytoplasmic MT arrays, and the γ-TuC is absent from MTOCs aside from the SPB. γ-TuC localization to SPBs in *mto1(1-549)*, *mto1(1-549)-GFP*, and *mto1(1-500)-GFP* is very likely limited to the nucleoplasmic face of the SPB. Note that the Mto1(1-549)-GFP and Mto1(1-500)-GFP signals are too faint to be detected in the presence of GFP-α-tubulin. Bar, 5 μm. [Strains: KS5356, KS5357, KS5641, KS5936]

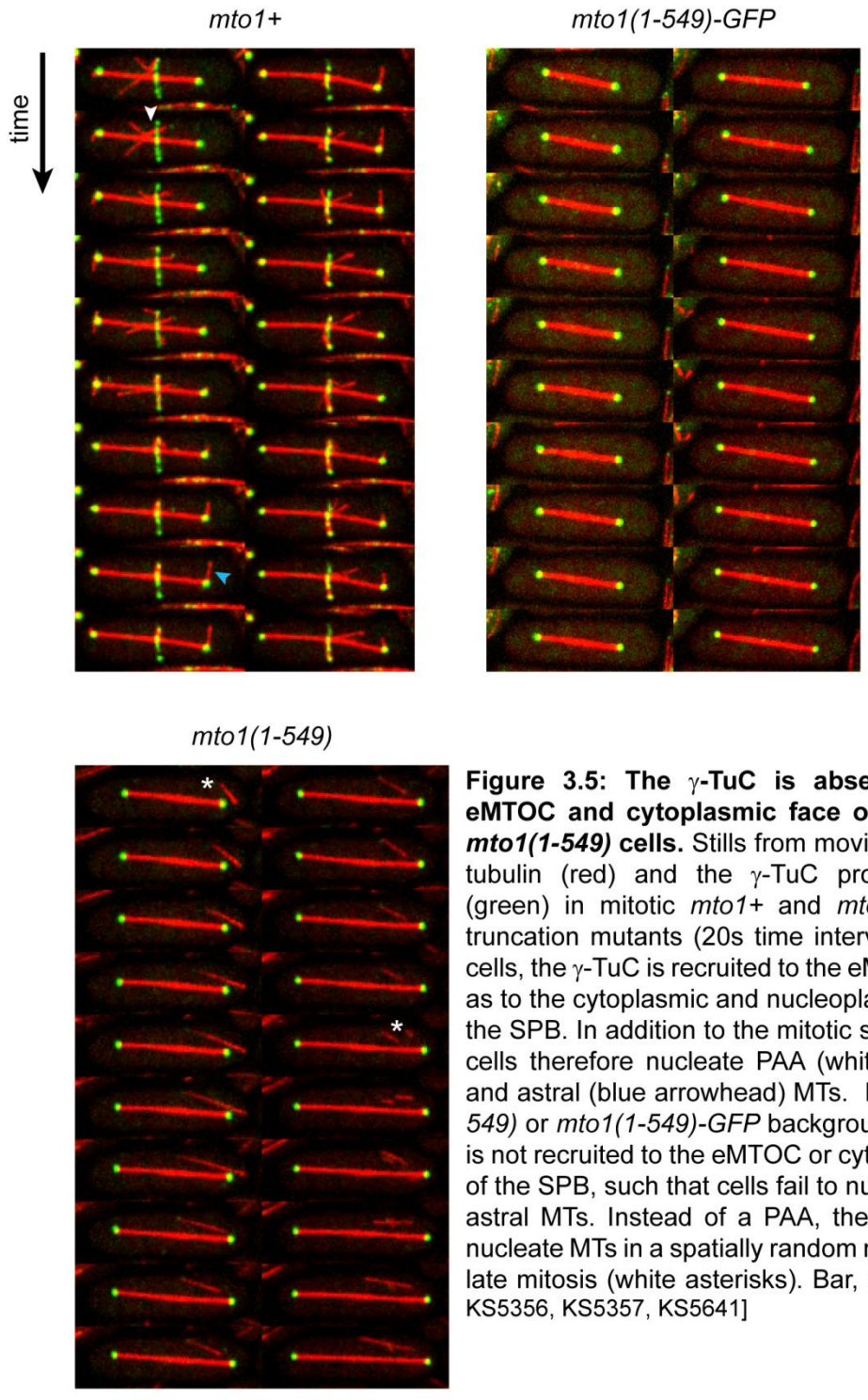

Figure 3.5: The γ-TuC is absent from the eMTOC and cytoplasmic face of the SPB in *mto1(1-549)* cells. Stills from movies of GFP-α-tubulin (red) and the γ-TuC protein Alp4-tdT (green) in mitotic *mto1+* and *mto1* C-terminal truncation mutants (20s time interval). In *mto1+* cells, the γ-TuC is recruited to the eMTOC, as well as to the cytoplasmic and nucleoplasmic faces of the SPB. In addition to the mitotic spindle, *mto1+* cells therefore nucleate PAA (white arrowhead) and astral (blue arrowhead) MTs. In an *mto1(1-549)* or *mto1(1-549)-GFP* background, the γ-TuC is not recruited to the eMTOC or cytoplasmic face of the SPB, such that cells fail to nucleate PAA or astral MTs. Instead of a PAA, these cells often nucleate MTs in a spatially random manner during late mitosis (white asterisks). Bar, 5 μm. [Strains: KS5356, KS5357, KS5641]

observed in *mto1Δ* and cells lacking the MASC region, and is thought to correspond to γ-TuC localized to the nucleoplasmic face of the SPB in an Mto1-independent manner (Samejima et al., 2010). This is supported by the absence of cytoplasmic astral MTs in both *mto1(1-549) and mto1(1-549)-GFP* (Figure 3.5). Astral MTs are also absent in mutants that lack the MASC region but retain most of mto1 C-terminus, such as *mto1(1-1051)-GFP* (Samejima et al., 2010).

In *mto1(1-500)-GFP*, Alp4-tdT showed no specific cytoplasmic localization, and cells failed to nucleate cytoplasmic MT arrays (Figure 3.4). This confirms that Mto1(1-500)-GFP, in which the Mto1-Mto2 binding region is disrupted, fails to promote MT nucleation from the γ-TuC.

Next, I wished to determine whether or not Mto1(1-549) retained localization to MT bundles. However, this was complicated by the fact that we suspect Mto1 localizes to MTs via two mechanisms. In the first mechanism, Mto1 associates directly with the MT lattice, and therefore localizes along the length of existing MT bundles. In the second mechanism, Mto1 remains associated with the minus-end of a MT following nucleation. Importantly, if this MT is incorporated into an existing MT bundle, Mto1 can *appear* as though it is associated with the MT lattice. Therefore, any *mto1* mutant capable of nucleating MTs is expected to show some Mto1 localization to MT bundles.

Localization of full-length Mto1 to the MT lattice is demonstrated by over-expression of *nmt81:*Mto1-GFP, which results in a complete decoration of MT bundles (Figure 3.6) (Samejima et al., 2005). Over-expressed *nmt81:*Mto1(1-549)-GFP, on the other hand, failed to decorate MTs. In fact, *nmt81:*Mto1(1-549)-GFP showed no increase in MT localization when compared to endogenously-expressed Mto1(1-549)-GFP (Figure 3.6). This suggests that Mto1(1-549) localization to MTs may be limited to MT minus ends. Consistent with this notion, endogenously-expressed Mto1(1-549)-GFP showed reduced localization to

MTs, when compared with Mto1-GFP (Figure 3.6). Similarly, Alp4-tdT had reduced localization to MTs in *mto1(1-549)-GF*P and *mto1(1-549)* cells, in comparison to cells expressing full-length Mto1 (Figure 3.4). Overall, these findings suggest that Mto1(1-549) is not targeted to the MT lattice. Given that Mto1(1-549)-GFP and Mto1(1-800)-GFP localization is essentially indistinguishable (Figure 3.3A) and that the MASC sequence is not necessary for MT localization (Samejima et al., 2010), residues between amino acid 800 and the MASC sequence probably mediate Mto1 targeting to MTs.

Mto1(1-549)-GFP was imaged together with Alp4-tdT, in order to confirm that they co-localized on the NE. As a control, Mto1-GFP was found to co-localize with Alp4-tdT on MTs, SPBs, and the eMTOC, as described previously (Figure 3.7) (Samejima et al., 2008). By contrast, Mto1(1-549)-GFP and Alp4-tdT co-localized predominantly on the NE, but also occasionally in the cytoplasm (Figure 3.7). In maximum projections through the full cell volume, Mto1(1-549)-GFP signal often overlapped partially with Alp4-tdT signal at the SPB. However, inspection of the specific Z-sections containing the SPB signal confirmed that Mto1(1-549)-GFP fails to localize to the SPB, as expected owing to deletion of the MASC sequence (Figure 3.7). Both Mto1-GFP and Mto1(1-549)-GFP were occasionally observed on their own, with no associated Alp4-tdT signal. This is consistent with the notion that Mto1 is a part of a sub-complex, which forms independent of the γ-TuC.

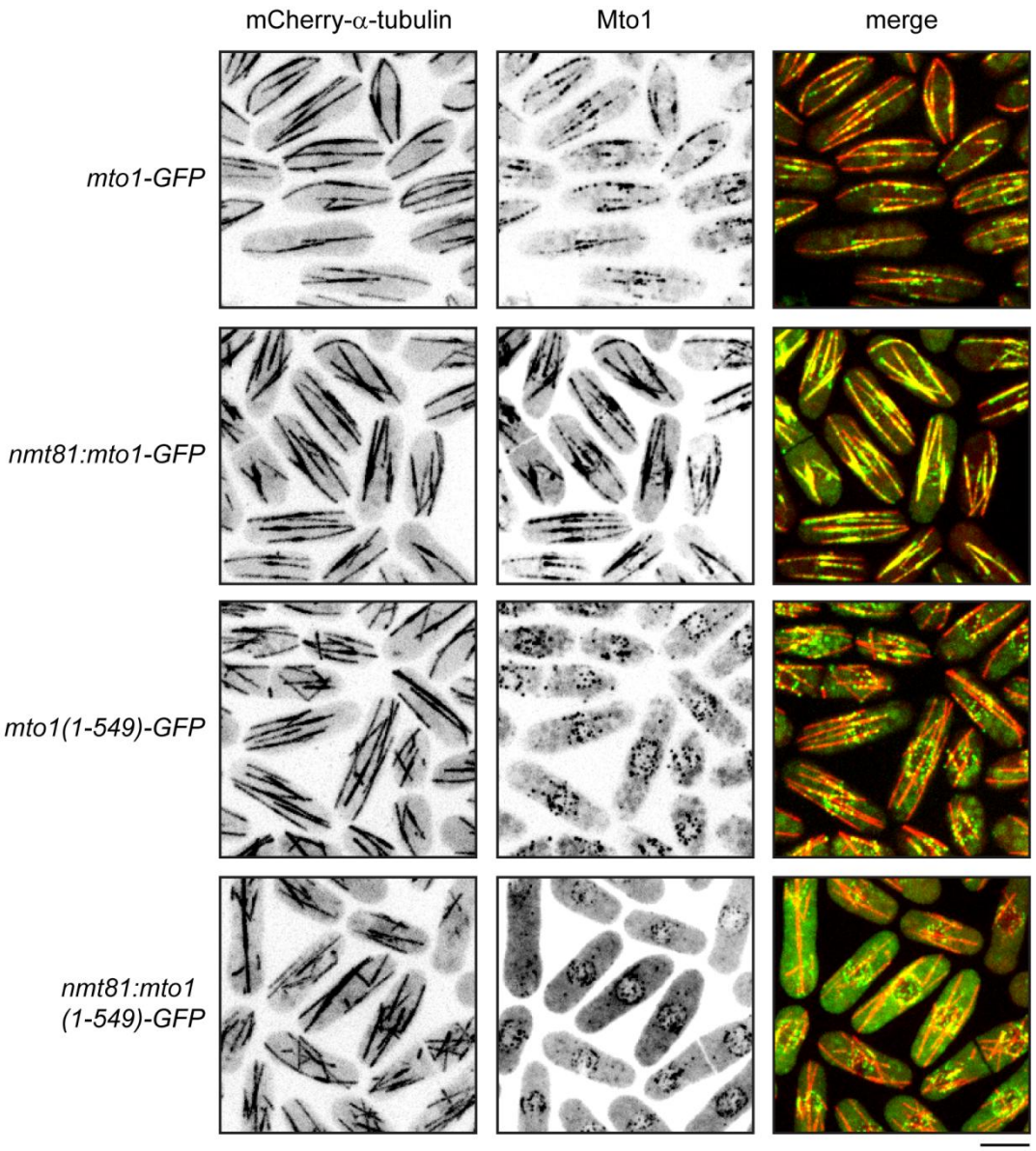

Figure 3.6: Mto1(1-549)-GFP does not localize to existing MT bundles. Endogenous expression and *nmt81* over-expression of Mto1-GFP and Mto1(1-549)-GFP with mCherry-α-tubulin. Over-expression of Mto1-GFP results in a virtually complete decoration of cytoplasmic MTs, which contrasts with the more punctate MT localization observed under endogenous expression. *nmt81:*Mto1-GFP is also more readily visible on the NE. Even when it is over-expressed, Mto1(1-549)-GFP shows limited MT localization in comparison to either endogenous or over-expressed Mto1-GFP. Primarily, over-expression of Mto1(1-549)-GFP appears to result in slightly increased NE localization and greater cytoplasmic background signal. Note that *nmt81* and endogenously-expressed Mto1 are presented at different contrasts, as *nmt81:*Mto1-GFP and *nmt81:*Mto1(1-549)-GFP signal would otherwise be nearly saturated (i.e. the increase in Mto1 signal upon over-expression is greater than displayed here). Bar, 5 μm. [Strains: KS6673, KS6672, KS6677, KS6679]

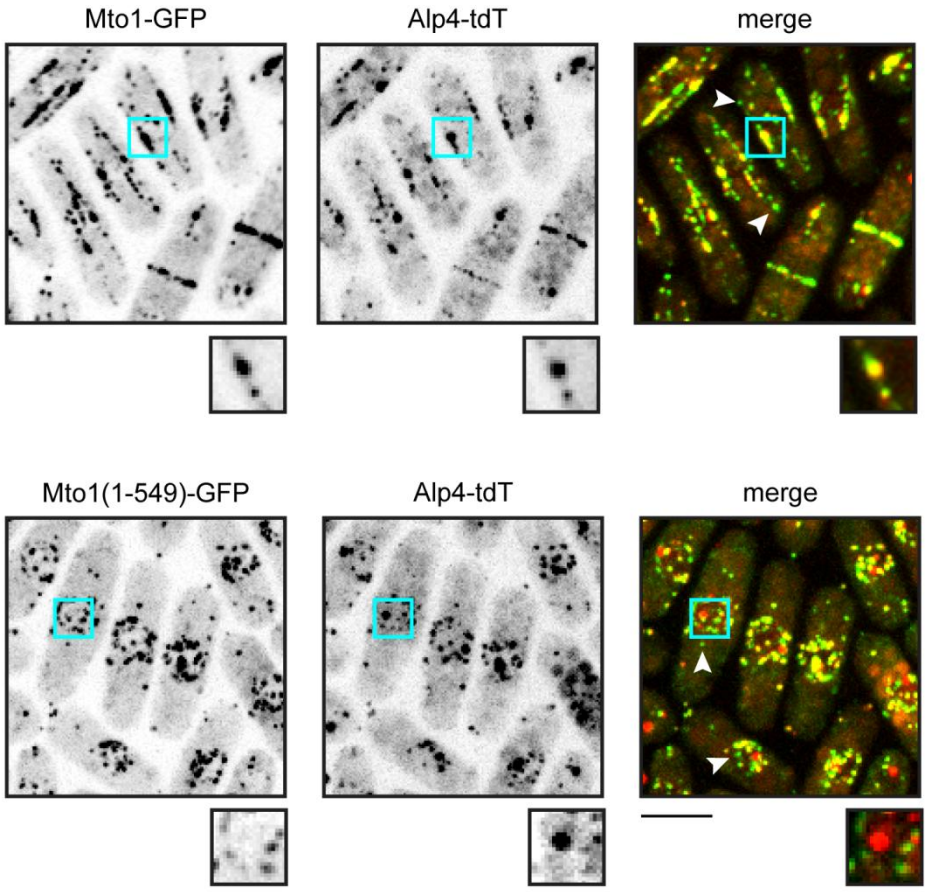

Figure 3.7: Mto1(1-549) and the γ-TuC co-localize on the NE. The co-localization of Mto1-GFP and Mto1(1-549)-GFP with Alp4-tdT is shown. Large panels are maximum projections of 8 Z-sections through the full cell volume. Smaller panels are maximum projections of 3 Z-sections containing the SPB volume, and correspond to a 2X zoom of the regions indicated by blue squares. Full-length Mto1-GFP and Alp4-tdT co-localized on the NE, SPBs, MTs, and eMTOC, as expected. Alp4-tdT co-localization with Mto1(1-549)-GFP was limited to the NE and occasional spots within the cytoplasm, which may have been MT-associated. Both Mto1-GFP and Mto1(1-549)-GFP were also observed alone, without any associated Alp4-tdT signal (white arrowheads). Bar, 5 μm. [Strains: KS5678, KS5674]

3.2.3 Mto1(1-549) promotes increased MT nucleation from the NE

Although MTs in *mto1(1-549)* were qualitatively normal (Figure 3.4), we wished to verify that the C-terminal truncation mutants were capable of nucleating MTs. We confirmed *de novo* MT nucleation using both fixed- and live-cell assays. *mto1-GFP* and *mto1(1-549)-GFP* cells were subjected to MT re-growth experiments, in which cells were chilled on ice to induce MT depolymerization and then returned to 25^{o}C to allow for MT re-assembly. Figure 3.8 shows cells fixed and stained by anti-tubulin immunofluorescence. Cells were fixed prior to chilling, and also 0, 1, 3, and 10 minutes after being returned to 25^{o}C. In both *mto1-GFP* and *mto1(1-549)-GFP*, equally robust MT re-growth could be observed by 1 minute, and MT arrays appeared to be at steady state by 3 minutes. This suggests that extensive truncation of the Mto1 C-terminus has little or no effect on the ability of cells to nucleate new MTs. Nucleation in both strains occurred predominantly from the area around the nucleus, as described previously for cold-shock experiments with *mto1+* cells (Anders et al., 2006; Samejima et al., 2005; Samejima et al., 2008; Sawin et al., 2004; Venkatram et al., 2005). In wild-type cells, the re-growth of MTs from the NE can be explained by the re-distribution of Mto1 to the nuclear surface following cold-shock (Sawin et al., 2004), while Mto1(1-549)-GFP is already present on the NE even under normal growth conditions.

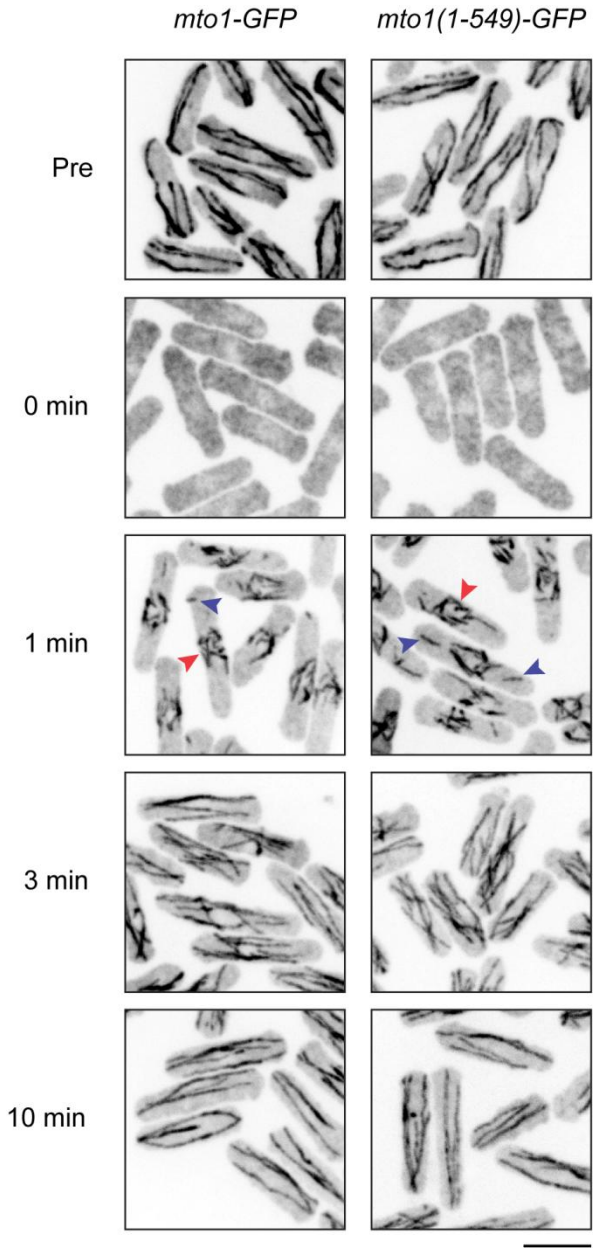

Figure 3.8: *mto1(1-549)-GFP* cells are capable of nucleating MTs. Cold-shock and MT regrowth in *mto1-GFP* and *mto1(1-549)-GFP*, with anti-tubulin staining of fixed cells. Cells were fixed prior to cold-induced MT depolymerization and also at the times indicated following return to 25ºC. Cells expressing either Mto1-GFP or Mto1(1-549)-GFP showed substantial MT nucleation within 1 minute of being returned to 25ºC. Almost all of this initial nucleation occurred from the NE (red arrowheads), although some MTs were nucleated elsewhere in the cytoplasm (blue arrowheads). By 3 minutes, MTs in both strains appeared to have returned to steady state. By this assay, MT nucleation in *mto1-GFP* and *mto1(1-549)-GFP* was indistinguishable. Bar, 5 μm. [Strains: KS819, KS5209]

Live-cell imaging of GFP-α-tubulin was used to compare MT nucleation in *mto1+* and *mto1(1-549)* strains. The aim was to address whether re-distribution of Mto1(1-549) to the NE—by removal of localization domains rather than cold-shock—would promote increased MT nucleation from the NE under normal growth conditions. Cells expressing *nmt81:*GFP-Atb2 in *mto1+*, *mto1-GFP*, *mto1(1-549)*, and *mto1(1-549)-GFP* backgrounds all clearly exhibited *de novo* MT nucleation (Figure 3.9). The frequency and spatial distribution of MT nucleation was analyzed by counting nucleation events, and classifying them as occurring in the NE region or elsewhere in the cytoplasm. The appearance of a new MT, that did not arise from breakage or release from an existing MT bundle, was taken as representing a *de novo* nucleation event. It is important to note that MT nucleation occurring along existing MT bundles cannot be identified with confidence, and thus was not counted in this experiment.

Both *mto1(1-549)* and wild-type *mto1+* cells exhibited MT nucleation almost exclusively from the region around the NE, with only very occasional nucleation events occurring freely in the cytoplasm. Further, the addition of a GFP tag in *mto1-GFP* and *mto1(1-549)-GFP* had no effect when compared to the respective untagged strain (Figure 3.9). Notably, the truncated *mto1* strains nucleated MTs from the NE at roughly twice the frequency of cells with full-length *mto1*. This can be explained by the redistribution of Mto1(1-549) and the γ-TuC to the NE, away from additional prospective nucleation sites on MTs and the SPB. In cells with full-length Mto1, a much smaller proportion of Mto1 and the γ-TuC are observed on the NE, such that MT nucleation from the NE likely represents only a subset of total cytoplasmic nucleation. Importantly, it is unlikely that *mto1+* cells nucleate fewer MTs overall than *mto1(1-549)* cells. Instead, much of the nucleation in *mto1+* probably occurs from the SPB and along existing MTs, such that it is not easily scored in this assay.

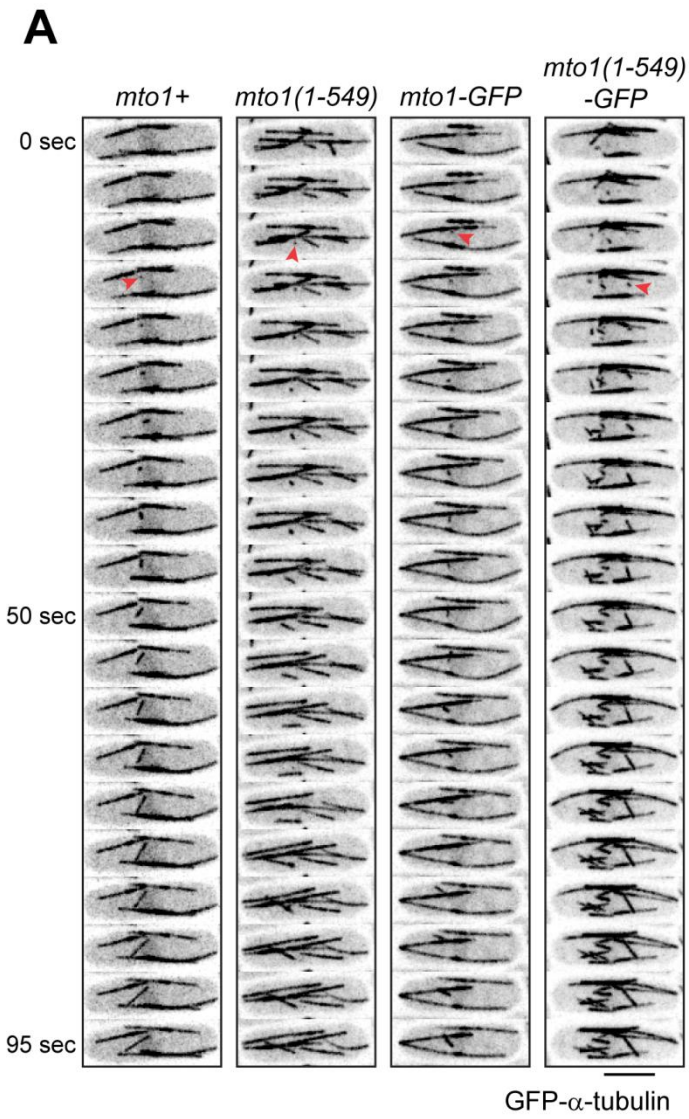

Figure 3.9: *mto1(1-549)* cells show increased MT nucleation from the NE. Interphase MT nucleation in cells expressing full-length Mto1 or Mto1 C-terminal truncations. (A) Stills from movies of GFP-α-tubulin in WT and mutant cells (5 sec time interval). Both full-length Mto1 and truncated Mto1(1-549) clearly exhibited *de novo* MT nucleation (red arrowheads), regardless of whether or not they were GFP-tagged. Note that Mto1-GFP and Mto1(1-549)-GFP are too faint to be detected when expressed together with GFP-α-tubulin. (B) Quantification of the MT nucleation observed in (A). Nucleation events in each strain were counted, and classified as occurring either in the region on/near the NE or elsewhere in the cytoplasm. In all strains, virtually all detectable nucleation occurred from the NE region. The frequency of nucleation from the NE region was greater in *mto1(1-549)* and *mto1(1-549)-GFP* in comparison to *mto1+* and *mto1-GFP* cells. GFP-tagging had little or no effect on nucleation frequency relative to the respective un-tagged strain. Bar, 5 μm. [Strains (cells counted, nucleation events counted): KS2802 (25,56), KS6086 (15,97) KS2738 (25,69), KS5491 (14,83)]

3.3 Discussion

The work presented in this chapter demonstrates that cytoplasmic MT nucleation is preserved in *mto1* C-terminal truncation mutants as small as *mto1(1-549)*. Mto1(1-549) retains the Mto1 regions required for γ-TuC and Mto2 binding but lacks sequences which mediate localization to SPBs, MTs, and the eMTOC. Further truncation results in cells which fail to nucleate cytoplasmic MT arrays, most likely due to deletion of Mto1 sequence required for interaction with Mto2. This is expected, as *mto2Δ* cells are only capable of nucleating MTs from the SPB (Samejima et al., 2005). Therefore, simultaneous removal of the SPB-localizing and Mto2-binding regions in *mto1(1-500)-GFP* completely abolishes cytoplasmic MT nucleation.

Various C-terminal truncations of Mto1, ranging in size from Mto1(1-549)-GFP to Mto1(1-800)-GFP, showed clear localization to the NE. Previously, Mto1 had only been clearly detectable on the NE when over-expressed or following cold-induced depolymerization of MTs (Samejima et al., 2005; Sawin et al., 2004). Mto1(1-549) was also found to recruit the γ-TuC to the NE, resulting in increased MT nucleation from the nuclear surface. This finding provides mechanistic insight to the largely unexplained observation that the fission yeast NE acts as a MTOC. Presumably, the same mechanism accounts for NE-derived nucleation in wild-type cells, but is simply harder to observe as full-length Mto1 localizes primarily to MTs and the SPB.

Significantly, the findings presented here reveal that re-localizing Mto1 and the γ-TuC in *mto1(1-549)* does not compromise MT nucleation, but rather alters the spatial distribution of MT nucleation within the cell. This provides an initial indication that the role of Mto1 in activating the γ-TuC may be independent of its role in localizing the γ-TuC. Given

its ability to recruit the γ-TuC to the NE, and thereby promote increased MT nucleation at the NE, Mto1(1-549) is henceforth referred to as "Mto1-NE".

4. The Mto1/2-bonsai complex activates MT nucleation by the γ-TuC

4.1 Introduction

Ultimately, I wished to determine whether or not a particular domain of Mto1 was directly involved in activating the γ-TuC. To address this question, I sought to generate a minimal Mto1 mutant which completely lacked localization domains, but retained the ability to promote cytoplasmic MT nucleation. In the previous chapter, we saw that the Mto1 C-terminus can be truncated to amino acid 549, without compromising MT nucleation in the cytoplasm. This Mto1 mutant, referred to as Mto1-NE, does not localize to SPBs, MTs, or the eMTOC, but instead shows enhance localization to the NE. In the following chapter, I investigate the role of the Mto1 N-terminus in MT nucleation, as well as localization of Mto1 and the γ-TuC.

To do this, I generated a series of *mto1* N-terminal truncation mutants. This revealed that the Mto1 N-terminus is required for localization of the Mto1/2 complex and γ-TuC to the NE. By combining the N- and C-terminal truncations in a single mutant, I generated Mto1-bonsai, a minimal fragment of Mto1 that retains the γ-TuC and Mto2 binding regions, but lacks both the N- and C-terminal localization domains. Mto1-bonsai promotes spatially random MT nucleation from the γ-TuC, completely independent of localization to conventional MTOCs. In addition, live-cell imaging revealed that puncta containing both the γ-TuC and Mto1/2-bonsai complex (Mto1-bonsai-Mto2 complex) are present at the ends of newly-nucleated MTs. This provides the most direct evidence to date that Mto1 contributes directly to γ-TuC activation.

Fluorescence quantification was used to determine the copy numbers of GFP-tagged Mto1-bonsai, Mto2, Alp4, and Alp6 in the puncta associated with MT nucleation. This quantification indicates that these nucleating puncta are single γ-TuRCs, associated with 13 copies each of Mto1-bonsai and Mto2. The copy numbers observed for Mto1-bonsai and Mto2 therefore match the 13 protofilaments of the MT lattice, as well as the 13 γ-tubulins thought to produce an effective template for MT nucleation. Most importantly, this finding suggests that the γ-TuC is activated by higher-order assemblies of the Mto1/2 complex.

4.2 Results

4.2.1 Over-expressed N-terminal truncations of Mto1 promote MT nucleation away from the NE

I produced a series of Mto1 N-terminal truncation mutants, in the context of both the full length Mto1 C-terminus and the truncated Mto1-NE mutant. The N-terminus was truncated to amino acid residue 131, 203, or 242, such that the CM1 region, which roughly spans amino acids 247-310 (Figure 3.1B) (Samejima et al., 2008), was left intact in all cases. Initially, truncations were generated such that Mto1 was over-expressed from the *nmt81* promoter, because construction of these strains was technically simpler than generating N-terminal truncations expressed from an endogenous promoter.

As a first test for MT nucleating function, *mto1* N-terminal truncation mutants were subjected to cold-shock and MT regrowth assays, exactly as described in section 3.2.3. All of the N-terminal truncation mutants were capable of nucleating MTs, but differed in the

localization and robustness of MT nucleation. Previous work has shown that wild-type cells nucleate MTs from the NE within 1 minute following return to warm media, and exhibit steady-state MT arrays within 2-4 minutes (Sawin et al., 2004). In contrast, cells completely lacking Mto1 exhibit new MTs only after 10-20 minutes and a return to steady state after 30-60 minutes (Sawin et al., 2004). Like wild-type and *mto1-GFP* cells, *nmt81:mto1(131-1115)-GFP*, *nmt81:mto1(131-549)-GFP*, *nmt81:mto1(203-549)-GFP*, and *nmt81:mto1(242-549)-GFP* all nucleated MTs within 1 minute, and appeared to have steady-state MT arrays by 3 minutes (Figure 4.1B). MT nucleation did not appear as robust in the N-terminal truncation mutants, in particular for *nmt81:mto1(203-549)-GFP* and *nmt81:mto1(242-549)-GFP.* Still, it was clear that all of the *mto1* N-terminal truncations retained at least some ability to nucleate cytoplasmic MTs. Significantly, unlike cells expressing full-length Mto1, the *mto1* N-terminal truncations did not exhibit MT re-growth from the NE, but rather showed spatially random MT nucleation throughout the cytoplasm (Figure 4.1B).

Analysis of Mto1 localization revealed that the N-terminal truncations were absent from the NE. This explains the spatially random nucleation observed in cold-shock experiments. *nmt81:*Mto1(131-1115)-GFP did not show the faint NE localization observed in *nmt81:*Mto1-GFP, and instead appeared to show an increased decoration of MTs (Figure 4.2). The lack of Mto1 at the NE was much more apparent when the N-terminus of Mto1-NE was truncated; while *nmt81:*Mto1-NE-GFP clearly localized to the NE, *nmt81:*Mto1(131-549)-GFP, *nmt81:*Mto1(203-549)-GFP, and *nmt81:*Mto1(242-549)-GFP were distributed throughout the cytoplasm, often as larger puncta (Figure 4.2). These larger spots may represent Mto1 aggregates, which could potentially account for the reduced nucleation observed in *nmt81:mto1(203-549)-GFP* and *nmt81:mto1(242-549)-GFP*. Indeed, *nmt81:*Mto1(242-549)-GFP showed both the largest spots and the weakest MT nucleation.

Overall, these findings suggested that truncation of the Mto1 N-terminus eliminates NE localization, without compromising cytoplasmic MT nucleation.

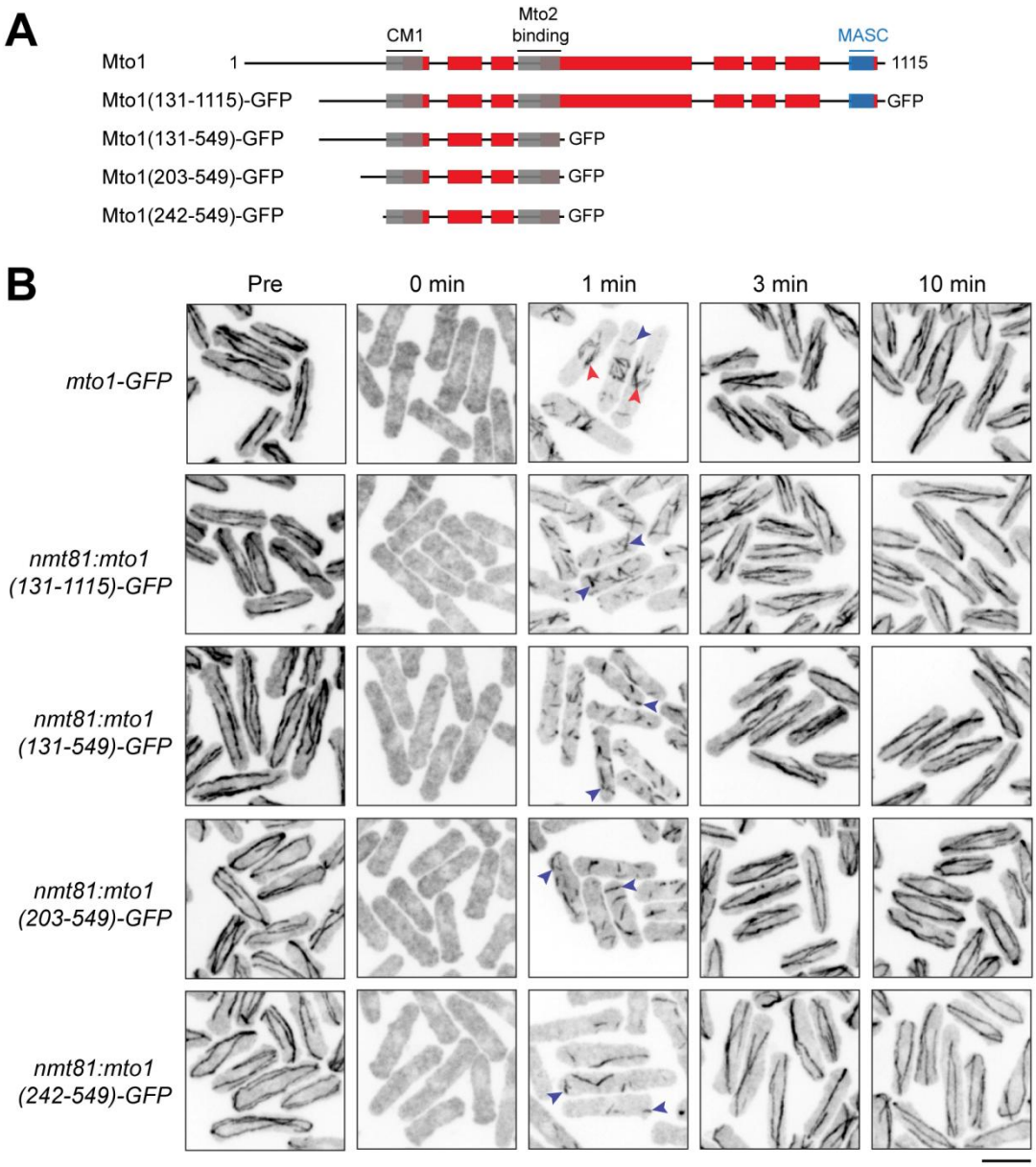

Figure 4.1: MT re-growth in *mto1* N-terminal truncation mutants occurs away from the NE. (A) Top: schematic representation of wild-type Mto1 with predicted coiled-coils shown in red and CM1, Mto2-binding, and MASC regions indicated. Bottom: various Mto1 N- and C-terminal truncation mutants with C-terminal GFP tags. (B) Cold-shock and MT regrowth with anti-tubulin staining of fixed cells. Cells were fixed prior to cold-induced MT depolymerization (Pre) and also at the times indicated following return to 25°C. In cells expressing full-length Mto1-GFP, MTs were nucleated predominantly from the NE (red arrows), while the *mto1* N-terminal truncations exhibited spatially random nucleation (blue arrows) throughout the cytoplasm. All strains returned to steady-state by 3 minutes, although initial MT nucleation (1 minute) appeared to be less efficient in *nmt81:mto1(203-549)-GFP* and *nmt81:mto1(242-549)-GFP*. Bar, 5 μm. [Strains: KS819, KS5381, KS5385, KS5517, KS5520]

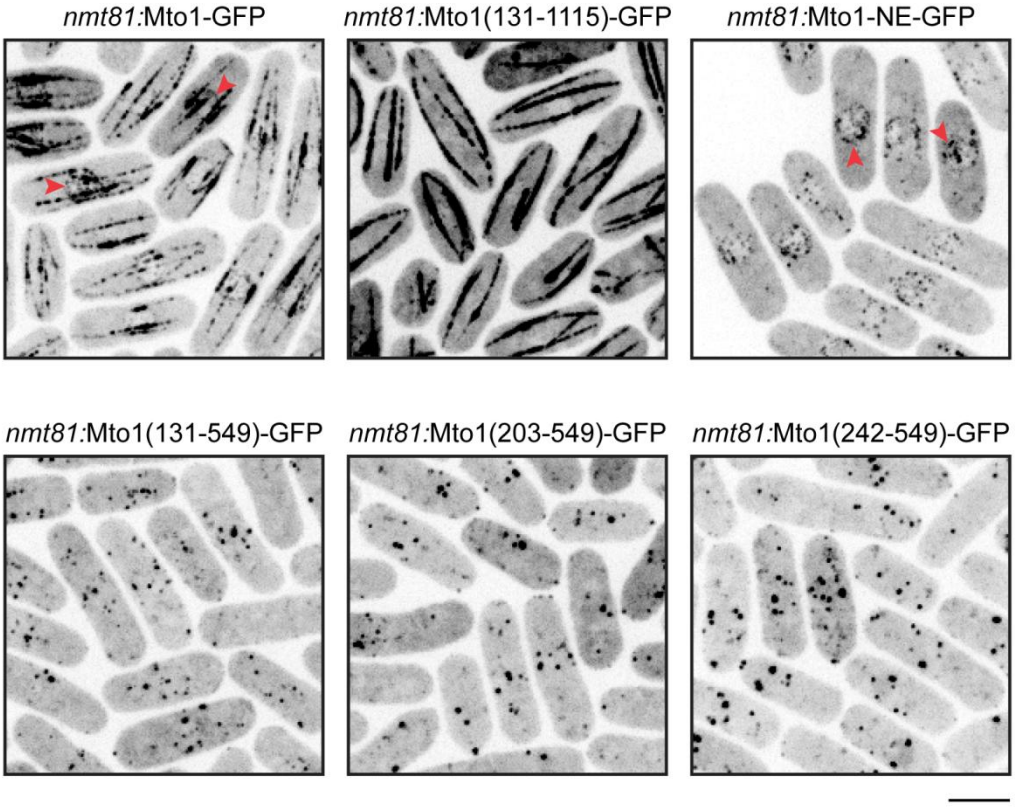

Figure 4.2: Over-expressed Mto1 N-terminal truncations do not localize to the NE. Full-length *nmt81:*Mto1-GFP is visible primarily along MTs, but can also be detected on the NE (red arrows). In contrast, *nmt81:*Mto1(131-1115)-GFP is absent from the NE, and appears to have increased localization to MTs. Localization to the NE is most apparent for *nmt81:*Mto1-NE-GFP, and is not observed with *nmt81:*Mto1(131-549)-GFP, *nmt81:*Mto1(203-549)-GFP, or *nmt81:*Mto1(242-549)-GFP, which instead appear as distinct puncta throughout the cytoplasm. Bar, 5 μm. [Strains: KS3887, KS5381, KS5647, KS5385, KS5517, KS5520]

4.2.2 The Mto1 N-terminus mediates localization to the NE

Strains expressing Mto1 N-terminal truncations from the endogenous *mto1* promoter were also constructed, in order to verify the phenotypes observed with the *nmt81*-expressed mutants. Like their over-expressed counterparts, endogenously-expressed Mto1(131-549)-GFP, Mto1(203-549)-GFP, and Mto1(242-549)-GFP failed to

localize to the NE, confirming that the Mto1 N-terminus was required for NE targeting (Figure 4.3).

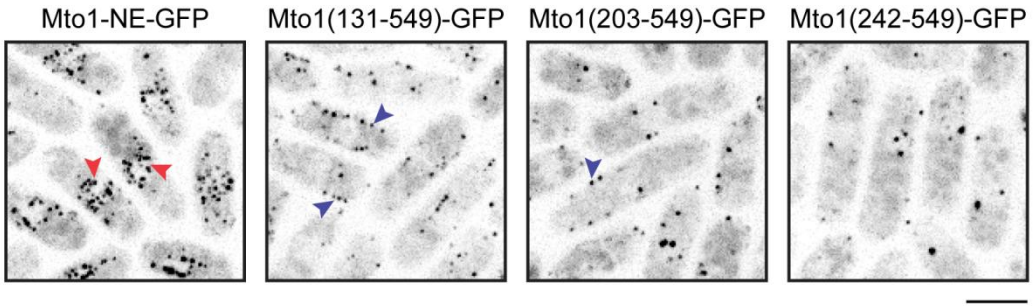

Figure 4.3: Endogenously-expressed Mto1 N-terminal truncations do not localize to the NE. The distinct NE localization (red arrows) of Mto1-NE-GFP was eliminated by truncation of the N-terminus in Mto1(131-549)-GFP, Mto1(203-549)-GFP, and Mto1(242-549)-GFP. Mto1(131-549)-GFP and Mto1(203-549)-GFP were often arranged in straight lines, indicating localization to MT bundles, presumably via association with MT minus-ends (blue arrows). Bar, 5 μm. [Strains: KS5209, KS5922, KS5924, KS5926]

To prove that this was true in context of the full-length Mto1 C-terminus, localization of endogenously-expressed Mto1(131-1115)-GFP was also analyzed. This required a modification of our localization assay, because under normal conditions, both Mto1-GFP and Mto1(131-1115)-GFP are visible primarily along MT bundles, and neither protein is easily detectable on the NE (Figure 4.4). Cells expressing Mto1-GFP or Mto1(131-1115)-GFP were treated with methyl benzimidazol-2-yl-carbamate (MBC) in order to disrupt MTs, and therefore the MT localization of Mto1 . Treatment with 50 μg/ml MBC caused Mto1-GFP, but not Mto1(131-1115)-GFP, to re-distribute to the NE, indicating that the Mto1 N-terminus contains a *bona fide* NE-localizing domain (Figure 4.4). That is, results obtained with the Mto1 C-terminal truncations were not simply an artefact due to the truncation. In the presence of MBC, Mto1(131-1115)-GFP was generally visible as 1-2 large spots per cell, which likely corresponded to the SPB and MT stubs left over from incomplete depolymerization (Figure 4.4).

These findings suggest a model in which Mto1 is dynamically partitioned between various cytoplasmic MTOCs. In wild-type cells, Mto1 is distributed amongst the SPB, MTs, and to a lesser extent the NE. Disrupting Mto1 localization to MTs, either by truncating the Mto1 C-terminus or depolymerizing MTs by cold-shock or MBC, results in a re-distribution of Mto1 to MTOCs on the NE. This suggests that the affinity of Mto1 for MTs and the SPB is greater than its affinity for MTOCs on the NE (Figure 4.5). Alternatively, MTs and the SPB may simply contain a greater number of Mto1 binding sites than the NE.

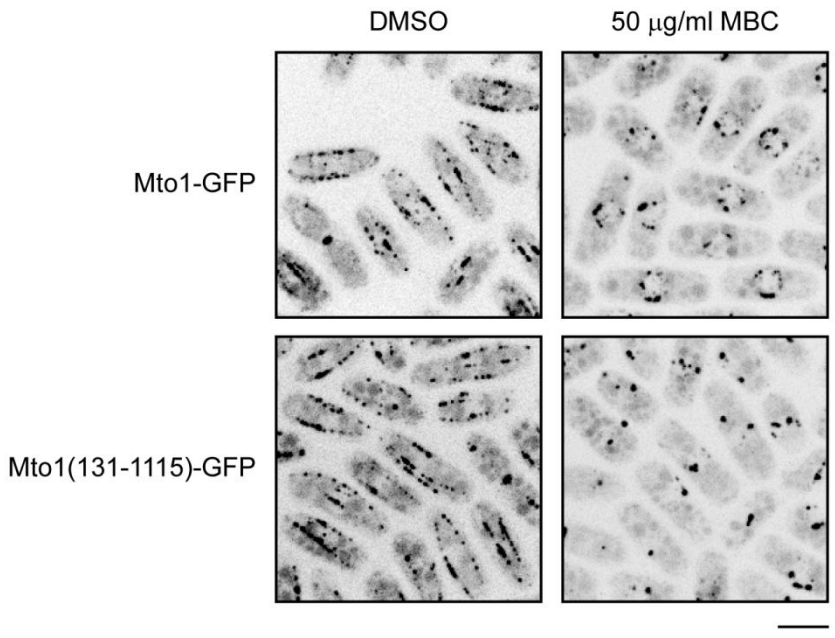

Figure 4.4 : Localization of full-length Mto1 to the NE requires the Mto1 N-terminus. Cells were treated with DMSO (control) or 50 μg/ml MBC. In controls, both Mto1-GFP and Mto1(131-1115)-GFP were visible primarily along MT bundles. Following treatment with MBC, Mto1-GFP re-distributed to the NE, while Mto1(131-1115)-GFP localized as 1-2 large spots per cell, which likely corresponded to MT stubs. Bar, 5 μm. [Strains: KS819, KS5940]

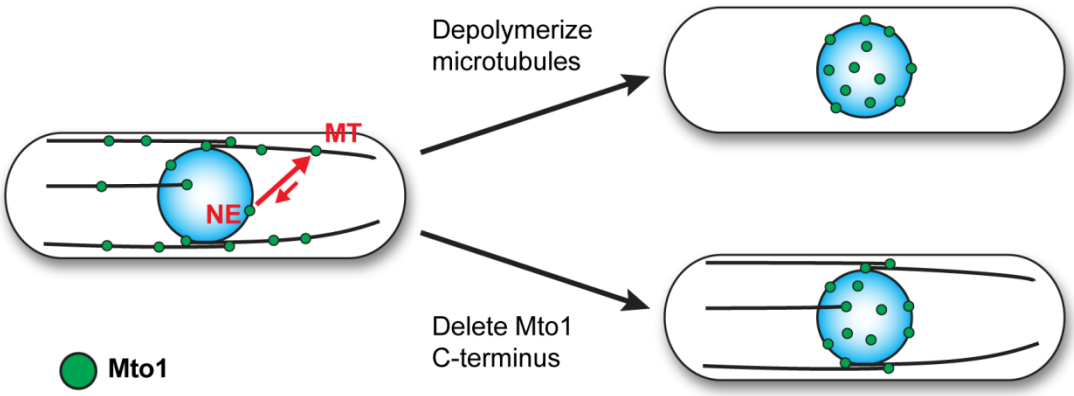

Figure 4.5: Mto1 is dynamically partitioned between different MTOCs. During interphase, full-length Mto1 is present on the SPB, MTs, and NE. Mto1 localization to the NE is fairly limited, suggesting Mto1 has a greater affinity for sites on the SPB and MTs. Depolymerizing MTs, by drug treatment or cold-shock, causes Mto1 to re-distribute to lower-affinity sites on the nuclear surface. Similarly, deleting the Mto1 C-terminal localization domains results in a re-distribution of Mto1 to the NE. In the latter case, Mto1 localization to MTs is most likely limited to MT minus-ends, where it persists following MT nucleation.

Next, I wanted to verify that Mto1(131-549)-GFP failed to decorate the MT lattice, as was seen with Mto1-NE-GFP (Figure 3. 6). Although Mto1(131-549)-GFP is observed on MT bundles, over-expression of *nmt81:*Mto1(131-549)-GFP does not result in the MT decoration observed with *nmt81:*Mto1-GFP (Figure 4.6; Figure 3.6). As described for Mto1-NE-GFP in Chapter 3, Mto1(131-549)-GFP localization to MTs may therefore be limited exclusively to MT minus ends following nucleation. To confirm this, I generated the CM1 mutant *mto1(131-9A1-549)-GFP*, which fails to nucleate cytoplasmic MTs. In the absence of *de novo* MT nucleation, Mto1(131-9A1-549)-GFP failed to associate with cytoplasmic MTs that had escaped from the nucleus (Figure 4.6), indicating that Mto1(131-549)-GFP is not targeted to the MT lattice. Therefore, Mto1(131-549) can be regarded as a "non-localizing" version of Mto1, being absent from conventional MTOCs on the SPBs, MTs, NE, and eMTOC.

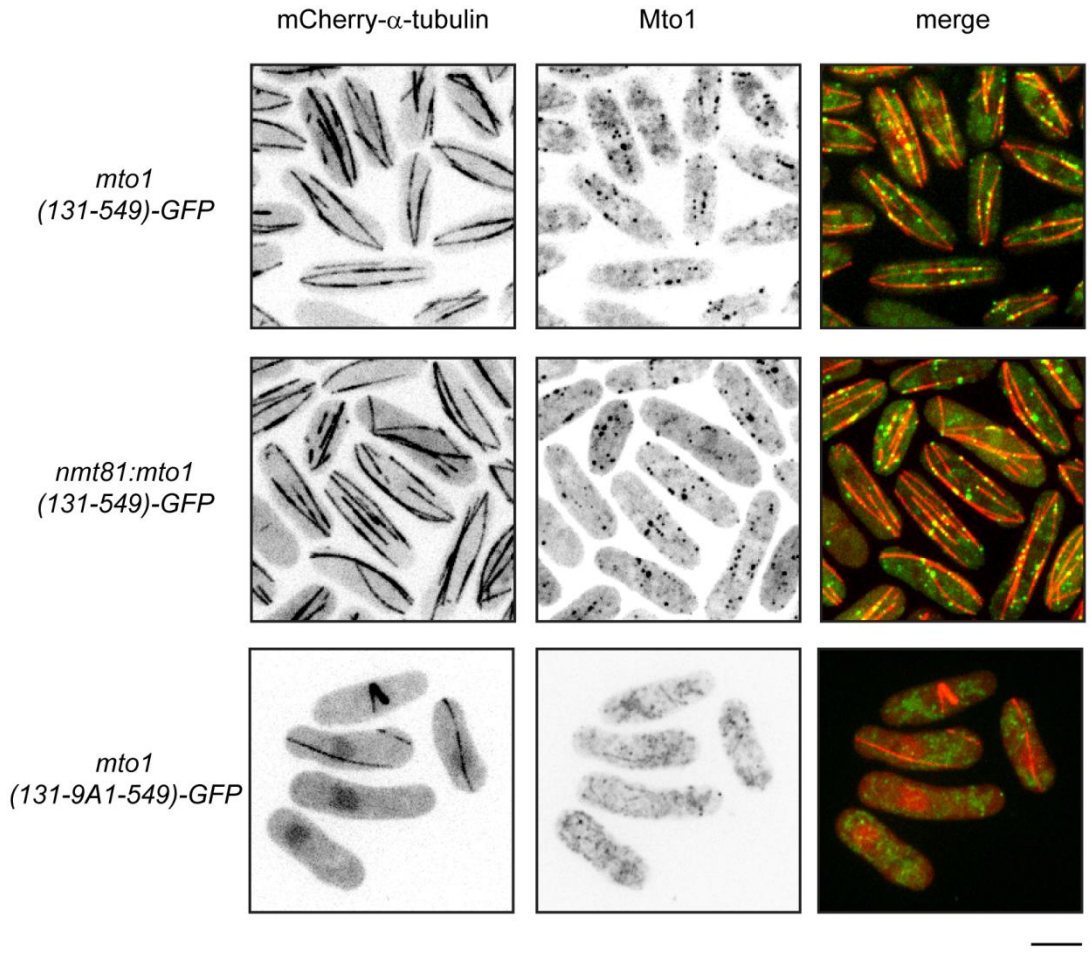

Figure 4.6: Mto1(131-549)-GFP does not decorate the MT lattice. Mto1(131-549)-GFP and over-expressed *nmt81:*Mto1(131-549)-GFP localized to MTs to essentially the same extent. This contrasts with full-length Mto1, which completely decorates MTs when over-expressed (see Figure 3.6), suggesting that Mto1(131-549)-GFP has little or no affinity for the MT lattice. Also, the CM1 mutant *mto1(131-9A1-549)-GFP* failed to nucleate cytoplasmic MTs, and Mto1(131-9A1-549)-GFP did not localize to MTs that had escaped from the nucleus. This implies that Mto1(131-549)-GFP localization to MTs may be limited to MT minus-ends following nucleation. Note that *nmt81:*Mto1(131-549)-GFP signal is presented at a different contrast than Mto1(131-549)-GFP and Mto1(131-9A1-549)-GFP, as *nmt81:*Mto1(131-549)-GFP signal would otherwise be nearly saturated. Bar, 5 μm. [Strains: KS6678, KS6680, KS6676]

Localization of the γ-TuC in the *mto1* N-terminal truncation mutants was also investigated, in order to determine whether or not Mto1 localization to the NE was required for γ-TuC localization to the NE. Simultaneous removal of the N- and C-terminal localization domains in *mto1(131-549)* and *mto1(131-549)-GFP* essentially abolished the Alp4-tdT NE localization observed in *mto1-NE* (Figure 4.7; Figure 3.4). However, cells expressing Mto1(131-1115), which retains the Mto1 C-terminal localization domains, showed normal Alp4-tdT localization to MTs, SPBs, and the eMTOC (Figure 4.7). Very faint Alp4-tdT signal could occasionally be detected on the NE in the *mto1* N-terminal truncation mutants, but overall it is apparent that robust localization of the γ-TuC to the NE requires the Mto1 N-terminus. Further, as seen in *mto1(1-549)*, Alp-tdT in *mto1(131-549)* and *mto1(131-549)-GFP* showed only very limited association with MT bundles, and was presumably limited to MT minus-ends (Figure 4.7). Thus, like Mto1(131-549) itself, the γ-TuC in *mto1(131-549)* appears to be essentially absent from conventional MTOCs.

Figure 4.8 shows the co-localization of Alp4-tdT with Mto1(131-1115)-GFP and Mto1(131-549)-GFP. As seen with Mto1-GFP and Mto1-NE-GFP, both Mto1(131-1115)-GFP and Mto1(131-549)-GFP were occasionally observed on their own, without any associated Alp4-tdT signal. Again, this is consistent with the notion that Mto1/2 forms a sub-complex independent of association with the γ-TuC.

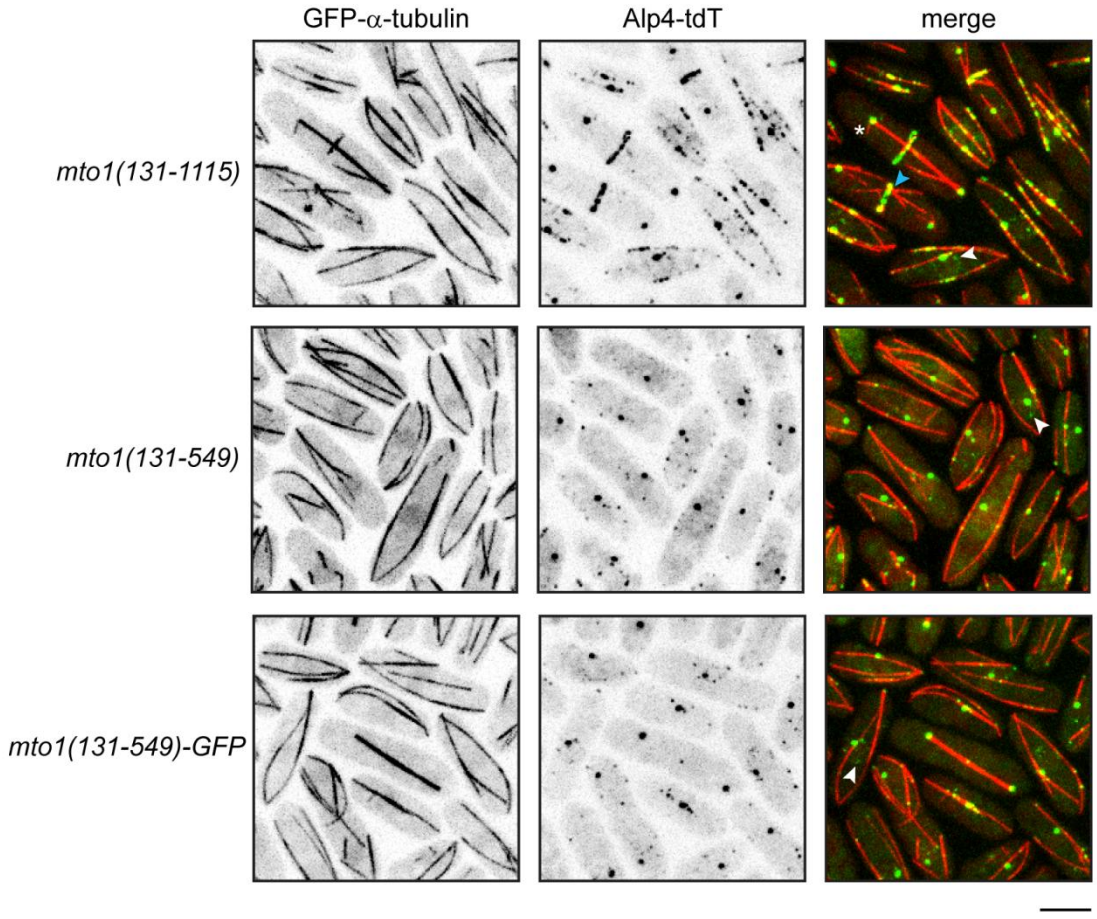

Figure 4.7: γ-TuC localization to the NE is virtually abolished in *mto1* N-terminal truncation mutants. Interphase MTs (red) and Alp4-tdT (γ-TuC; green) localization in *mto1* N-terminal truncation strains. Alp4-tdT exhibited only very limited localization to the NE (white arrows) when the *mto1* N-terminus was truncated in *mto1(131-1115)*, *mto1(131-549)*, and *mto1(131-549)-GFP*. Localization of Alp4-tdT to MTs, SPBs, and the eMTOC was unaffected in *mto1(131-1115)*, as confirmed by the observation of astral (white asterisk) and PAA (blue arrow) MTs. Bar, 5 μm. [Strains: KS5942, KS6635, KS5937]

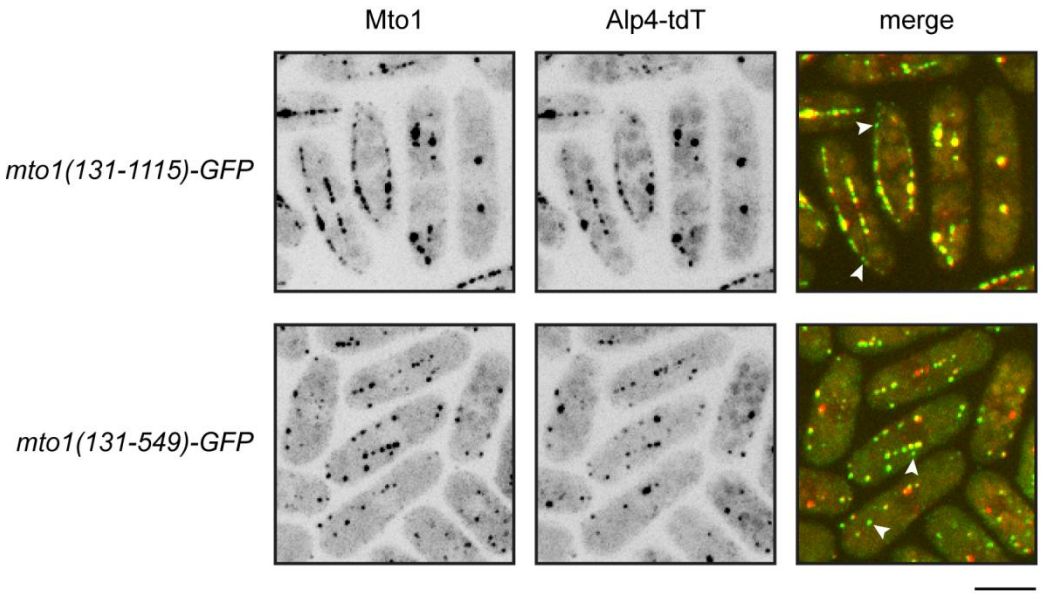

Figure 4.8: N-terminal truncations of Mto1 co-localize with the γ-TuC. During interphase, Mto1(131-549)-GFP co-localized with Alp4-tdT at suspected MT minus-ends, while Mto1(131-1115)-GFP and Alp4-tdT co-localized at the SPB and along the MT lattice. On occasion, both Mto1(131-549)-GFP and Mto1(131-1115)-GFP were observed alone, with no corresponding Alp4-tdT signal (white arrows). Bar, 5 μm. [Strains: KS6103, KS5933]

4.2.3 Mto1-bonsai promotes spatially random MT nucleation

The ability to remove the Mto1 N- and C-terminal localization sequences allowed me to directly address an important question: Can cells which express a "non-localizing" version of Mto1 still effectively nucleate cytoplasmic MTs, or is γ-TuC localization to conventional MTOCs necessary for MT nucleation?

First, I wished to determine *how much* of the Mto1 N-terminus could be removed while preserving cytoplasmic MT nucleation. The more extensive 203- and 242- N-terminal truncations of Mto1 appeared to have impaired function. Both *mto1(203-1115)* and *mto1(242-1115)* cells showed somewhat curved morphology, and this was more pronounced when the C-terminus was also truncated, as in *mto1(203-549)-GFP and*

mto1(242-549)-GFP (Figure 4.9A). By contrast, *mto1(131-1115)* had wild-type morphology, and *mto1(131-549)-GFP* cells showed only occasional, slight curving. More importantly, however, the more extensive *mto1* truncation mutants exhibited abnormal cytoplasmic MT arrays. Imaging of GFP-α-tubulin revealed that *mto1(203-549)-GFP* and *mto1(242-549)-GFP* cells typically contained 1-2 long, curved MT bundles, a characteristic feature of *mto1Δ* (Figure 4.9B). Also, *de novo* nucleation of MTs was rarely observed in *mto1(203-549)-GFP* and *mto1(242-549)-GFP*, consistent with the weak MT nucleation observed in regrowth experiments with *nmt81:*mto1(203-549)-GFP and *nmt81:*mto1(242-549)-GFP (Figure 4.1B).

When expressed from the endogenous *mto1* promoter, the steady state levels of Mto1(203-549)-GFP and Mto1(242-549)-GFP were lower than Mto1(131-549)-GFP (75% and 50% of the Mto1(131-549)-GFP expression level, respectively) (Figure 4.9C). This reduced expression could account, at least in part, for the compromised MT nucleation observed in *mto1(203-549)-GFP* and *mto1(242-549)-GFP* cells.

Cells expressing Mto1(131-549)-GFP, on the other hand, had qualitatively normal MT arrays and frequently nucleated new MTs (Figure 4.9; Figure 4.10). Because it represented a minimal, trimmed but functional version of Mto1, Mto1(131-549) was given the name "Mto1-bonsai". Quantification of nucleation events revealed that *mto1-bonsai* and *mto1-bonsai-GFP* nucleated MTs in a spatially random manner (Figure 4.10). This clearly differs from *mto1+* or *mto1-NE* cells, where MT nucleation occurrs almost exclusively from the NE or the region around the NE (Figure 3.9; Figure 4.10). It is important to note that MT nucleation counted in the "nuclear envelope region" includes nucleation from the NE itself, as well as nucleation occurring in the cytoplasm adjacent to the NE. Therefore, if MT nucleation was spatially random, we would expect to see most nucleation events occurring in the larger "cytoplasmic region", but would also expect some nucleation in the "nuclear envelope region". This is precisely what we observe in *mto1-bonsai* and

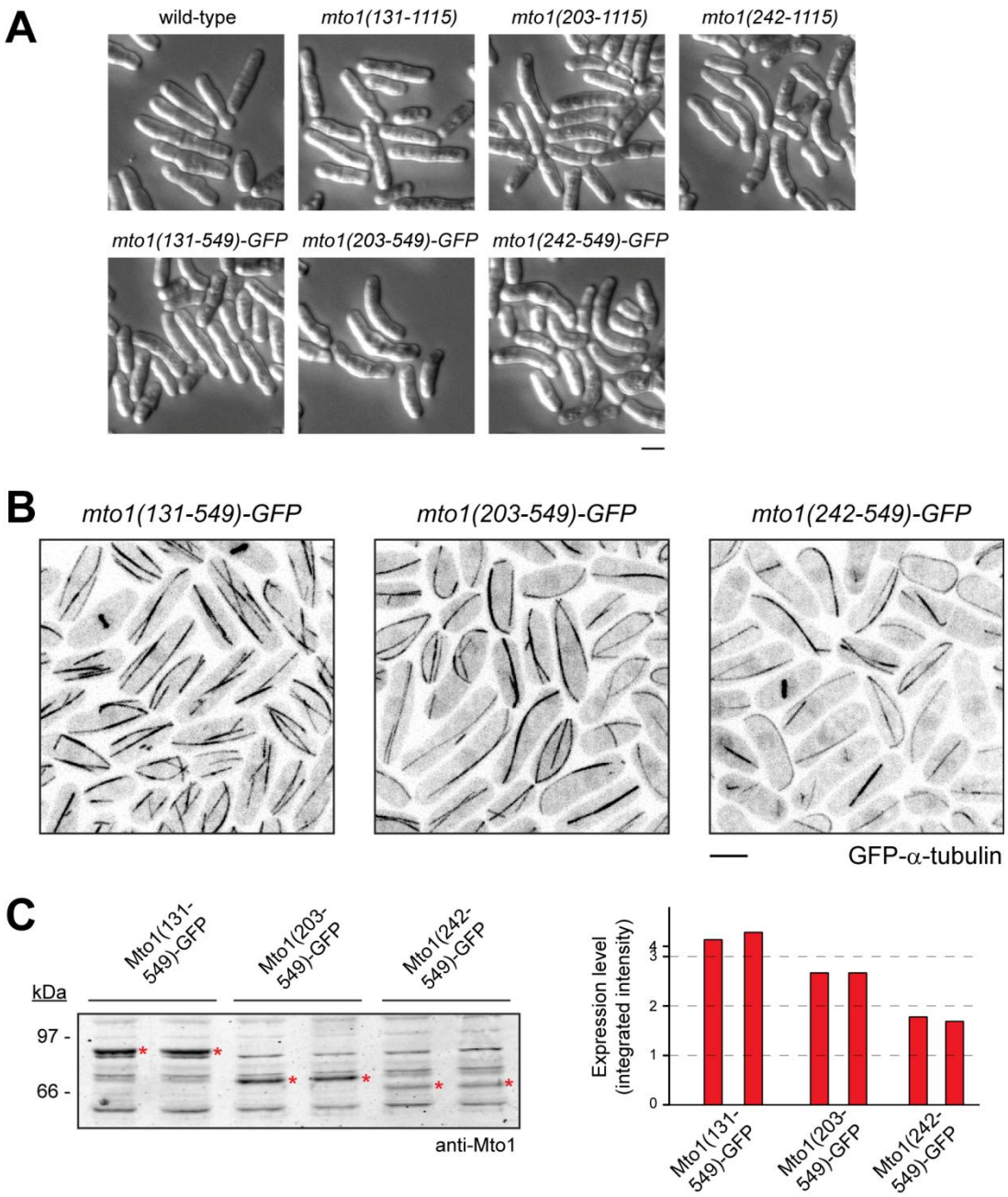

Figure 4.9: Extensive truncation of the Mto1 N-terminus impairs Mto1 function. (A) Cell morphology following growth to stationary phase and re-introduction to fresh medium. *mto1(131-1115)* was found to have wild-type morphology, but further N-terminal truncation in *mto1(203-1115)* and *mto1(242-1115)* resulted in a curved shape characteristic of *mto1*Δ. Similarly, *mto1(203-549)-GFP* and *mto1(242-549)-GFP* were clearly curved, while *mto1(131-549)-GFP* showed only occasional, slightly curved cells. (B) Imaging of GFP-α-tubulin revealed that *mto1(131-549)-GFP* exhibited qualitatively normal MT arrays, while *mto1(203-549)-GFP* and *mto1(242-549)-GFP* typically contained 1-2 abnormal MT bundles, indicative of impaired MT nucleation. (C) Anti-Mto1 western blot of whole cell extracts (left) and quantification of Mto1 expression levels (right) in various *mto1* truncation mutants. Two isolates of each strain were analyzed. Red asterisks indicate Mto1 bands. Mto1(203-549)-GFP and Mto1 (242-549)-GFP were expressed at lower levels than Mto1(131-549)-GFP. Bar, 5 μm. [Strains: KS516, KS5851, KS5853, KS5855, KS5922, KS5924, KS5926, KS5929, KS5930, KS5931]

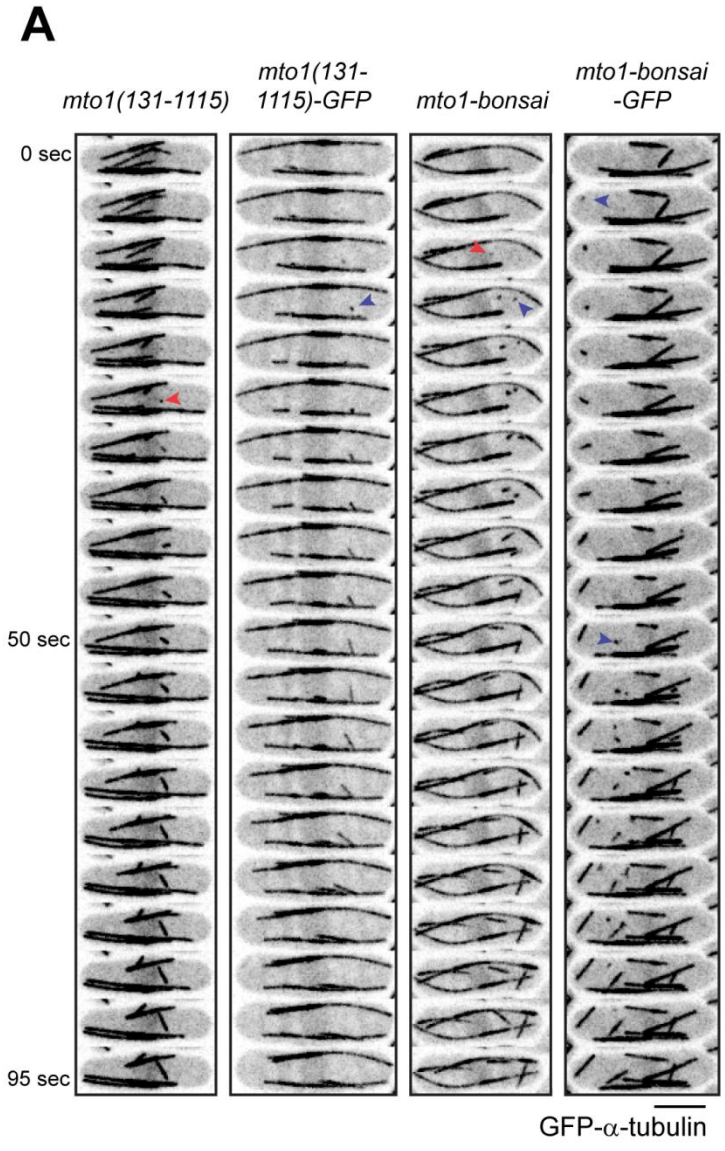

Figure 4.10: MT nucleation is spatially random in *mto1-bonsai*. (A) Stills from movies of GFP-α-tubulin (5 sec time interval), with MT nucleation from the NE region (red arrows) and freely in the cytoplasm (blue arrows) indicated. *mto1(131-1115)*, *mto1(131-1115)-GFP*, *mto1-bonsai*, and *mto1-bonsai-GFP* all exhibited *de novo* MT nucleation. (B) Quantification of MT nucleation in the cytoplasmic and NE regions. Both *mto1-bonsai* and *mto1-bonsai-GFP* nucleated MTs in a spatially random manner, with the majority of nucleation events occurring freely in the cytoplasm. A low MT nucleation frequency was reported for *mto1(131-1115)* and *mto1(131-1115)-GFP*, likely because MT nucleation from the SPB and along MTs is not easily quantified. Data for *mto1+*, *mto1-GFP*, *mto1-NE*, and *mto1-NE-GFP* are identical to figure 3.9, and are presented for comparison. Average nucleation frequency ± SEM is reported. Bar, 5 μm. [Strains (cells counted, nucleation events counted): KS5944 (28, 40), KS6102 (45, 28), KS6637 (20, 43), KS5929 (16,71)]

mto1-bonsai-GFP cells (Figure 4.10). Most importantly, these findings demonstrate that targeting of Mto1-bonsai/Mto1-bonsai-GFP and the γ-TuC to conventional MTOCs is not necessary for cytoplasmic MT nucleation. This indicates that additional factors present at MTOCs are not required for activation of the γ-TuC.

The frequency of MT nucleation in un-tagged *mto1-bonsai* was considerably lower than in *mto1-bonsai-GFP*. This can be explained by the low expression level of Mto1-bonsai, relative to both Mto1-bonsai-GFP and the other Mto1 truncations, as determined by western blotting (Figure 4.11). Still, the fairly limited amount of Mto1-bonsai present in cells was clearly sufficient to promote MT nucleation. The effect of GFP-tagging on Mto1 expression levels varied. While tagging increased steady-state levels of Mto1-bonsai, it decreased levels of full-length Mto1 and Mto1(131-1115), and had no effect on Mto1-NE (Figure 4.11). In a previous study, C-terminal GFP-tagging was found to decrease the levels of full-length Mto1, while increasing the stability of various C-terminal truncation mutants ranging in size from Mto1(1-1051) to Mto1(1-1095) (Samejima et al., 2010). Nonetheless, with the exception of full-length Mto1, a decrease in protein levels for any given Mto1 fragment corresponded to a reduction in MT nucleation frequency (Figure 3.9; Figure 4.10; Figure 4.11).

Truncation of the Mto1 N-terminus did not appear to have a significant effect on the frequency of MT nucleation, as Mto1-NE-GFP and Mto1-bonsai-GFP are expressed at similar levels and nucleate MTs at comparable rates (0.7 $cell^{-1}min^{-1}$ compared to 0.5 $cell^{-1}min^{-1}$) (Figure 3.9; Figure 4.10; Figure 4.11). Very little nucleation was observed in *mto1(131-1115)* and *mto1(131-1115)-GFP* (Figure 4.10). However, this is most likely because MT nucleation in these strains occurs primarily along existing MTs or from the SPB, and therefore tends to go undetected. Given the normal MT arrays observed in both *mto1(131-1115)* and *mto1(131-1115)-GFP*, it is clear that these strains are not genuinely

deficient in *de novo* MT assembly (Figure 4.10). Taken together, these results suggest that Mto1 has a distinct role in activating MT nucleation from the γ-TuC, that is independent of its role in recruiting the γ-TuC to MTOCs.

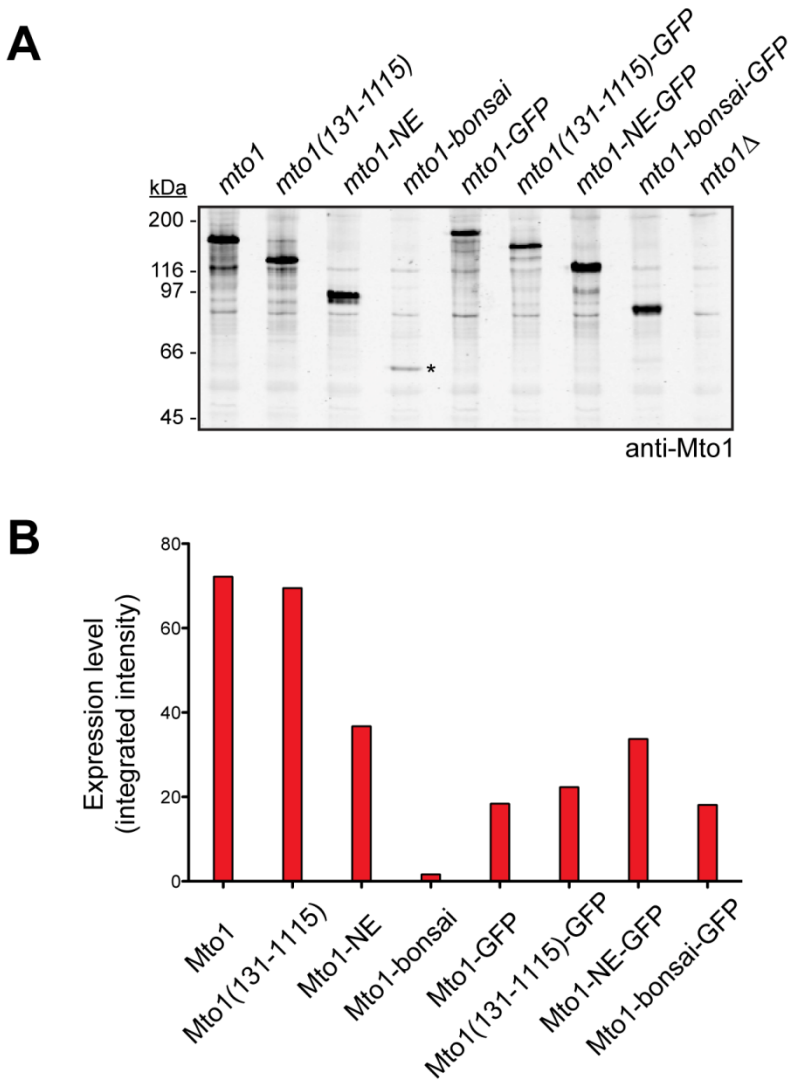

Figure 4.11: The various Mto1 truncations are expressed at different levels. (A) Whole cell extracts from wild-type and mutant *mto1* strains were analyzed by anti-Mto1 western blot. An asterisk indicates the position of the faint Mto1-bonsai band. (B) Quantification of wild-type and mutant Mto1 expression levels. All of the GFP-tagged versions of Mto1 were expressed at similar levels, making direct comparison of phenotypes in these *mto1* mutants possible. Un-tagged Mto1-bonsai had a particularly low expression level. [Strains: KS515, KS5851, KS5607, KS6626, KS819, KS5940, KS5209, KS5922, KS1017]

4.2.4 Mto1/2-bonsai activates MT nucleation by the γ-TuC

I hypothesized that if the Mto1/2 complex was directly involved in activating the γ-TuC, it would have to be associated with the γ-TuC upon MT nucleation, even when MT nucleation occurred away from MTOCs in the *mto1-bonsai* mutant. In other words, I predicted that both the γ-TuC and Mto1/2-bonsai complex would be present at the minus-ends of MTs during *de novo* MT nucleation. Indeed, live-cell imaging with mCherry-α-tubulin revealed that Mto1-bonsai-GFP, as well as Mto2-GFP, Alp4-GFP, and Alp6-GFP in an *mto1-bonsai* background, were associated with the ends of newly-nucleated MTs (Figure 4.12). Imaging was performed at a high time resolution of 1.63 seconds, allowing for the unambiguous detection of *de novo* nucleation events and associated Mto1/2 and γ-TuC puncta. The nucleation of MTs from puncta containing Mto1-bonsai-GFP and Mto2-GFP, in addition to the γ-TuC, strongly suggests that Mto1/2 has a direct role in γ-TuC activation.

Fluorescence quantification was used to determine the stoichiometry of Mto1/2-bonsai and γ-TuC components in the puncta associated with MT nucleation. Such quantification would be extremely difficult in *mto1+* or *mto1-NE*, given the "crowded" nature of MTOCs in these strains. The spatially random nucleation observed in *mto1-bonsai*, on the other hand, allowed for easy identification of individual nucleation events and associated nucleating puncta. The intensity of Mto1-bonsai-GFP, Mto2-GFP, Alp4-GFP, and Alp6-GFP nucleating puncta at or near the moment of MT nucleation was measured, and converted into a number of molecules by comparison to standards imaged under the same conditions (Figure 4.13; 4.14). This technique was initially developed in Tom Pollard's lab, where the copy numbers of a large variety of cytokinesis proteins were determined by a combination of fluorescence microscopy, flow cytometry, and quantitative immunoblotting (Wu and Pollard, 2005). Here, I employed GFP-tagged Polo kinase (Plo1-

GFP) and myosin regulatory light chain (Rlc1-GFP) as standards in determining copy numbers for my proteins of interest.

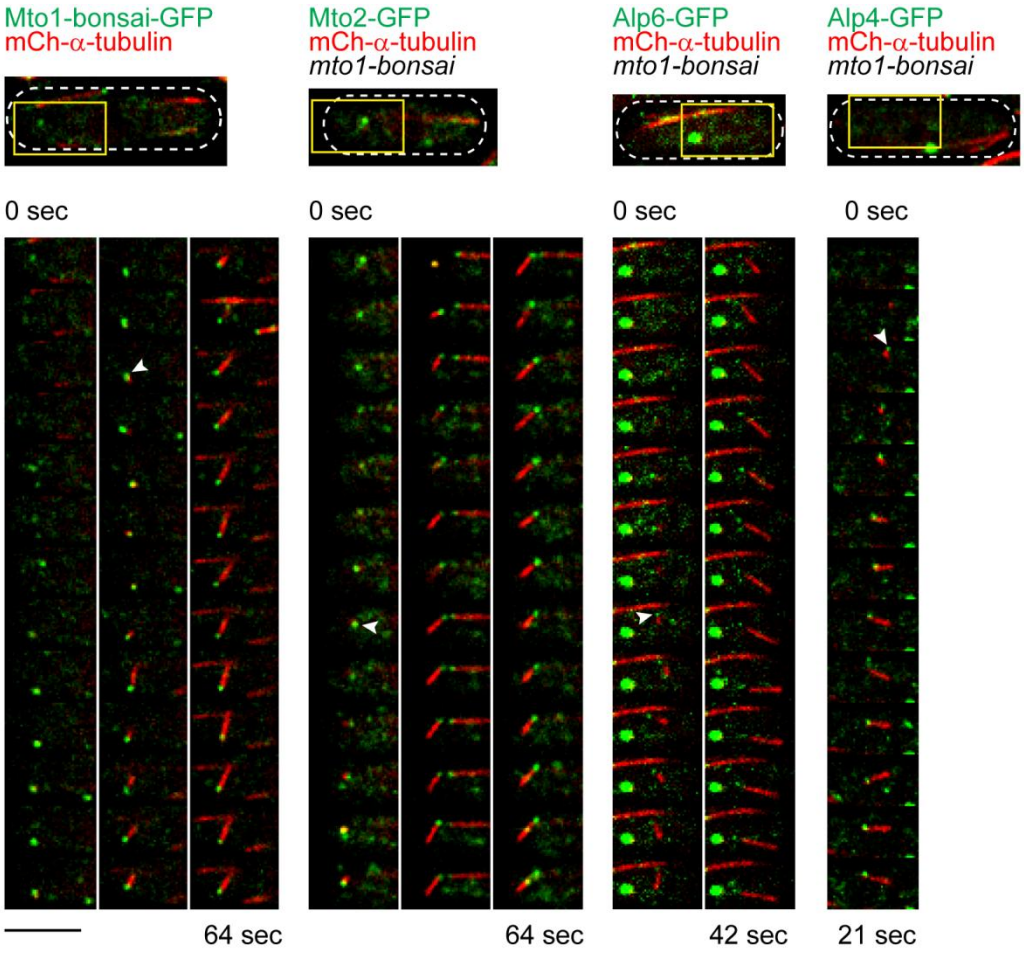

Figure 4.12: Discrete puncta containing Mto1/2-bonsai and the γ-TuC nucleate MTs. Stills from movies of Mto1-bonsai-GFP, Mto2-GFP, Alp4-GFP, and Alp6-GFP imaged together with mCherry-α-tubulin (1.63 second time resolution). Mto2-GFP, Alp4-GFP, and Alp6-GFP were imaged in an *mto1-bonsai* background. The images shown are single Z-sections (Mto1-bonsai-GFP and Mto2-GFP) or sum projections of 2 Z-sections (Alp4-GFP and Alp6-GFP).The dashed white lines show the cell outline, and yellow boxes indicate the region of the cell shown in the montages below. MT nucleation was associated with Mto1-bonsai-GFP, Mto2-GFP, Alp4-GFP, and Alp6-GFP puncta (white arrows). These nucleating puncta persisted at MT ends as they polymerized. Bar, 5 μm. [Strains: KS6678, KS6791, KS6776, KS6898]

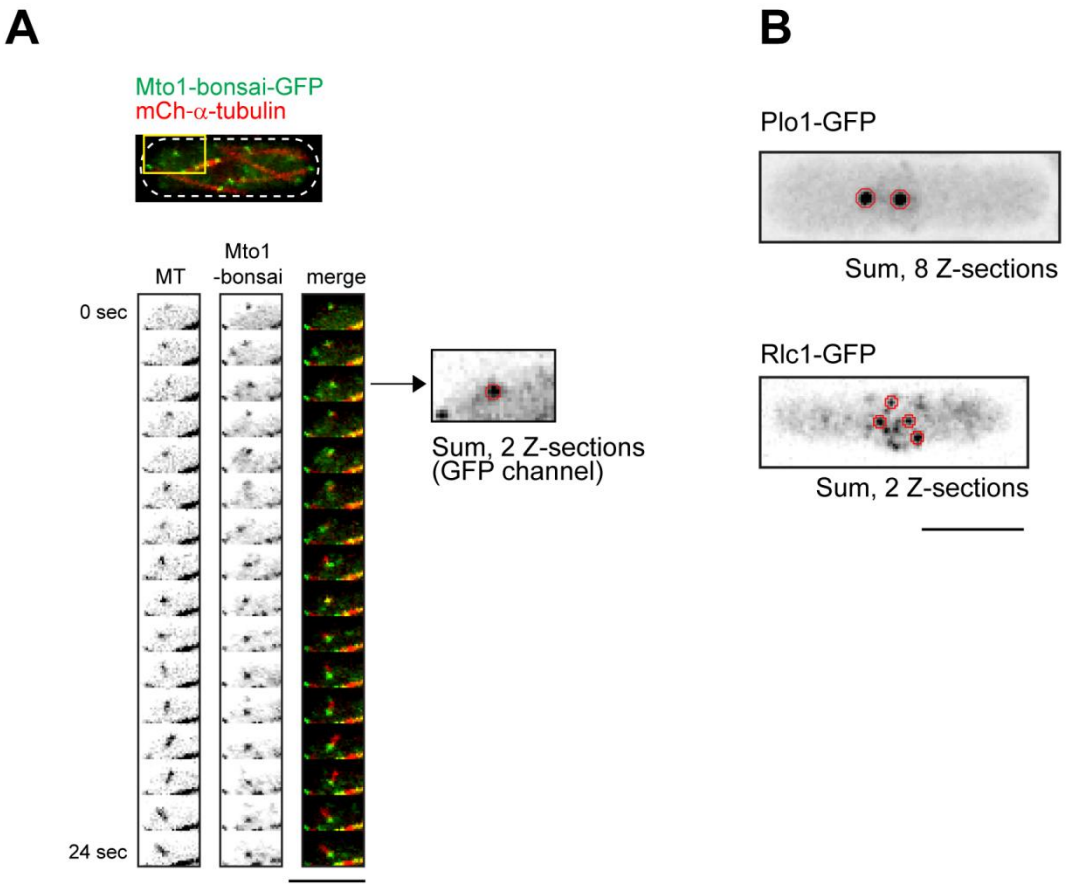

Figure 4.13: The number of molecules in Mto1-bonsai, Mto2, Alp4, and Alp6 nucleating puncta was determined by comparison to known standards. (A) An example of the quantification method. Stills from a movie of Mto1-bonsai-GFP with mCherry-α-tubulin are presented as in Figure 4.12 (single Z-sections), with MTs and Mto1-bonsai also shown separately. The intensity of the nucleating particle (red circle) at or very near the moment of MT nucleation was quantified in a sum projection of 2 Z-sections (shown at 2X zoom). Mto2-GFP, Alp4-GFP, and Alp6-GFP were quantified in an identical manner. (B) Plo1-GFP at recently separated SPBs and Rlc1-GFP at cytokinesis nodes have known copy numbers, and were thus used as standards. They were quantified in sum projections of 8 and 2 Z-sections, respectively. The increased number of Z-sections used in quantifying Plo1-GFP was necessary to ensure that all signal was included. For all quantification, adjacent cytoplasmic signal, corresponding to the appropriate number of Z-sections, was subtracted as background. Bar, 5 μm. [Strains: KS6678, KS6684, KS6682]

Previous studies have demonstrated that cytokinesis nodes contain on average 41.3 ± 23 molecules of Rlc1 (Laporte et al., 2011), while around 220 molecules of Plo1 are present at each SPB during early mitosis (Wu and Pollard, 2005). The intensities of Mto1/2-bonsai and γ-TuC puncta were closer to those observed for Rlc1-GFP nodes than for Plo1-

GFP, with Plo1-GFP signal being approximately an order of magnitude greater (Figure 4.14; Figure 4.15). Rlc1-GFP nodes were therefore used as the standard in determining Mto1-bonsai-GFP, Mto2-GFP, Alp4-GFP, and Alp6-GFP copy numbers. Plo1-GFP intensity was analyzed during each imaging session, in order to confirm the fidelity of intensity measurements . As seen in Figure 4.15, the distribution of intensities and average intensity for Plo1-GFP was reproducible across multiple experiments.

The Mto1-bonsai-GFP and Mto2-GFP nucleating particles were composed of an average of 12.8 and 13.0 molecules, respectively (Figure 4.14). Evidently, this reveals a 1:1 stoichiometry of Mto1-bonsai:Mto2 in the complexes associated with MT nucleation, and suggests that these larger assemblies are composed of some sort of core Mto1/2-bonsai subunit, such as a dimer or tetramer. Notably, the value 13 also matches the number of protofilaments in a MT, as well as the number of γ-tubulins thought to be present in single γ-TuRCs.

Alp4-GFP and Alp6-GFP also showed very similar intensities, corresponding to an average of 8.5 and 8.4 molecules per nucleating puncta, respectively (Figure 4.14). This is consistent with existing models of the γ-TuC, where GCP2 and GCP3 are present in equal copy number (Kollman et al., 2010; Kollman et al., 2008). In addition, the values are remarkably close to the 6-7 copies of each protein required to produce a γ-TuC with a 13 γ-tubulin template.

Overall, these values indicate that the puncta observed correspond to single γ-TuRCs, making this the first direct, *in vivo* observation of individual γ-TuCs nucleating individual MTs. Further, the presence of 13 copies of both Mto1-bonsai and Mto2 implies that there are roughly 2 copies of Mto1 and 2 copies of Mto2 associated with each γ-TuSC in a nucleation-competent complex. This suggests that higher-order assemblies of the Mto1/2 complex contribute to γ-TuC activation.

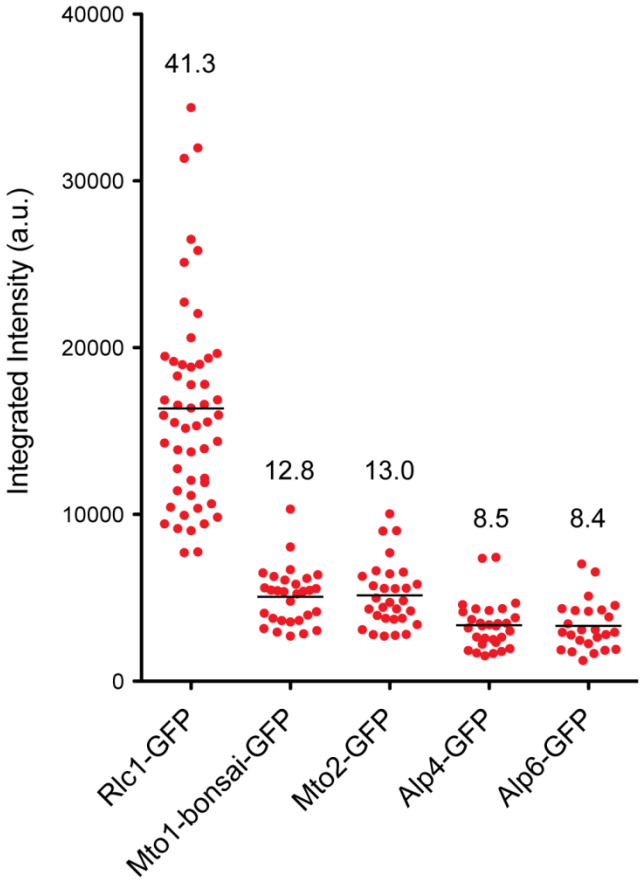

Figure 4.14: MTs are nucleated by complexes containing approximately 13 copies each of Mto1-bonsai and Mto2. The intensities of individual Rlc1-GFP nodes and Mto1-bonsai-GFP, Mto2-GFP, Alp4-GFP, and Alp6-GFP nucleating puncta were plotted. The black bar indicates the average intensity for each protein, with the corresponding copy number indicated above. A previous study revealed that cytokinesis nodes contain on average 41.3 molecules of Rlc1-GFP (Laporte et al., 2011). This value was used as a standard in calculating the average copy numbers indicated for Mto1-bonsai-GFP, Mto2-GFP, Alp4-GFP, and Alp6-GFP. [Strains: KS6682, KS6678, KS6791, KS6776, KS6898]

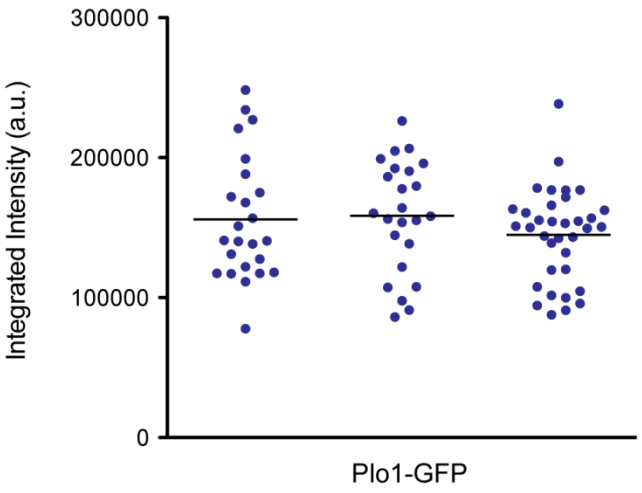

Figure 4.15: The intensity observed per GFP molecule is consistent across multiple experiments. Plo1-GFP was imaged and quantified during each imaging session involving fluorescence quantification, in order to verify that constant intensity/GFP was being observed. In three different experiments, the average Plo1-GFP intensity at recently-separated SPBs (black bars) was nearly identical. [Strain: KS6684]

4.3 Discussion

Analysis of the *mto1-bonsai* mutant provides strong evidence that the Mto1/2 complex is a γ-TuC activator. MT nucleation occurred directly from particles containing Mto1-bonsai-GFP and Mto2-GFP, in addition to the γ-TuC. Further, MT nucleation was found to be spatially random in *mto1-bonsai*, occurring without γ-TuC localization to conventional MTOCs. Significantly, this reveals that the role of Mto1/2 in activating the γ-TuC is independent of its role in localizing the γ-TuC to specific sub-cellular sites. This also shows that additional factors present at MTOCs are not required for γ-TuC activation and MT nucleation. Of course, I cannot rule out the possibility that additional, unidentified factors also contribute to γ-TuC activation, regardless of γ-TuC localization to MTOCs.

I have described Mto1-bonsai as the minimal fragment of Mto1 that is capable of promoting MT nucleation by the γ-TuC. However, some nucleation may be retained in more extensively truncated *mto1* mutants. I showed in chapter 3 that further truncation of the Mto1 C-terminus abolishes cytoplasmic MT nucleation, likely by eliminating the Mto1-Mto2 interaction. More extensive truncation of the Mto1 N-terminus, on the other hand, does not appear to completely eliminate MT nucleation. Both *mto1(203-549)-GFP* and *mto1(242-549)-GFP* cells show only limited MT nucleation, but this clearly differs from *mto1Δ* cells which are completely incapable of nucleating cytoplasmic MTs. Mto1(203-549)-GFP and Mto1(242-549)-GFP have lower steady-state expression levels than Mto1-bonsai-GFP, which may account for the reduced nucleation observed in these mutants. Indeed, over-expression of *nmt81:*Mto1(203-549)-GFP results in MT nucleation comparable to that seen in *nmt81:mto1-bonsai-GFP*, as determined by MT regrowth experiments. Over-expression of *nmt81:*Mto1(242-549)-GFP has a more modest effect, although it is clear that *nmt81:*mto1(242-549)-GFP cells can in fact nucleate MTs. Thus, in principle, N-terminal truncations smaller than Mto1-bonsai-GFP may be capable of promoting MT nucleation by the γ-TuC. Still, *mto1-bonsai* remains the smallest mutant identified that is capable of robust MT nucleation, when expressed from the endogenous *mto1* promoter.

Higher-order assemblies of Mto1/2 appear to be responsible for activating the γ-TuC. Fluorescence quantification revealed that MTs were nucleated by γ-TuCs associated with approximately 13 copies each of Mto1-bonsai-GFP and Mto2-GFP. This implies that in an actively nucleating γ-TuC, each γ-TuSC is associated with roughly 2 copies of Mto1 and 2 copies of Mto2. Therefore, one might predict that Mto1/2 contributes to γ-TuC activation by promoting γ-TuSC multimerization. Also, Mto1/2-binding could induce conformational changes in the γ-TuC, which are thought to be necessary for generating an effective γ-

tubulin template for MT assembly (Kollman et al., 2011; Kollman et al., 2010). A model for γ-TuC activation by the Mto1/2-bonsai complex is shown in figure 4.16.

Recently, a similar study performed in budding yeast determined the stoichiometry of γ-TuC components present at the ends of MTs released from the SPB. MTs were found to be associated with 17 γ-tubulin, 7 Spc97, and 9 Spc98 molecules (Erlemann et al., 2012), values which are comparable to those seen here for Alp4 and Alp6. Significantly, however, both analyses revealed copy numbers that exceed the 7 γ-TuSCs that produce a 13 γ-tubulin template *in vitro* (Kollman et al., 2010). The authors of the budding yeast study proposed that the additional γ-tubulin and Spc98 may help to stabilize the γ-TuC or determine the site of the MT seam, rather than contributing directly to the γ-tubulin template (Erlemann et al., 2012). A similar model could account for the additional Alp4 and Alp6 molecules observed here.

Importantly, my fluorescence quantification was performed on γ-TuCs and Mto1/2-bonsai complexes that were in the process of nucleating MTs. This allowed me to determine the composition of complexes that were "active" and capable of MT nucleation. Ideally, I would also like to have determined the composition of complexes that were *not* actively nucleating MTs. This would allow me to address, for example, whether or not Mto1/2-bonsai exists primarily as smaller sub-complexes, which promote MT nucleation only upon multimerization into higher order assemblies. However, these "non-nucleating" particles diffused rapidly around the cell and persisted for only short periods of time, making them essentially impossible to accurately identify and quantify. In contrast, the actively nucleating puncta were much easier to identify, owing to their clear association with nascent MTs.

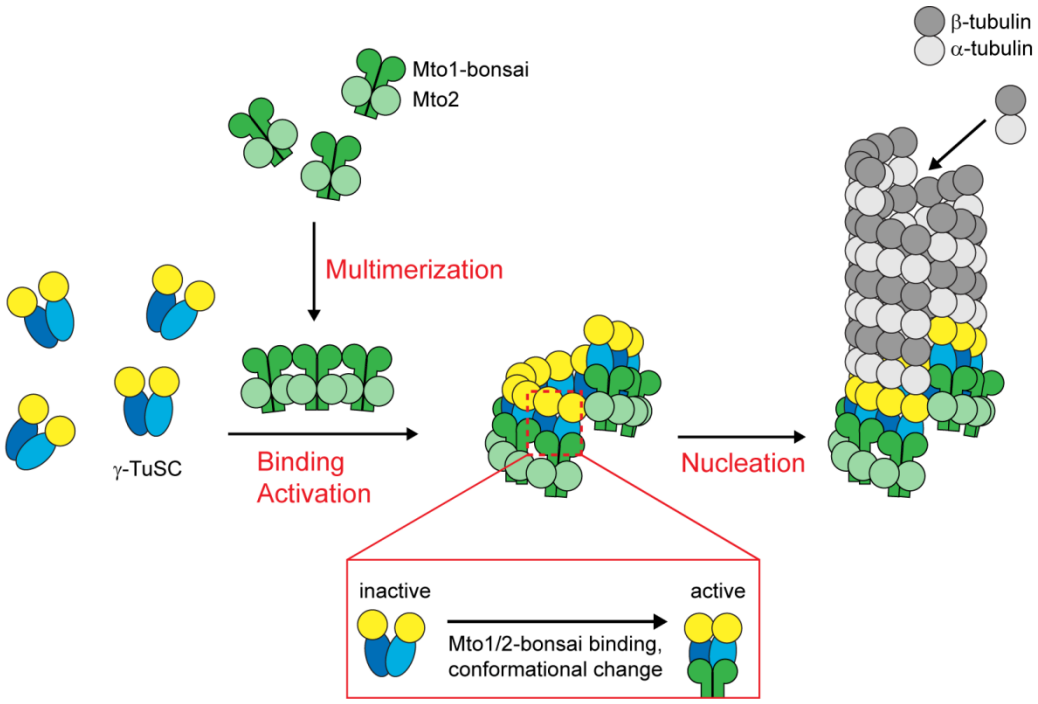

Figure 4.16: Multimers of Mto1/2-bonsai activate the γ-TuC. Mto1/2-bonsai multimerizes into higher-order complexes, which promote γ-TuSC assembly into rings. An active γ-TuC comprises approximately 7 γ-TuSCs associated with 13 copies each of Mto1-bonsai and Mto2. This suggests each γ-TuSC is associated with 2 copies of Mto1-bonsai and 2 copies of Mto2. Activation of the γ-TuC is thought to require a conformational change in GCP3, which adjusts the spacing of γ-tubulins to match the spacing of adjacent protofilaments in the MT lattice. Binding of Mto1/2-bonsai at each γ-TuSC in the ring could induce this conformational change (red box), thereby producing an effective template for MT nucleation.

5. Mto2 multimerizes Mto1 into higher-order complexes that activate the γ-TuC

5.1 Introduction

Previous work has indicated that Mto1/2 localization depends on Mto1 but not Mto2. However, in *mto2Δ* cells, Mto1 promotes MT nucleation exclusively from the SPB (Samejima et al., 2005; Venkatram et al., 2005). This reveals that Mto2 contributes to Mto1/2 activation of MT nucleation at non-SPB sites. Because they fail to localize to the SPB, the Mto1-NE and Mto1-bonsai mutants therefore provided an opportunity to directly assess the role of Mto2 in MT nucleation. Through analysis of Mto1-NE-GFP and Mto1-bonsai-GFP in an *mto2Δ* background, I concluded that Mto2 is required for multimerization of Mto1 at sites on the NE, MTs, and free in the cytoplasm. Further, I found that multimerization of Mto1/2 into higher-order assemblies is required for MT nucleation.

The *mto1-NE* and *mto1-bonsai* mutants also allowed me to address the role of various MTOCs in nuclear positioning. According to current models, MTs are associated with the nucleus via their minus ends. The forces produced as MT plus-ends grow and push against the cell cortex are thought to position the nucleus at the centre of the cell (Tran et al., 2001). Physical connection of MTs to the nucleus could be achieved by nucleation of MTs from MTOCs on the NE , or alternatively by additional factors that link existing MTs to the nuclear surface. Here, I demonstrate that MT nucleation from the NE does in fact contribute to nuclear positioning; in *mto1(131-1115)* and *mto1-bonsai* cells, where the NE no longer acts as a MTOC, nuclei were more eccentric than in wild-type cells. By contrast, the lack of MT nucleation from the SPB and existing MTs in *mto1-NE* had no effect on nuclear positioning.

In this chapter, I also analyzed the role of the γ-TuRC-specific proteins Alp16, Gfh1, and Mod21 in MT nucleation in the *mto1-NE* and *mto1-bonsai* mutants. Previous work has shown that the γ-TuRC-specific proteins are not required for MT nucleation in wild-type cells (Anders et al., 2006). However, individual or simultaneous deletion of Alp16, Gfh1, and Mod21 results in a roughly 2-fold reduction in the frequency of MT nucleation, in mto1+ cells (Anders et al., 2006). In *mto1-NE* and *mto1-bonsai*, on the other hand, the absence of the γ-TuRC specific proteins has no effect on the frequency of MT nucleation. We propose that the γ-TuSC proteins in association with Mto1/2-bonsai may form a minimal, non-localizing γ-TuC that is sufficient for MT nucleation.

5.2 Results

5.2.1 Higher-order multimerization of Mto1/2 is required for γ-TuC activation

Mto1-GFP localization to MTs is fairly weak in *mto2Δ* cells, showing only faint decoration of MTs rather than the more robust, punctate signal observed in the presence of Mto2 (Figure 5.1) (Samejima et al., 2005; Venkatram et al., 2005). This led us to speculate that Mto2 may have a role in multimerization of Mto1 at iMTOCs. Indeed, in an *mto2Δ* background, Mto1-NE-GFP and Mto1-bonsai-GFP completely failed to assemble into distinct puncta, and instead produced only a diffuse signal (Figure 5.1). Mto1(131-9A1-549)-GFP also formed puncta in an Mto2-dependent manner, suggesting that multimerization of the Mto1/2 complex can occur independent of interaction with the γ-TuC or localization to MTOCs (Figure 5.1). Mto1(131-9A1-549)-GFP showed no specific localization, but rather

formed puncta that appeared to diffuse freely throughout the cytoplasm. Notably, however, these puncta were less numerous and generally fainter than those observed with Mto1-bonsai-GFP, hinting that association with the γ-TuC may contribute to Mto1/2-bonsai assembly and/or stability.

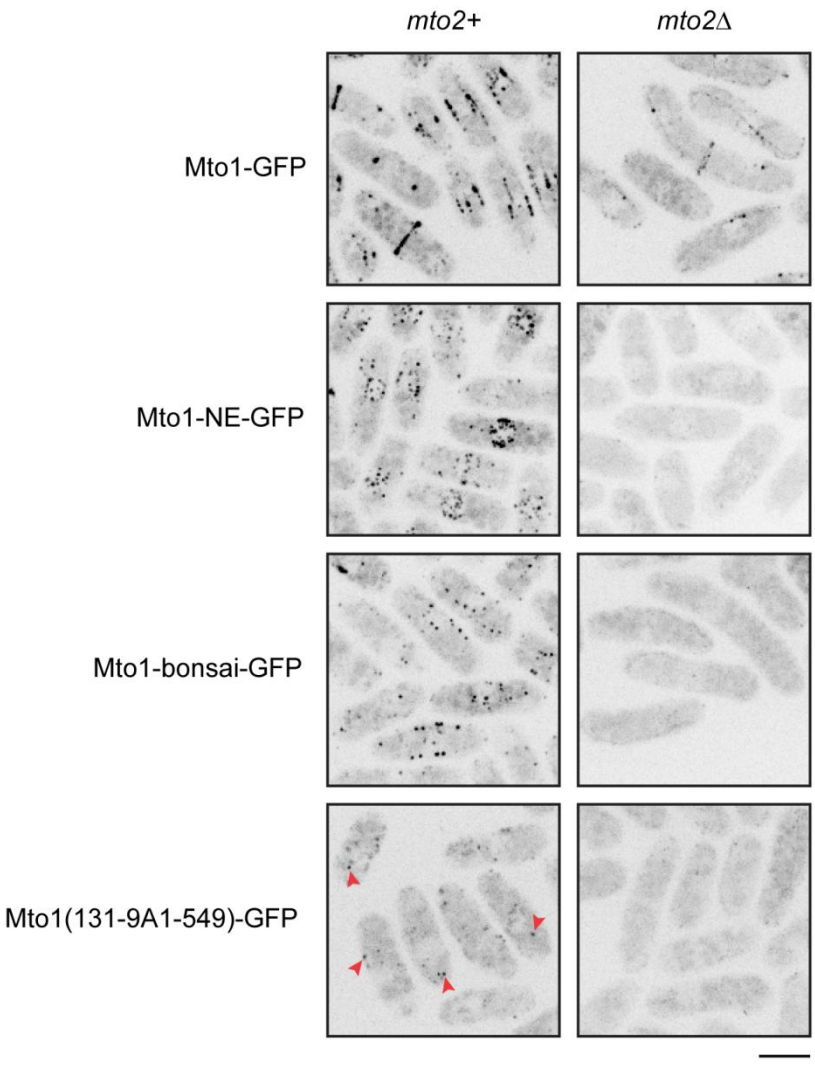

Figure 5.1: Multimerization of Mto1-bonsai-GFP and Mto1-NE-GFP requires Mto2. Various GFP-tagged mutants of Mto1 were imaged in *mto2*+ and *mto2*Δ backgrounds. In *mto2*Δ cells, full-length Mto1-GFP localized to SPBs and weakly to MTs and the eMTOC, as described previously. In the absence of Mto2, Mto1-NE-GFP, Mto1-bonsai-GFP, and Mto1(131-9A1-549)-GFP were no longer visible as discrete puncta, but rather produced a diffuse signal. Note that Mto1(131-9A1-549)-GFP puncta (red arrows) were much fainter and less numerous than Mto1-NE-GFP and Mto1-bonsai-GFP. Bar, 5 μm. [Strains: KS819, KS1407, KS5209, KS5349, KS5922, KS6456, KS6080, KS6098]

We saw in the previous chapter that MTs were nucleated from puncta containing higher-order assemblies of Mto1/2-bonsai (Figure 4.12; Figure 4.14). Therefore, we predicted that the apparent lack of Mto1-NE-GFP and Mto1-bonsai-GFP puncta in *mto2Δ* cells would correspond to a lack of MT nucleation. To test this, I made movies of GFP-α-tubulin in various *mto2+* and *mto2Δ* strains. As expected, *mto1+ mto2Δ* cells were capable of nucleating interphase MTs from the SPB (Figure 5.2)(Samejima et al., 2005; Venkatram et al., 2005). In contrast, *mto1-NE-GFP mto2Δ* and *mto1-bonsai-GFP mto2Δ* mutants failed to nucleate any cytoplasmic MTs (no MT nucleation was observed in 50 cells imaged over 500 seconds) (Figure 5.2). Overall, this suggests that MT nucleation from non-SPB sites requires multimerization of Mto1 by Mto2.

The absence of MT nucleation in *mto1-NE-GFP mto2Δ* and *mto1-bonsai-GFP mto2Δ* cells was confirmed by quantifying numbers of MT bundles. Both *mto1-NE-GFP mto2Δ* and *mto1-bonsai-GFP mto2Δ* behaved like *mto1Δ,* often having one or no MT bundles, indicating a complete lack of cytoplasmic MT nucleation. These strains differed from *mto1+ mto2Δ* and *mto1-GFP mto2Δ,* in which MT nucleation from the SPB typically maintained arrays of 1-2 MT bundles per cell (Figure 5.2).

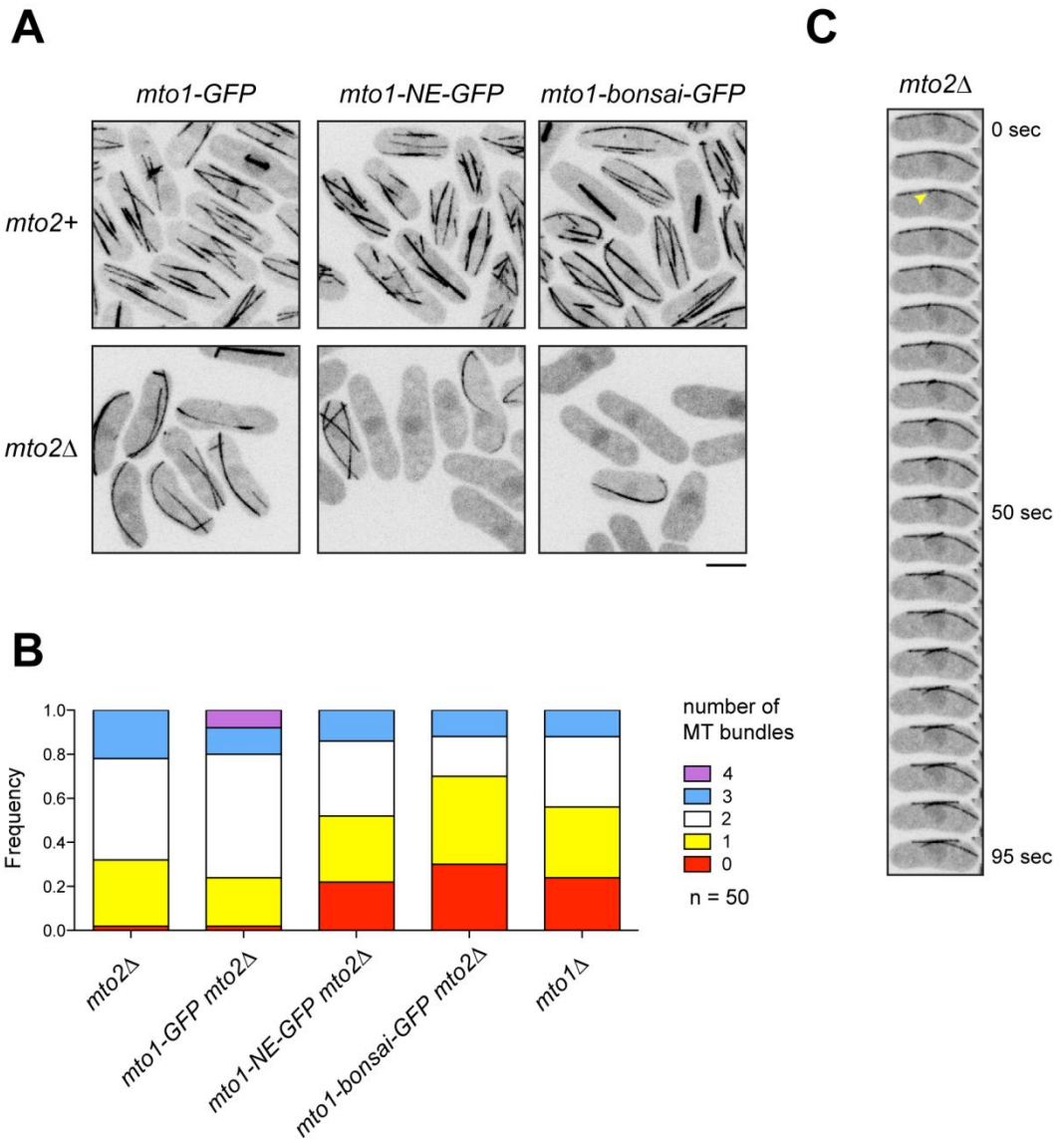

Figure 5.2: Mto2 is required for MT nucleation in *mto1-NE-GFP* and *mto1-bonsai-GFP*. (A) GFP-α-tubulin was imaged in wild-type and truncated *mto1* strains, in both an *mto2+* and *mto2Δ* background. No cytoplasmic MT nucleation was observed in *mto1-NE-GFP mto2Δ* or *mto1-bonsai-GFP mto2Δ* (50 cells of each were imaged over 500 seconds). (B) The number of MT bundles present in the various *mto1* and *mto2* mutants was counted. *mto2Δ* cells expressing full-length Mto1 (with or without a GFP tag) typically contained 1-2 MT bundles, while *mto1Δ* cells often contained no MTs whatsoever. The number of MT bundles in *mto1-NE-GFP mto2Δ* and *mto1-bonsai-GFP mto2Δ* cells was comparable to *mto1Δ*, consistent with these strains being completely deficient in cytoplasmic MT nucleation. (C) In the presence of full-length Mto1, *mto2Δ* cells can nucleate cytoplasmic MTs from the SPB (yellow arrow). Stills from a movie of GFP-α-tubulin in *mto2Δ* are shown (5 second time interval). Bar, 5 μm. [Strains: KS2738, KS6459, KS5491, KS6461, KS5929, KS6457, KS6458, KS5816]

5.2.2 Mto2 shows limited multimerization in the absence of Mto1

Next, I wished to address whether or not Mto1 makes any contribution to Mto2 multimerization. Previously, it was shown that Mto2-GFP failed to localize to MTOCs in an *mto1Δ* background, instead being visible as a diffuse signal throughout the cytoplasm (Samejima et al., 2005; Venkatram et al., 2005). Here, more sensitive spinning disk confocal microscopy was used to address whether or not deletion of *mto1* results in disassembly of Mto2 puncta. As seen in figure 5.3, faint particles of Mto2-GFP were still detected in *mto1Δ* cells. Generally, these Mto2-GFP puncta showed no specific localization and diffused rapidly around the cell, making them difficult to detect. These diffusing particles were in fact Mto2-GFP, as an imaging control showed some autofluorescence on the GFP channel, but lacked discrete puncta (Figure 5.3). Mto2-GFP puncta in *mto1Δ* were occasionally observed along MTs, perhaps indicating that Mto2 has a very weak affinity for the MT lattice (Figure 5.3). Overall, however, it was apparent that robust assembly of Mto2 puncta required the presence of Mto1.

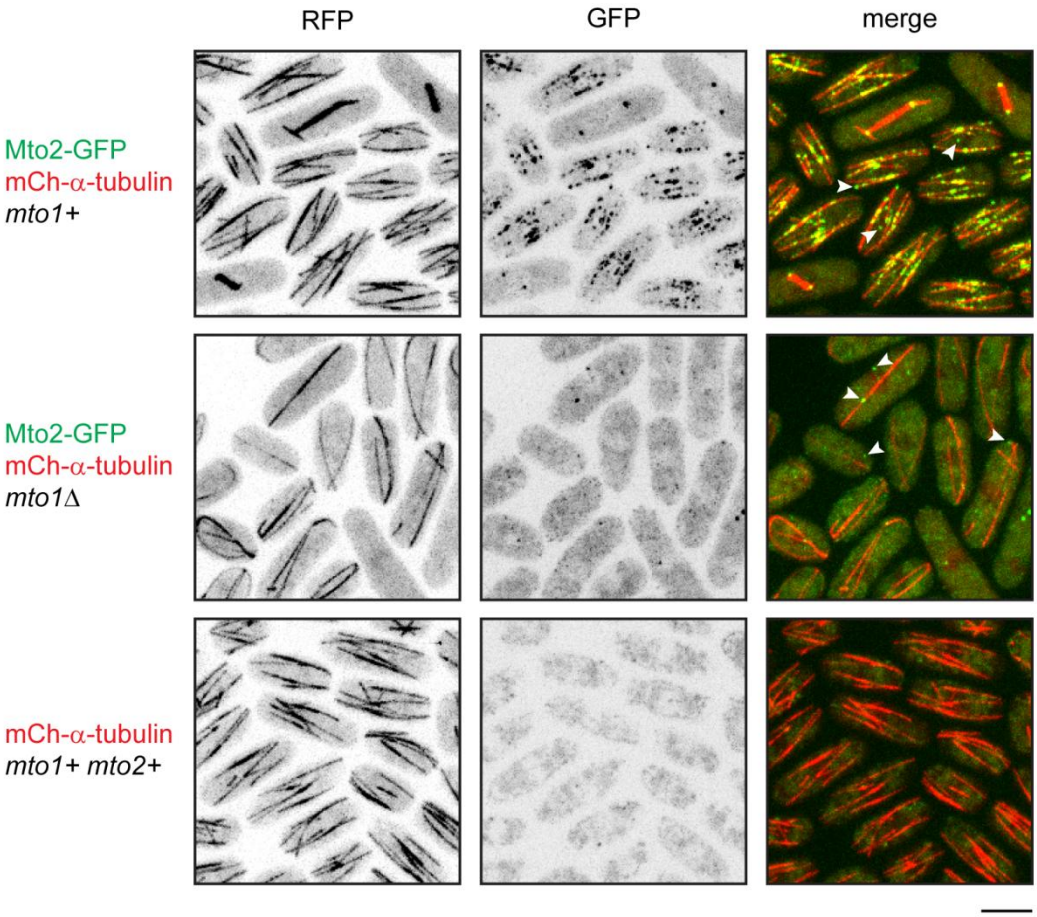

Figure 5.3: Faint Mto2-GFP puncta are observed in the absence of Mto1. Mto2-GFP was imaged together with mCherry-α-tubulin, in *mto1+* and *mto1*Δ backgrounds. In *mto1+* cells, Mto2-GFP was observed on the NE, MTs, SPBs, and eMTOC (not shown), as expected. Mto2-GFP on MTs and the NE was visible as distinct puncta (white arrows). In *mto1*Δ cells, limited numbers of faint Mto2-GFP puncta were still observed, which were occasionally associated with MTs. These puncta were absent from an imaging control lacking Mto2-GFP (compare images of GFP channel). Bar, 5 μm. [Strains: KS7055, KS7056, KS6715]

5.2.3 MT nucleation from the NE has a minor role in nuclear positioning

Nuclear positioning in fission yeast is a MT-dependent process (Sawin et al., 2004; Tran et al., 2001). Previous work has revealed that MT minus-ends are linked to the nucleus via the SPB and additional sites on the nuclear surface, in a process which may involve the SPB protein Sad1 (Tran et al., 2001). As MT plus-ends grow and push against the cell cortex, they are thought to exert forces that position the nucleus at the centre of the cell (Tran et al., 2001). Linkage of MTs to the nuclear surface could be achieved by two general mechanisms: MTOCs on the NE and SPB could nucleate and therefore anchor MTs via their minus-ends. Alternatively, existing MTs could be captured and attached to the SPB and/or NE.

I therefore tested if nuclear positioning was affected in the various *mto1* truncation mutants, where the SPB and/or NE no longer function as cytoplasmic MTOCs. Wild-type and truncated *mto1* strains were DAPI-stained, and the distances from the centre of the nucleus to the nearest cell tip (S) and the farthest cell tip (L) were determined (Figure 5.4). The ratio S/L was used as a measure of nuclear positioning, where a value of 1.0 would represent a perfectly centred nucleus. Because they have comparable expression levels (Figure 4.11), the GFP-tagged versions of the *mto1* mutants were used in this experiment.

Disrupting localization of Mto1 and the γ-TuC was found to have a limited effect on nuclear positioning. Roughly 60% of cells expressing full-length Mto1-GFP exhibited an S/L ratio greater than 0.8 (Figure 5.4). By contrast, nuclei in *mto1Δ* showed significant displacement from the cell centre (Figure 5.4), as shown previously (Sawin et al., 2004). Only 20% of *mto1Δ* cells had an S/L ratio greater than 0.8, due to a lack of proper cytoplasmic MT organization. However, nuclear positioning in *mto1-NE-GFP* was essentially indistinguishable from *mto1-GFP* (Figure 5.4). This demonstrates that eliminating Mto1

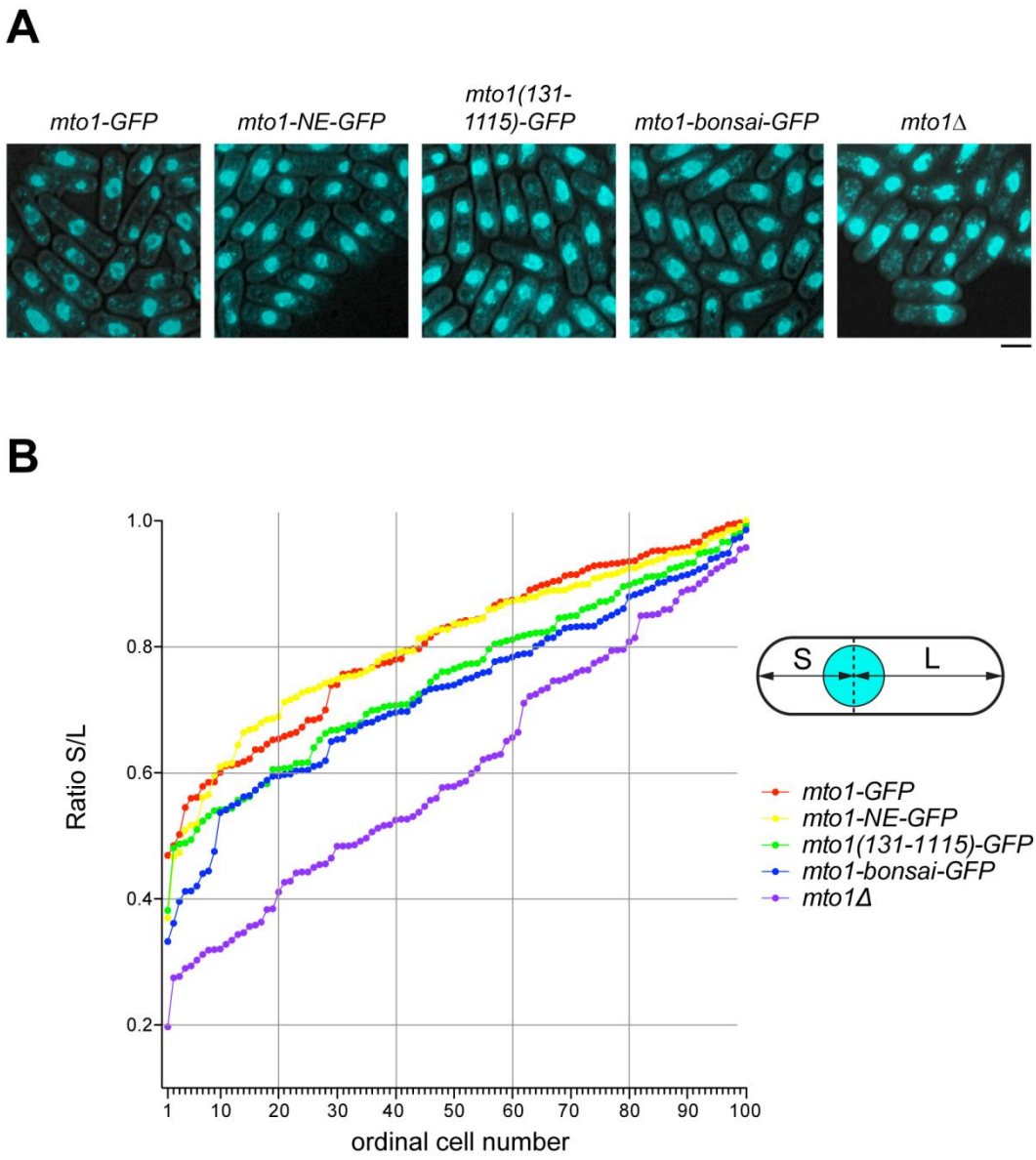

Figure 5.4: MT nucleation from the NE has a minor role in ensuring correct nuclear positioning. (A) Various *mto1* mutants were stained with DAPI in order to measure nuclear positioning. (B) The distance from the centre of the nucleus to the nearest cell tip (S) and farthest cell tip (L) was determined, and the ratio S/L was reported as a measure of nuclear displacement from the cell centre. Cells from different *mto1* strains were plotted in ascending order of the ratio S/L. *mto1*Δ cells showed the greatest displacement of the nucleus from the cell centre, when compared to full-length *mto1-GFP*. Eliminating MT nucleation from the SPB and pre-existing MTs in *mto1-NE-GFP* had no appreciable effect on nuclear positioning. *mto1(131-1115)-GFP* and *mto1-bonsai-GFP* cells had slightly more eccentric nuclei, indicating that MT nucleation from the NE does contribute to nuclear positioning. Bar, 5 μm. [Strains: KS819, KS5209, KS5940, KS5922, KS1017]

localization to the SPB and pre-existing MTS, and thereby abolishing cytoplasmic MT nucleation from these sites, has no appreciable effect on MT-dependent nuclear positioning. Eliminating NE localization in *mto1(131-1115)-GFP* and *mto1-bonsai-GFP*, on the other hand, had a moderate effect on nuclear positioning, with roughly 40% of cells having an S/L ≥ 0.8 (Figure 5.4). MT nucleation from MTOCs on the NE therefore contributes at least somewhat to ensuring correct nuclear positioning.

5.2.4 *mto1-NE-GFP* and *mto1-bonsai-GFP* nucleate MTs in the absence of γ-TuRC-specific proteins

The γ-TuRC-specific proteins Alp16, Gfh1, and Mod21 are not essential for MT nucleation, but appear to enhance the MT-nucleating activity of the γ-TuC; *alp16Δ gfh1Δ mod21Δ* cells retain the ability to nucleate MTs, but nucleate at a reduced frequency (approximately half the frequency of wild-type cells)(Anders et al., 2006). Moreover, in the absence of Alp16, Gfh1 and Mod21 fail to interact with the γ-TuSC, such that *alp16Δ* cells can effectively be regarded as *alp16Δ mod21Δ gfh1Δ* triple deletion mutants.

We wanted to confirm that the γ-TuRC-specific proteins were also dispensable for MT nucleation in *mto1-NE* and *mto1-bonsai* cells. Therefore, I made movies of GFP-α-tubulin in cells expressing Mto1-GFP, Mto1-NE-GFP, or Mto1-bonsai-GFP in an *alp16Δ* background, and quantified nucleation events as before. As expected, the frequency of MT nucleation in *mto1-GFP alp16Δ* was clearly reduced when compared to *mto1-GFP alp16+ cells* (Figure 5.5). In *mto1-NE-GFP* and *mto1-bonsai-GFP*, however, deleting *alp16* had no appreciable effect on the frequency of MT nucleation (Figure 5.5). This suggests that the γ-TuRC-specific proteins make no obvious contribution to MT nucleation in *mto1-NE* or *mto1-bonsai*, although the reason for this remain unclear.

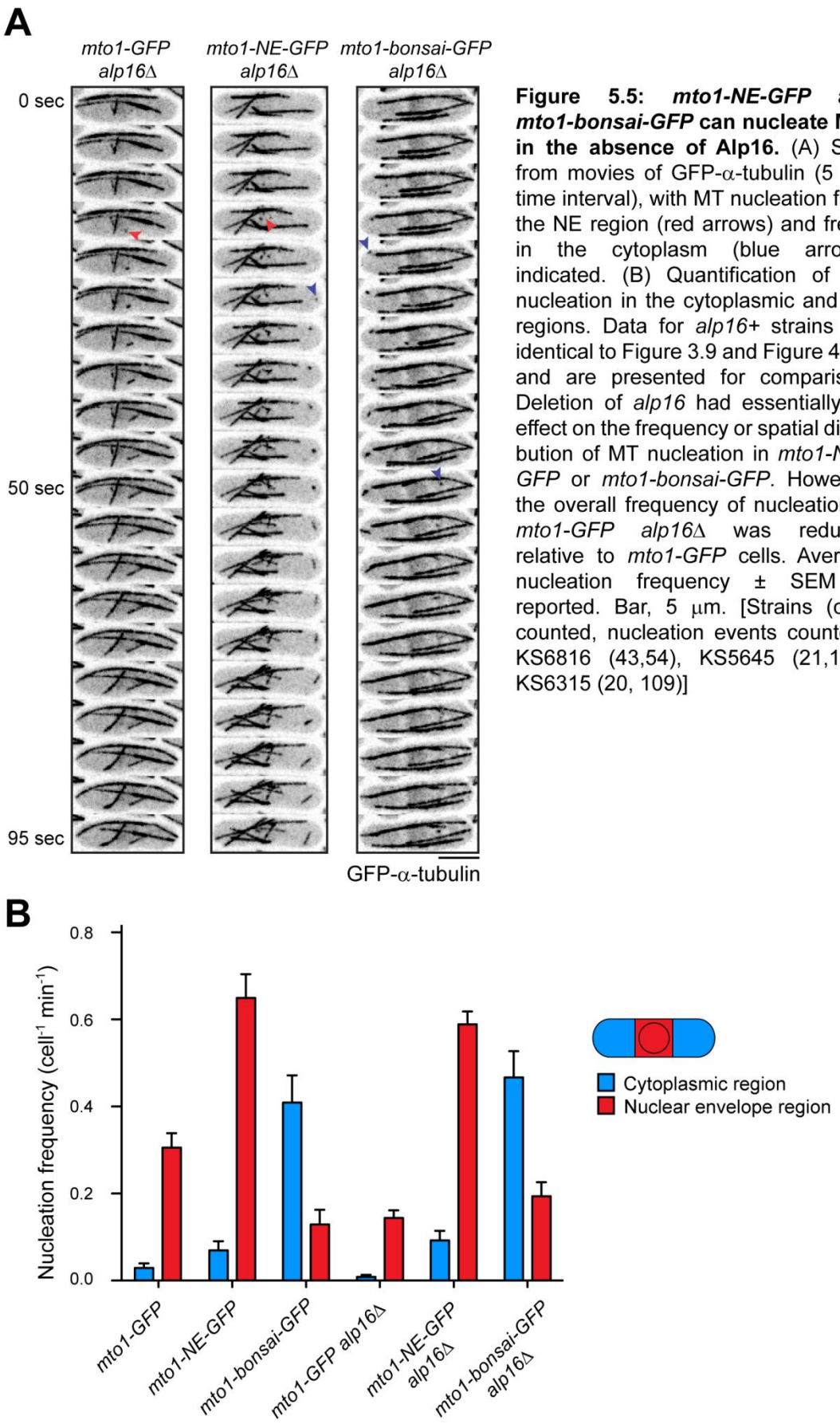

Figure 5.5: *mto1-NE-GFP* and *mto1-bonsai-GFP* can nucleate MTs in the absence of Alp16. (A) Stills from movies of GFP-α-tubulin (5 sec time interval), with MT nucleation from the NE region (red arrows) and freely in the cytoplasm (blue arrows) indicated. (B) Quantification of MT nucleation in the cytoplasmic and NE regions. Data for *alp16+* strains are identical to Figure 3.9 and Figure 4.10, and are presented for comparison. Deletion of *alp16* had essentially no effect on the frequency or spatial distribution of MT nucleation in *mto1-NE-GFP* or *mto1-bonsai-GFP*. However, the overall frequency of nucleation in *mto1-GFP alp16Δ* was reduced relative to *mto1-GFP* cells. Average nucleation frequency ± SEM is reported. Bar, 5 μm. [Strains (cells counted, nucleation events counted): KS6816 (43,54), KS5645 (21,118), KS6315 (20, 109)]

5.3 Discussion

In cells lacking Mto2, Mto1-NE and Mto1-bonsai puncta are no longer observed. This results in a complete lack of cytoplasmic MT nucleation, highlighting the importance of Mto1 multimerization in γ-TuC activation. However, MT nucleation from the SPB is preserved in *mto2Δ* cells expressing full-length Mto1, as shown in previous studies (Samejima et al., 2005; Venkatram et al., 2005). Thus, Mto2 may be specifically required for multimerizing Mto1 at iMTOCs on MTs, the NE, and free in the cytoplasm. Additional, redundant factors at the SPB could be responsible for multimerizing Mto1 in an Mto2-independent manner.

The notion that Mto2 promotes Mto1 multimerization also helps us interpret observations regarding Mto1 localization. In the absence of Mto2, localization of full-length Mto1 to the SPB is unaffected, although localization to MT bundles is clearly reduced (Samejima et al., 2005; Venkatram et al., 2005). Further, Mto1 is completely absent from the NE in an *mto2Δ* background, a phenomenon clearly demonstrated by comparison of *mto1-NE-GFP* and *mto1-NE-GFP mto2Δ* cells. In principle, Mto2 could contribute to Mto1 localization to MTs and the NE in at least two ways. First, Mto2 itself could contain sequences which help target Mto1/2 to MTs and the NE. This is unlikely, however, due to the lack of Mto2 localization to these MTOCs in an *mto1Δ* background. The second, perhaps more plausible explanation is that multimerization of Mto1 by Mto2 increases the avidity of the Mto1/2 complex for sites on MTs and the NE. This explanation is consistent with the idea that Mto1 is the predominant factor involved in localizing the Mto1/2 complex and γ-TuC to MTOCs.

In this chapter, we also demonstrated that MT nucleation from MTOCs on the NE contributes to nuclear positioning. This is in line with the view that physical linkage

between MTs and the NE is required to position the nucleus at the centre of the cell (Tran et al., 2001). Eliminating the NE as a MTOC in the *mto1* N-terminal truncations, however, had a much milder effect on nuclear positioning than completely abolishing cytoplasmic MT nucleation in *mto1Δ* cells. Even in *mto1-bonsai* cells, where MT nucleation is spatially random, nuclei were only somewhat more eccentric than in wild-type cells. Simply maintaining cytoplasmic MT arrays, therefore, appears to be more important to nuclear positioning than nucleating MTs from the NE. Overall, this suggests that other factors, in addition to MTOCs on the NE, must link the MT cytoskeleton to the nuclear surface.

Finally, this chapter revealed that the γ-TuRC-specific proteins Alp16, Gfh1, and Mod21 are not required for MT nucleation in *mto1-bonsai-GFP*. This suggests that complexes composed solely of Mto1/2-bonsai and γ-TuSCs may be sufficient for MT nucleation. Owing to its simplicity, this is an attractive model for a minimal MT-nucleating complex, that functions independent of localization to conventional MTOCs. Nonetheless, other proteins that contribute to γ-TuC activation may remain to be identified.

6. Recombinant Mto1/2-bonsai complex self-assembles into large multimers

6.1 Introduction

In the preceding chapters, I provided evidence that the Mto1/2 complex is a γ-TuC activator. We suspect that Mto1/2-bonsai in association with γ-TuSCs may be sufficient for MT nucleation. However, the possibility that other proteins are also required for MT nucleation can never be formally excluded by *in vivo* studies. Ultimately, identification of the minimal components that are sufficient for robust physiological MT nucleation will require *in vitro* reconstitution of an actively-nucleating complex.

Towards this more long-term objective, I expressed and purified Mto1-bonsai and Mto2 individually, and also together as the Mto1/2-bonsai complex. To do this, I employed the MultiBac system, a baculovirus expression system developed by Imre Berger and colleagues (Berger et al., 2004; Bieniossek and Berger, 2009; Fitzgerald et al., 2006; Fitzgerald et al., 2007; Trowitzsch et al., 2010). The MultiBac system is specifically designed for the expression of multiprotein complexes. Multiple genes of interest (GOIs) are cloned into a transfer vector, which is then integrated into the MultiBac Bacmid (a baculovirus shuttle vector that can be propagated in both *E. coli* and insect cells). Transfection of the recombinant Bacmid into insect cells then allows for virus production and, ultimately, protein expression. GOIs can easily be added to existing MultiBac transfer vectors, using conventional cloning techniques or by Cre-LoxP fusion with "donor vectors" carrying additional GOIs (Trowitzsch et al., 2010). This means that one can easily express various combinations (or truncations) of proteins from a multiprotein complex, and also add additional components at a later date.

I used the MultiBac system to co-express Mto2 together with full-length Mto1, Mto1-NE, or Mto1-bonsai. Mto1-bonsai showed the most robust expression, and further analysis was therefore limited to Mto1-bonsai and Mto2. Using N-terminal 6-histidine tags, Mto1-bonsai, Mto2, and Mto1/2-bonsai complex were Nickel-purified. Following a subsequent gel filtration step, the individual proteins and protein complex could be obtained with roughly 95% purity.

Size exclusion chromatography with multi-angle light scattering (SEC-MALS) revealed that Mto1/2-bonsai complex eluted as a broad peak containing complexes ranging in size from ~75-800 kDa. This large size-range across a single peak suggested that Mto1/2-bonsai was in a dynamic equilibrium between complexes with various degrees of multimerization. Indeed, dilution of the sample caused Mto1/2-bonsai to elute later, indicating a shift in equilibrium towards disassembly into smaller multimers. A similar effect was seen with Mto2 alone, indicating that Mto2 also multimerizes and is in a dynamic equilibrium. By contrast, in the absence of Mto2, Mto1-bonsai appeared to be monodisperse. In addition, I found that Mto1-bonsai and Mto2 purified separately were able to self-assemble into Mto1/2-bonsai complex when combined *in vitro*.

6.2 Results

6.2.1 Mto1/2-NE and Mto1/2-bonsai are expressed at higher levels in insect cells than full-length Mto1/2

Initially, I constructed bacmids for the co-expression of 6His-Mto1, 6His-Mto1-NE, or 6His-Mto1-bonsai together with Mto2. I generated various constructs of Mto1 because

we suspected that the smaller Mto1 truncations might be expressed at higher levels than full-length Mto1. The various bacmids were transfected into Sf9 insect cells to generate virus stocks, and the approximate titre of virus stocks was then determined (see materials and methods). Suspension cultures of Sf9 cells were infected with equal amounts of each virus, and total and soluble expression of Mto1 and Mto2 was monitored by western blotting for 4 days following infection (Figure 6.1). In all cases, Mto2 expression appeared to peak after 2-3 days, and essentially all Mto2 appeared to be soluble. Similarly, Mto1-NE and Mto1-bonsai expression also peaked around 3 days, and both proteins appeared to be entirely soluble. However, full-length Mto1 appeared to show much weaker expression. The Mto1 band was fainter in comparison to background signal, perhaps indicating that it was largely degraded. All three anti-Mto1 western blots were performed with serum, rather than affinity-purified antibodies, such that some non-specific bands were likely present in all cases. However, with full-length Mto1, additional high molecular weight bands were observed, which were absent from the Mto1-NE and Mto1-bonsai blots (Figure 6.1). These high molecular weight bands likely corresponded to degradation of full-length Mto1. Further, only a fraction of Mto1 appeared to be soluble, and the amount of soluble Mto1 did not appear to increase beyond one day post-infection. Therefore, I decided to pursue Mto1/2-bonsai for further analysis — this complex clearly showed better expression than full-length Mto1 with Mto2, and has biological relevance as the "minimal" Mto1/2 complex.

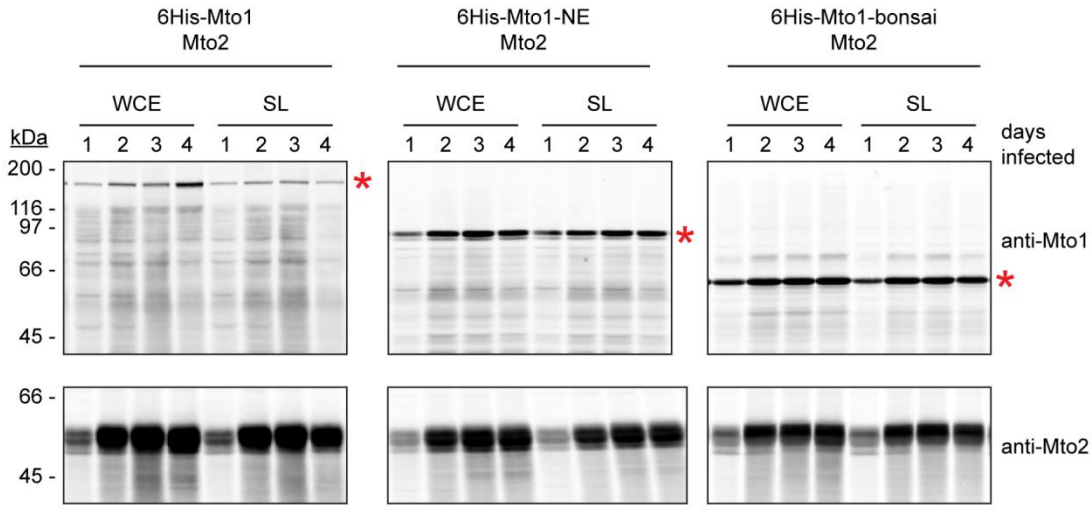

Figure 6.1: Mto1-NE and Mto1-bonsai are expressed at higher levels than full-length Mto1. Sf9 cells were infected with virus stock for expression of Mto2 together with 6His-tagged full-length Mto1, Mto1-NE, or Mto1-bonsai. Samples of whole cell extracts (WCE) and soluble lysates (SL) were taken 1, 2, 3, and 4 days following addition of virus. WCE and SL samples were run on 10% SDS-PAGE and analyzed by anti-Mto1 and anti-Mto2 immunoblotting. Each blot was performed separately, so intensities cannot be rigorously compared quantitatively. However, it was apparent that 6His-Mto1 showed reduced expression levels and perhaps increased degradation when compared to 6His-Mto1-NE and 6His-Mto1-bonsai. Expression levels of 6His-Mto1-NE, 6His-Mto1-bonsai, and Mto2 peaked after 2-3 days, while 6His-Mto1 levels showed little increase over time. The positions of Mto1 bands are indicated by red asterisks.

6.2.2 6His-Mto1/2-bonsai has a particularly high-affinity for nickel

In developing a protocol for nickel-purification of 6His-Mto1/2-bonsai, I first sought to determine the range of imidazole concentrations in which the complex would bind to Ni-charged beads. Soluble lysate from Sf9 cells expressing 6His-Mto1-bonsai and Mto2 was incubated with Ni-charged His-Bind Fractogel, in the presence of increasing concentrations of imidazole. Samples of the supernatant were analyzed by western blot, in order to quantify the amount of unbound 6His-Mto1-bonsai and Mto2. The recovery of both proteins following elution from the beads was also analyzed by western blot (Figure 6.2). Surprisingly, 6His-Mto1-bonsai appeared to show efficient binding and recovery from beads

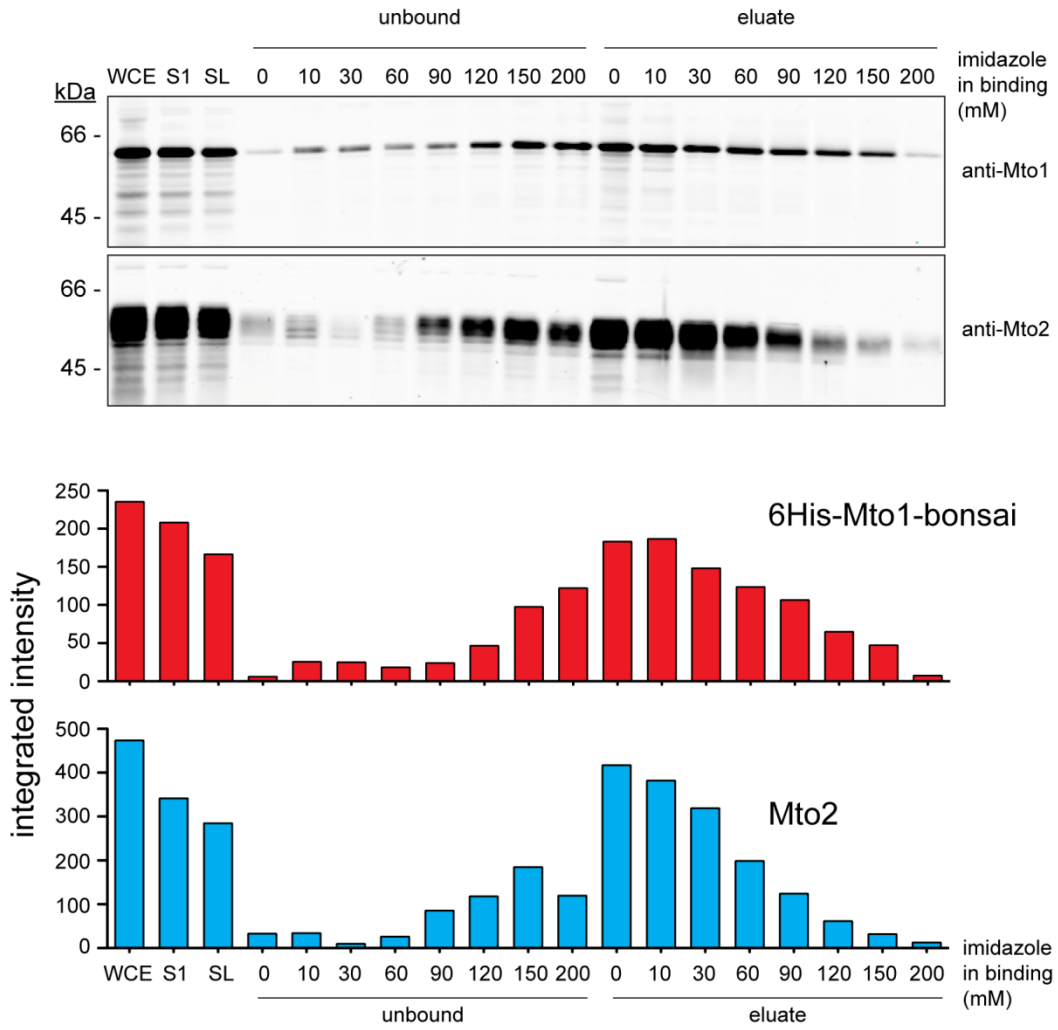

Figure 6.2: 6His-Mto1/2-bonsai complex binds nickel even at high imidazole concentrations. Soluble lysate (SL) from Sf9 cells co-expressing 6His-Mto1-bonsai and Mto2 was incubated with Ni^{2+}-charged His-bind fractogel beads. Incubation was performed in binding buffers with imidazole concentrations ranging from 0-200 mM. Samples of the unbound material and material recovered by elution with 300 mM imidazole were taken, and analyzed by 10% SDS-PAGE followed by anti-Mto1 and anti-Mto2 immunoblotting. Quantification of Mto1 and Mto2 levels is shown below the western blots. 6His-Mto1-bonsai was found to bind efficiently to beads even at high imidazole concentrations of 60-90 mM. Binding and recovery of both 6His-Mto1-bonsai and Mto2 was efficient with up to 30-60 mM imidazole in binding buffer. WCE, whole cell extract; S1, supernatant from initial low-speed spin.

even at 60-90 mM imidazole. Mto2 recovery was also efficient at relatively high imidazole concentrations of 30-60 mM. We took this as an initial indication that recombinant Mto1/2-bonsai may be multimerized; the presence of multiple 6His tags on a single complex would increase the avidity of the complex for Ni-charged beads, and allow for binding at relatively high imidazole concentrations.

I was therefore able to perform nickel purifications under fairly stringent conditions (45 mM and 90 mM imidazole in binding and wash buffers, respectively; see materials and methods). This allowed me to partially purify 6His-Mto1/2-bonsai complex, in addition to 6His-Mto1-bonsai and 6His-Mto2 individually (Figure 6.3). Co-purification of un-tagged Mto2 with 6His-Mto1-bonsai confirmed that the recombinant proteins formed a complex.

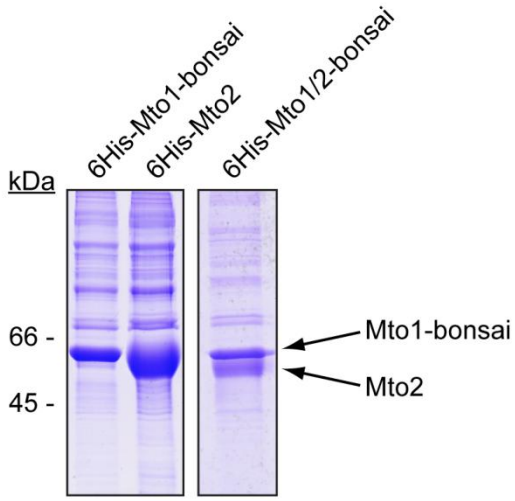

Figure 6.3: Mto1-bonsai and Mto2 were Nickel-purified separately or together as the Mto1/2-bonsai complex. Samples of Ni-purified proteins were analyzed by 10% SDS-PAGE followed by coomassie staining. For individual purification, Mto1-bonsai and Mto2 were both expressed with N-terminal 6His tags. For purification of the Mto1/2-bonsai complex, 6His-Mto1-bonsai was co-expressed with un-tagged Mto2.

6.2.3 Recombinant Mto1/2-bonsai forms a range of complexes roughly 75-800 kDa in size

As a second purification step, Ni-purified Mto1/2-bonsai complex was fractionated by gel filtration on a Superose 6 10/300 GL column. The Mto1/2-bonsai complex eluted over a relatively broad range, with a peak elution volume of roughly 10.5 mL. The purity in the peak fractions was estimated to be about 95%, with most contaminants present either in the void volume or in low molecular weight fractions (Figure 6.4A).

Quantification from coomassie-stained gels revealed that Mto1-bonsai and Mto2 co-migrated with an approximately 1:1 stoichiometry during gel-filtration (Figure 6.4B). This was consistent with the 1:1 stoichiometry of Mto1-bonsai-GFP and Mto2-GFP observed in the MT nucleating puncta described in chapter 4 (Figure 4.14). This also suggested that recombinant Mto1/2-bonsai complex was composed of a stable core subunit, such as an Mto1/2-bonsai heterodimer or heterotetramer, that failed to dissociate when subjected to gel filtration. Further, the broad elution profile of the complex suggested that species of different sizes were present, hinting that Mto1/2-bonsai may exist in a variety of multimeric states.

In order to determine the absolute size of the complex, Mto1/2-bonsai was analyzed by SEC-MALS. The peak Mto1/2-bonsai fractions from a Superose 6 run (10.0-10.5 mL) (Figure 6.4) were pooled and run again over a Superose 6 column with online MALS detection [SEC-MALS analysis was performed by Martin Wear]. Mto1/2-bonsai was found to be highly polydisperse, with complexes ranging from approximately 75-800 kDa observed across the Mto1/2-bonsai peak (Figure 6.5). Given the 1:1 stoichiometry of Mto1-bonsai and Mto2 (Figure 6.4), the smaller 75 kDa complexes were fairly consistent with an Mto1/2-bonsai heterodimer (both proteins are approximately 45 kDa). By the same logic,

the largest ~800 kDa complexes would be predicted to contain ~9 copies each of Mto1-bonsai and Mto2. Therefore, these higher-order assemblies are comparable in size to the nucleating puncta observed *in vivo* by fluorescence microscopy, which contained ~13 copies each of Mto1-bonsai and Mto2 (Figure 4.14).

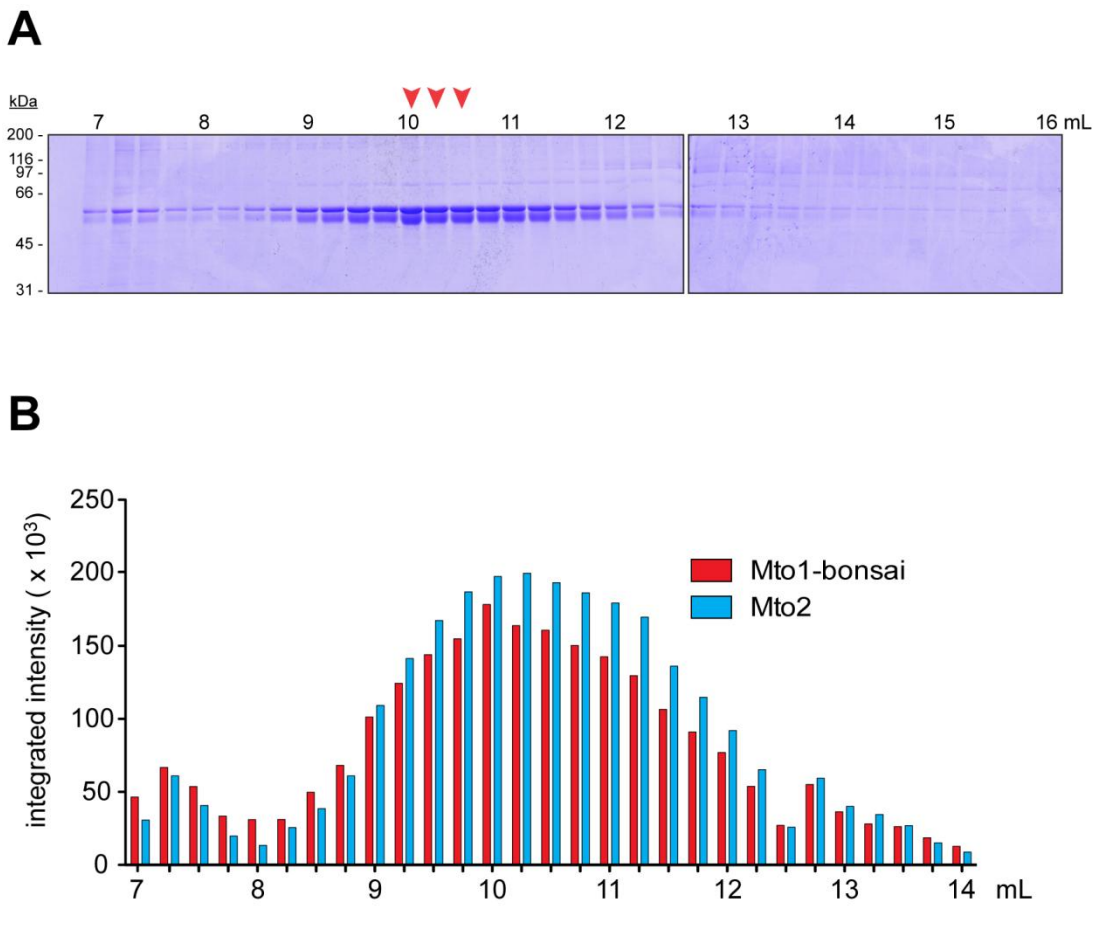

Figure 6.4: Mto1-bonsai and Mto2 co-fractionate with a 1:1 stoichiometry during gel filtration. (A) Ni-purified Mto1/2-bonsai complex was fractionated by gel filtration on a Superose 6 10/300 GL column, and fractions were analyzed by 10% SDS-PAGE followed by coomassie staining. Mto1/2-bonsai eluted over a broad range, with a peak around 10 mL. Purity in the peak fractions (red arrows) was estimated to be about 95%. Limited amounts of Mto1/2-bonsai could also be seen in the void volume (7-8 mL). (B) Quantification of Mto1-bonsai and Mto2 levels from the gel shown in (A). Mto1-bonsai and Mto2 co-fractionated with a 1:1 stoichiometry across the entire peak.

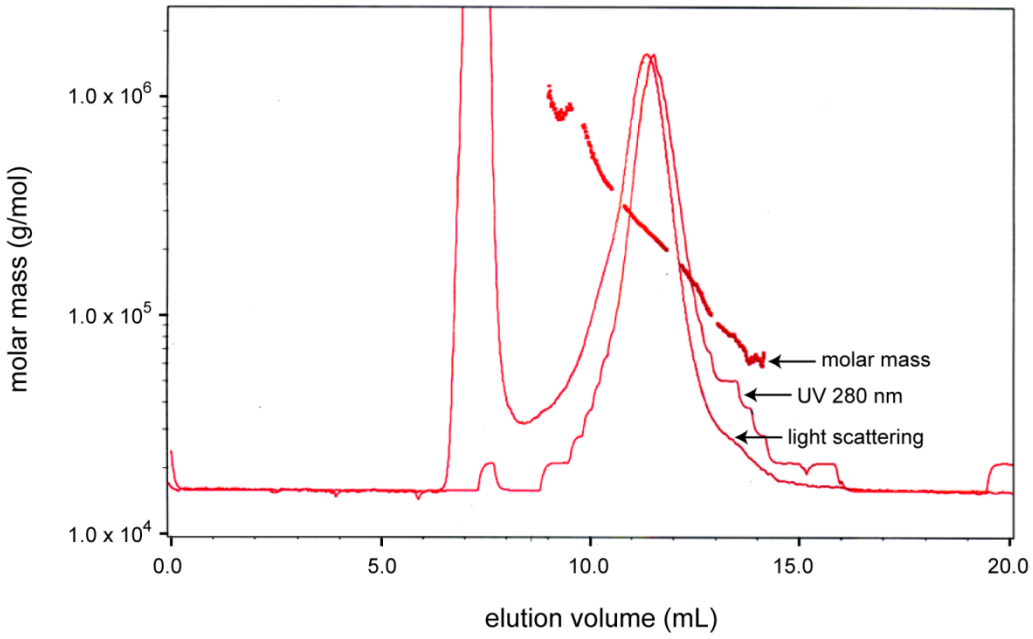

Figure 6.5: Recombinant Mto1/2-bonsai forms complexes ranging from ~75-800 kDa. Mto1/2-bonsai complex was analyzed by SEC-MALS, with gel filtration on a Superose 6 10/300 GL column. Chromatogram traces for UV 280 nm and light scattering are shown, along with calculated molar mass across the Mto1/2-bonsai peak. Mto1/2-bonsai was clearly polydisperse, with complexes ranging from approximately 75-800 kDa observed. The intense scattering signal around 7.5 mL corresponds to the void volume. [SEC-MALS analysis was performed by Martin Wear].

6.2.4 The Mto1/2-bonsai complex is in a dynamic equilibrium

Because the Mto1/2-bonsai peak contained species with a broad range of molecular weights, we suspected that the Mto1/2-bonsai complex may be in a dynamic equilibrium between multimers of various sizes. If this were true, then dilution of the Mto1/2-bonsai complex would lead to disassembly of the complex into smaller multimers. This would result in a shift towards later elution during gel filtration. To test this, "undiluted" (~20 μM) Mto1/2-bonsai complex was ran over a Superose 6 column, followed by 10- and 100-fold dilutions of the same sample. Dilution clearly resulted in a shift towards

later elution, suggesting disassembly of the complex into smaller subunits; relative to the undiluted sample, 10- and 100-fold dilution increased the elution volume by roughly 1 and 2.5 mL, respectively (Figure 6.6A). This indicates that the Mto1/2-bonsai complex is indeed in a dynamic equilibrium.

This dilution-induced shift toward smaller complexes was confirmed by SDS-PAGE and coomassie staining or western blot analysis of the fractions from gel filtration (Figure 6.6B). The Mto1-bonsai and Mto2 bands in the 10-fold diluted sample were only faintly detectably by coomassie staining, but still appeared to co-fractionate, suggesting that some sort of Mto1/2-bonsai subunit remained intact. That is, interaction between Mto1-bonsai and Mto2 was preserved upon dilution, despite the disassembly of higher-order Mto1/2-bonsai complexes. Similarly, in the 100-fold dilution, Mto1-bonsai and Mto2 appeared to peak in the same fraction (12.5 mL) as determined by immunoblotting, although the signal on these blots was very faint (Figure 6.6B). This may imply that higher-order multimers of Mto1/2-bonsai are assembled from a core, heteromeric subunit consisting of both Mto1-bonsai and Mto2.

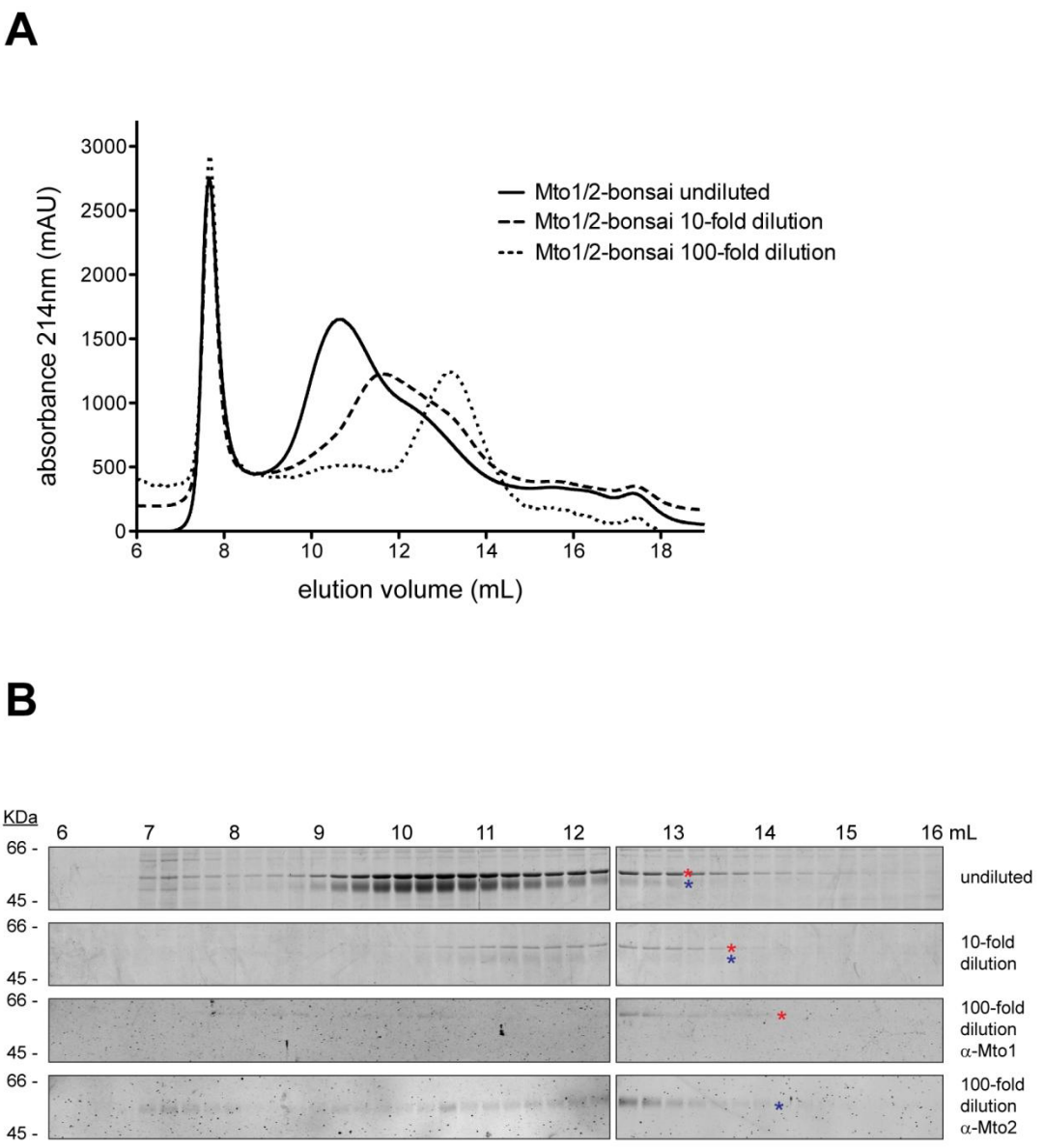

Figure 6.6: The Mto1/2-bonsai complex is in dynamic equilibrium. (A) Various dilutions of Ni-purified Mto1/2-bonsai were fractionated by gel filtration on a Superose 6 10/300 GL column (undiluted sample was roughly 20 μM). Upon 10- and 100-fold dilution of the sample, the Mto1/2-bonsai peak shifted towards a higher elution volume, indicating a disassembly into smaller complexes. Note that absorbance values are only accurate for the undiluted sample; values for the 10- and 100-fold dilutions were arbitrarily re-scaled to make them visible. (B) The shift in Mto1/2-bonsai elution was confirmed by subjecting fractions to 10% SDS-PAGE followed by coomassie staining (undiluted and 10-fold dilution) or anti-Mto1 and anti-Mto2 western blot (100-fold dilution). The positions of Mto1-bonsai (red asterisks) and Mto2 (blue asterisks) bands are indicated.

6.2.5 Mto2 multimerizes and is in a dynamic equilibrium, while Mto1-bonsai is likely monodisperse

I wished to address if either Mto1-bonsai or Mto2, when purified individually, was also multimerized and in a dynamic equilibrium. I therefore performed the same analysis as with the Mto1/2-bonsai complex, running various concentrations of Mto1-bonsai and Mto2 individually on a Superose 6 column. Mto2 showed a clear shift to later elution when diluted (Figure 6.7) (undiluted sample was approximately 50 μM). When diluted 10- and 100-fold, Mto2 was found to elute about 0.5 and 1.0 mL later, respectively. This reveals that Mto2 is in a dynamic equilibrium and therefore must be multimerized to at least some degree. Mto1-bonsai, by contrast, showed only a very modest (and possibly negligible) shift upon 10-fold dilution, and an even less apparent shift when diluted 100-fold (Figure 6.8). This suggests that Mto1-bonsai is likely monodisperse when purified alone, and assembles into more dynamic, higher-order assemblies only upon association with Mto2.

Next, I wanted to know if Mto1-bonsai and Mto2 were able to assemble into Mto1/2-bonsai complex *in vitro*. To test this, Mto1-bonsai and Mto2 were purified separately, and subsequently combined. Gel filtration on a Superose 6 column was then used to analyze the individual and combined proteins. When run individually, Mto1-bonsai and Mto2 were found to elute around 13.5 and 12.5 mL, respectively (Figure 6.9A). When combined and ran together, however, both proteins eluted as a broad peak centred around 11.5 mL, indicating multimerization into Mto1/2-bonsai complex (Figure 6.9A). SDS-PAGE and coomassie staining confirmed that Mto1-bonsai and Mto2 co-fractionated as Mto1/2-bonsai complex when combined (Figure 6.9B). Overall, this reveals that Mto1-bonsai and Mto2 have the intrinsic ability to self-assemble into higher-order complexes, outside of a cellular environment and independent of association with other proteins.

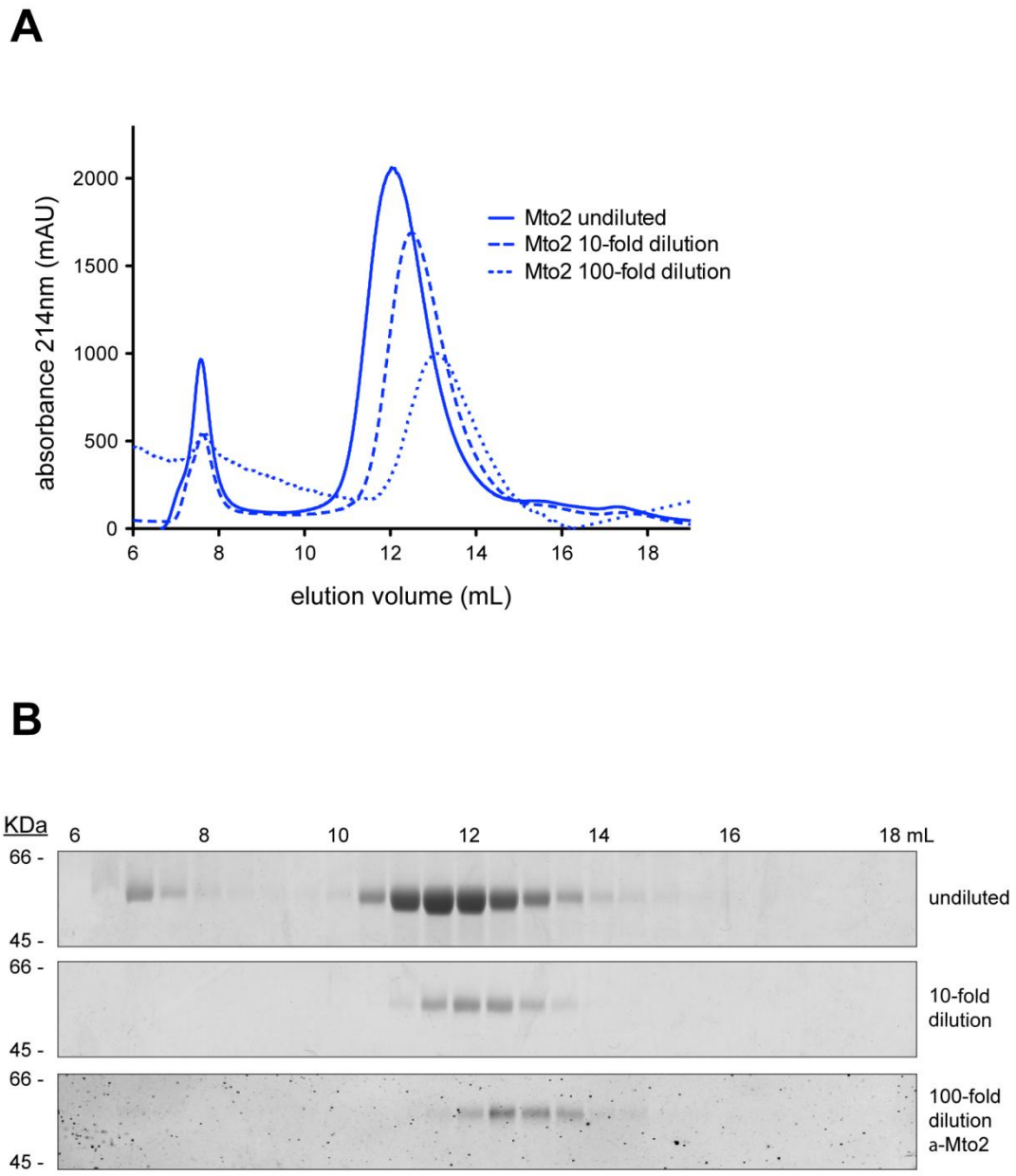

Figure 6.7: Mto2 multimerizes and is in a dynamic equilibrium. (A) Various dilutions of Ni-purified Mto2 were fractionated by gel filtration on a Superose 6 10/300 GL column (undiluted sample was roughly 50 μM). 10- and 100-fold dilution of the original sample caused Mto2 to elute at increased elution volumes. This suggests that Mto2 is in a dynamic equilibrium between complexes with different degrees of multimerization. Note that absorbance values are only accurate for the undiluted sample; values for the 10- and 100-fold dilutions were arbitrarily re-scaled to make them visible. (B) The shift of Mto2 to later elution was confirmed by running fractions on 10% SDS-PAGE and staining with coomassie (undiluted and 10-fold dilution) or anti-Mto2 western blotting (100-fold dilution).

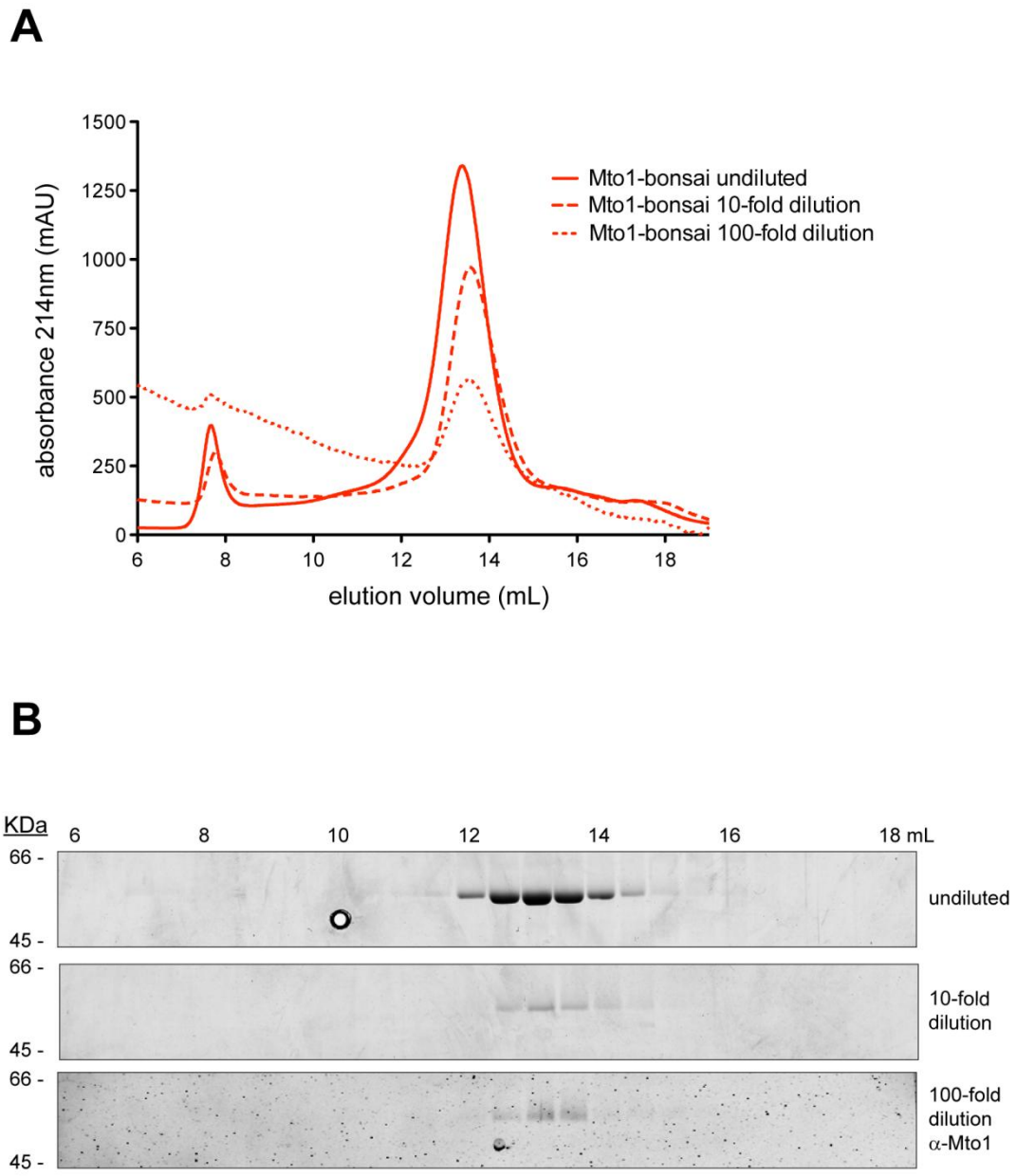

Figure 6.8: Mto1-bonsai is likely monodispersed. (A) Various dilutions of Ni-purified Mto1-bonsai were fractionated by gel filtration on a Superose 6 10/300 GL column (undiluted sample was roughly 30 μM). 10-fold dilution of the original sample only slightly increased the elution volume of Mto1-bonsai, and 100-fold dilution had no additional effect. This suggests that Mto1-bonsai is present as a single species. Note that absorbance values are only accurate for the undiluted sample; values for the 10- and 100-fold dilutions were arbitrarily re-scaled to make them visible. (B) Fractions were analyzed by 10% SDS-PAGE followed by coomassie staining (undiluted and 10-fold dilution) or anti-Mto1 western blot (100-fold dilution). This confirmed that the elution volume of Mto1-bonsai was essentially unaltered by dilution.

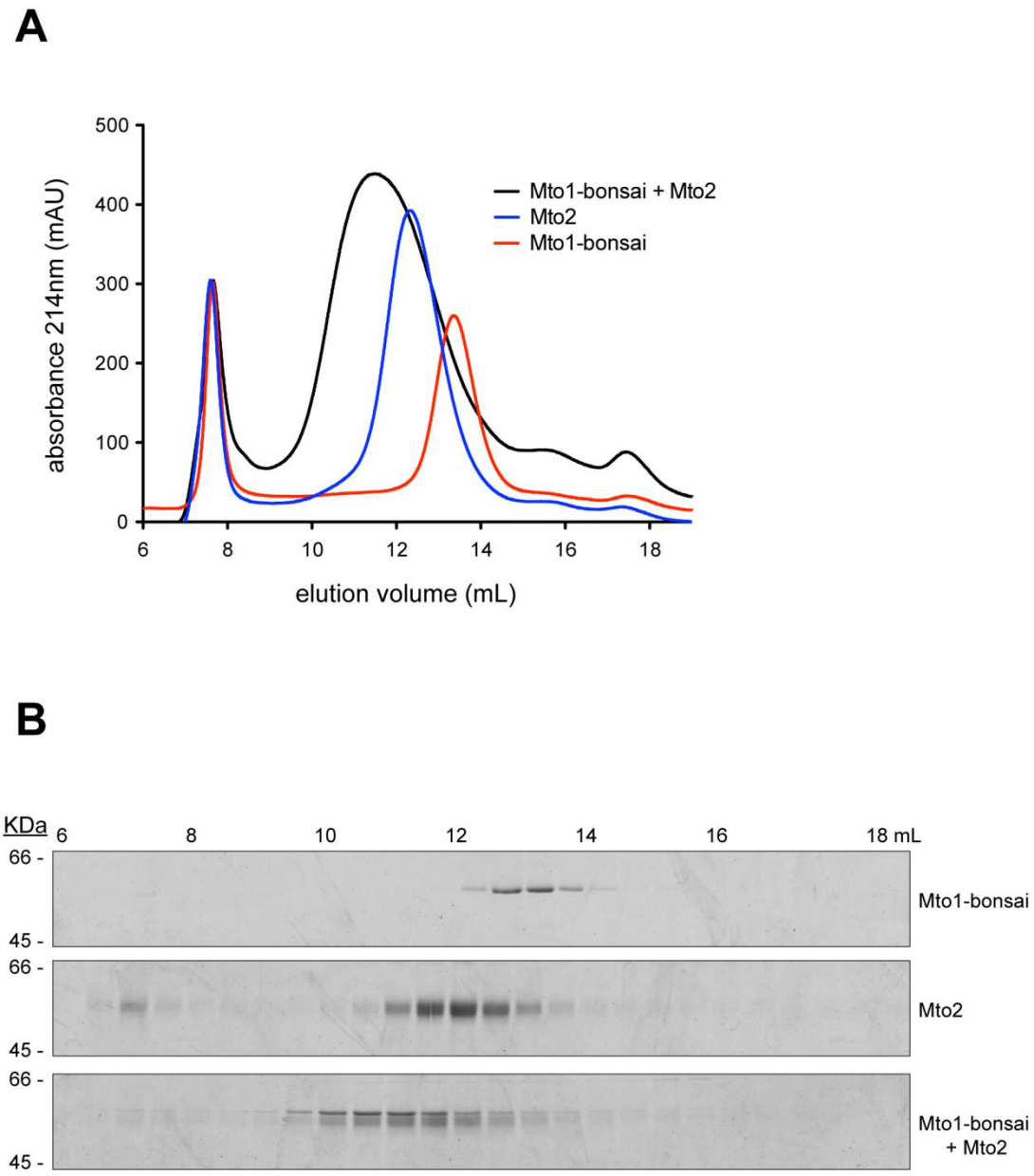

Figure 6.9: Mto1-bonsai and Mto2 multimerize efficiently *in vitro*. (A) Mto1-bonsai and Mto2 were Ni-purified separately and later combined *in vitro*. Samples of the individual and combined proteins were analyzed by gel filtration on a Superose 6 10/300 GL column. Equal amounts of Mto1-bonsai and Mto2 were present when ran individually and together. When combined, Mto1-bonsai and Mto2 assembled into a larger complex that eluted earlier. (B) Fractions from the gel filtration experiment were analyzed by 10% SDS-PAGE followed by coomassie staining. When combined, Mto1-bonsai and Mto2 clearly co-migrated and eluted earlier, indicating that they assembled into Mto1/2-bonsai complex.

6.3 Discussion

The fact that recombinant Mto1/2-bonsai assembles into large, dynamic multimers is consistent with observations of endogenous fission yeast Mto1/2 complex and likely relates to its function. SEC-MALS analysis of the recombinant complex suggests that Mto1/2-bonsai heterodimers associate to form multimers with a range of sizes. At about 800 kDa, the largest of these multimers would correspond to ~9 copies each of Mto1-bonsai and Mto2. These values are comparable to the 13 copies of Mto1-bonsai-GFP and Mto2-GFP observed in nucleating puncta by fluorescence microscopy. In addition, fluorescence microscopy of nucleating puncta and biochemical analysis of recombinant Mto1/2-bonsai both suggest that Mto1-bonsai and Mto2 associate with a 1:1 stoichiometry. Consistent with this, endogenous Mto1(1-800) and Mto2 from fission yeast extracts may form a heterotetramer, as determined by hydrodynamic analysis (Lynda M. Groocock, PhD Thesis 2010). Overall, the data therefore suggest that Mto1 and Mto2 associate in a core subunit, such as a heterodimer or heterotetramer, which then multimerizes into larger complexes. As we saw in chapter 4, higher-order multimers of Mto1/2-bonsai may activate MT nucleation from the γ-TuC. Significantly, this multimerization is preserved in purified, recombinant Mto1/2-bonsai complex.

The oligomeric states of Mto1-bonsai and Mto2 when purified individually were less clear. Previous work has shown that Mto1 and Mto2 self-interact *in vivo*, and that recombinant Mto2 (expressed in *E. coli,* where it is poorly soluble) may be pentameric (Lynda M. Groocock, PhD Thesis 2010). Here, the dilution experiments with recombinant Mto2 from insect cells clearly show that Mto2 is in a dynamic equilibrium, confirming that Mto2 must be multimerized to some extent. Mto1-bonsai, on the other hand, appeared to be monodisperse. From gel filtration alone, we cannot directly infer the oligomeric state of

Mto1-bonsai or Mto2, given the dependence of elution volume on additional features such as molecular shape and non-specific interaction with the column matrix. However, we can make some general predictions regarding Mto1-bonsai and Mto2 oligomerization, based on the typical migration of calibration proteins on Superose 6 (as described by GE Healthcare in protocols provided with the Superose 6 10/300 GL column). For example, bovine serum albumin (BSA), a globular protein of 67 kDa, is expected to elute around 16 mL. By contrast Mto1-bonsai and Mto2, which would both be 45 kDa as monomers, elute much earlier — Mto1-bonsai elutes at 13.5 mL, while Mto2 elutes around 12-13 mL (depending on concentration). These elution volumes fall between those generally expected for thyroglobulin and ferritin, which have molecular weights of 660 and 440 kDa, respectively. Overall, this implies that Mto1-bonsai, as well as Mto2, is very likely multimerized to some unknown degree. Given that it contains coiled-coils, we might predict that Mto1-bonsai is at least dimeric. However, this is somewhat inconsistent with the SEC-MALS data for the Mto1/2-bonsai complex, which suggests that Mto1-bonsai and Mto2 elute partly as heterodimers. It is possible that binding of Mto1-bonsai to Mto2 disrupts Mto1-Mto1 and Mto2-Mto2 self-interaction, although this seems unlikely. Ultimately, a technique such as SEC-MALS will be required to accurately determine the oligomeric states of Mto1-bonsai and Mto2 when purified alone.

7. Conclusions and Future Work

Throughout this study, I have attempted to characterize the role of Mto1/2 in activating the γ-TuC, while also adding to our knowledge of how Mto1/2 targets the γ-TuC to cytoplasmic MTOCs. Primarily, this was done through analysis of the *mto1-NE* and *mto1-bonsai* mutants. Also, as a first step towards reconstituting MT nucleation *in vitro*, I expressed, purified, and characterized recombinant Mto1/2-bonsai complex.

Very little is known about the factors involved in regulating MT nucleation by the γ-TuC, making the identification of γ-TuC activators a subject of particular interest. Currently, CDK5RAP2 remains the only protein which has been shown to have a direct role in activating the γ-TuC (Choi et al., 2010). CDK5RAP2 is also involved in recruiting the γ-TuC to the centrosome and, like Mto1, associates with the γ-TuC via a CM1 domain (Choi et al., 2010; Fong et al., 2008). *In vivo*, over-expression of a CM1-containing fragment of CDK5RAP2 displaces the γ-TuC from the centrosome, and results in extensive acentrosomal nucleation (Choi et al., 2010). However, it is uncertain if the MT nucleation observed under conditions of CDK5RAP2 over-expression occurs by a physiologically relevant mechanism. Indeed, cells over-expressing the CM1 fragment of CDK5RAP2 nucleate MTs in an abnormal manner, with many short MTs appearing throughout the entire cytoplasm. *In vitro*, both full-length CDK5RAP2 and the CM1-containing fragment are capable of activating MT nucleation from purified γ-TuRCs (Choi et al., 2010). Still, the mechanism by which CDK5RAP2 stimulates MT nucleation by the γ-TuRC remains unknown.

In the present work, I have provided strong evidence that the Mto1/2 complex is also a γ-TuC activator. Previous work has shown that in the absence of Mto1, the γ-TuC is no longer localized to cytoplasmic MTOCs and cells are completely deficient in cytoplasmic MT nucleation (Sawin et al., 2004; Venkatram et al., 2004). However, this did not tell us

whether or not Mto1/2 had a direct role in γ-TuC activation — it remained possible that Mto1/2 is responsible only for localizing the γ-TuC to MTOCs, where additional factors then activate γ-TuC. For example, kinases or structural proteins that are specifically localized to MTOCs could be required for activating the γ-TuC. To address this issue, I therefore generated the Mto1-bonsai mutant, which lacked the N- and C-terminal domains required for localizing the Mto1/2 complex and γ-TuC to cytoplasmic MTOCs. Significantly, the Mto1/2-bonsai complex is able to promote spatially random MT nucleation from the γ-TuC. This suggests that Mto1/2 has a direct role in activating the γ-TuC, that is independent of its role in localizing the γ-TuC to MTOCs. Consistent with this, live-cell imaging revealed that newly-nucleated MTs are always associated with Mto1-bonsai and Mto2, in addition to the γ-TuC. This confirmed that actively-nucleating γ-TuCs are associated with Mto1/2-bonsai complexes. Overall, the *mto1-bonsai* mutant provides the strongest evidence to date that Mto1/2 is a γ-TuC activator. However, we cannot rule out the possibility that additional proteins are also required for activating the γ-TuC by *in vivo* analysis alone. That is, additional γ-TuC-associated proteins that are required for MT nucleation may simply remain to be identified.

Importantly, *mto1-bonsai* has qualitatively normal MT arrays and shows only very minor defects in MT-dependent processes such as nuclear positioning and maintenance of cell morphology. These processes require that MTs are oriented with minus-ends overlapping at the cell centre and plus-ends towards the cell tips. This allows MTs to correctly target polarity factors to cell tips, and also to exert forces on the nucleus to position it at the centre of the cell. *mto1-bonsai* appears to be able to maintain this orientation of MTs, despite lacking any conventional MTOCs. This could be confirmed by imaging a MT plus-end tracking protein, such as GFP-tagged Mal3 (Busch and Brunner, 2004), in an *mto1-bonsai* background. Following spatially random MT nucleation in *mto1-*

bonsai, proper MT organization is likely ensured by additional factors, including the MT bundling proteins Ase1 and Dis1, as well as motor proteins such as Klp2 (Roque et al., 2010; Yamashita et al., 2005). The minus-end directed motor Klp2 and anti-parallel bundling protein Ase1 act cooperatively to orient MTs with plus-ends towards the cell tips and minus-ends overlapping at the cell centre (Braun et al., 2011; Roque et al., 2010). In fact, cells completely lacking nuclei and SPBs are capable of organizing and correctly orienting MTs in this manner (Carazo-Salas and Nurse, 2006; Daga et al., 2006). Notably, MT nucleation in these anucleate cells was found to be spatially random and Mto1-dependent. The mechanism for this spatially random nucleation is clearly explained here, using the *mto1-bonsai* mutant. Overall, the findings in anucleate cells and *mto1-bonsai* may lead us to question the functional purpose of nucleating MTs from specific subcellular sites. Perhaps, the function of site-specific MT nucleation is simply redundant with the MT organization achieved by bundling factors and motor proteins.

In both *mto1-NE* and *mto1-bonsai*, existing MTs no longer appear to function as MTOCs. The lack of MT nucleation from existing MTs has no obvious effect on these cells: *mto1-NE* cells are perfectly viable, and exhibit wild-type polarity and nuclear positioning. Polarity and nuclear positioning defects only arise when MT nucleation from the NE is eliminated in *mto1-bonsai* and *mto1(131-1115)*. MT-based MT nucleation in fission yeast may simply "amplify" existing MT bundles. This type of MT nucleation from the sides of existing bundles is important in other organisms. In Drosophila and human cells, the 8 subunit augmin complex has been show to recruit the γ-TuC to MTs within the mitotic spindle (Goshima et al., 2008; Uehara et al., 2009). This promotes MT nucleation from existing spindle MTs, thereby increasing the density and stability of the mitotic spindle. Augmin-dependent MT nucleation within the spindle also appears to increase the frequency of kinetochore capture (Goshima et al., 2008). Augmin depletion in Drosophila S2

cells is largely rescued by centrosome-mediated MT nucleation (Goshima et al., 2008), which itself depends on the CM1 protein Centrosomin (Megraw et al., 1999; Zhang and Megraw, 2007). By contrast, augmin depletion in human HeLa cells leads to severe spindle defects and metaphase arrest (Uehara et al., 2009).

The *mto1-NE* mutant will likely prove useful in understanding how the NE acts as a MTOC in fission yeast. The role of the NE as a MTOC is of interest in other systems as well. For example, the NE acts as a MTOC in differentiated muscle cells, referred to as myotubes. Myotubes are multinucleate cells, that form by the fusion of several myoblasts. During this differentiation process, centrosomal proteins such as γ-tubulin, pericentrin, and ninein re-distribute to the NE, thus establishing the NE as a site of MT nucleation (Bugnard et al., 2005; Tassin et al., 1985). In plants, which lack centrosomes, the NE acts as a primary MTOC (Seltzer et al., 2007; Stoppin et al., 1994). Arabidopsis γ-tubulin, GCP2, and GCP3 localize to the NE, and deletions within GCP2 and GCP3 abolish this localization (Seltzer et al., 2007). Precisely how the γ-TuC associates with the nuclear surface in plant cells remains unclear, although we might predict that this requires γ-TuC binding to some sort of anchoring complex on the NE. Mto1-NE may help us identify anchoring proteins of this sort. When compared to wild-type Mto1, Mto1-NE shows greatly increased localization to the nuclear surface. Thus, pull-down experiments with Mto1-NE could facilitate the identification of proteins which are specifically involved in linking the Mto1/2 complex to the nuclear surface.

Further analysis of the *mto1-bonsai* mutant allowed us to propose a general model for how Mto1/2 may activate the γ-TuC. Previously, sucrose gradients have revealed that the vast majority of fission yeast γ-tubulin is present in small complexes, suggesting that fission yeast cells contain only limited numbers of γ-TuRCs (Anders et al., 2006). Through fluorescence quantification of nucleating puncta, I found that actively-nucleating γ-TuCs are

associated with ~13 copies each of Mto1-bonsai and Mto2. The value 13 matches the number of protofilaments in a MT, and also the number of γ-tubulins thought to be present in a single γ-TuRC. We found that nucleating puncta contained ~8 copies each of Alp4-GFP and Alp6-GFP, values which are consistent with single γ-TuRCs. Overall, these values indicate that each γ-TuSC in an active γ-TuC associates with ~2 copies each of Mto1-bonsai and Mto2. Therefore, we propose that Mto1/2-bonsai may help promote the multimerization of γ-TuSCs into active γ-TuRCs.

Higher-order multimers of Mto1/2 appear to be required for activating the γ-TuC. Deletion of *mto2* results in the disappearance of Mto1-NE-GFP and Mto1-bonsai-GFP puncta. In the absence of these puncta, which correspond to Mto1/2-NE and Mto1/2-bonsai multimers, cells are completely deficient in cytoplasmic MT nucleation. Importantly, in the absence of Mto2, full-length Mto1 retains normal localization to the SPB and can promote MT nucleation from the SPB (Samejima et al., 2005; Venkatram et al., 2005)(this study). This demonstrates that Mto2 is not required for MT nucleation *per se*. Rather, the main role of Mto2 may be in multimerizing Mto1 at non-SPB MTOCs. A redundant mechanism of multimerization could allow full-length Mto1 to stimulate MT nucleation at the SPB. Local concentration of Mto1 at the SPB, for example, could be sufficient for promoting Mto1 multimerization. However, because they fail to localize to the SPB, Mto1-NE and Mto1-bonsai are completely dependent on Mto2 for assembly into the higher-order complexes required for MT nucleation.

Based on EM structural data, it has been proposed that activation of the γ-TuC may also require a conformational change in GCP3. This conformational change would adjust the spacing of γ-tubulins to match the spacing of adjacent protofilaments in the MT lattice (Kollman et al., 2011; Kollman et al., 2010). Perhaps, binding of Mto1/2-bonsai at each γ-

TuSC in a complete γ-TuRC could induce this conformational change, thus producing an effective template for MT nucleation.

Cells may regulate Mto1/2 multimerization as a means of controlling cytoplasmic MT nucleation throughout the cell cycle. Previous work has revealed that Mto2 is phosphorylated throughout the cell cycle and hyperphosphorylated during mitosis (Lynda Groocock, PhD Thesis). The mitotic phosphorylation of Mto2 is correlated with disruption of the Mto1-Mto2 interaction and disassembly of Mto1/2 puncta (Lynda Groocock, PhD Thesis). This suggests that Mto2 phosphorylation may cause Mto1/2 multimers to disassemble during mitosis, leading to inactivation of cytoplasmic γ-TuCs and depolymerization of cytoplasmic MT arrays. This is an attractive model that remains to be directly demonstrated. That is, current data shows only a correlation between Mto2 hyperphosphorylation, disassembly of Mto1/2 multimers, and the depolymerization of cytoplasmic MTs during mitosis.

The budding yeast proteins Spc72 and Spc110 also appear to associate with the γ-TuC as multimers. Spc72 and Spc110 mediate γ-TuC attachment to the nucleoplasmic and cytoplasmic face of the SPB, respectively (Knop and Schiebel, 1997; Knop and Schiebel, 1998). Recent work in Elmar Schiebel's lab (publish during this thesis work) indicates that MTs nucleated from γ-TuCs on the nucleoplasmic or cytoplasmic face of the SPB are associated with ~15 copies of Spc72 or Spc110 (Erlemann et al., 2012). These values are comparable to the 13 copies of Mto1-bonsai and Mto2 per γ-TuC seen here, and similarly suggest that Spc72 and Spc110 may act as a scaffold for γ-TuSC multimerization and activation. Notably, the SPB acts as the only MTOC in budding yeast, which lack an Mto2 homologue. One might suspect, therefore, that Spc72 and Spc110 must be multimerized by association with the SPB in order to promote MT nucleation from the γ-TuC — a similar mechanism as described for Mto1 in *mto2Δ* cells. Thus, a lack of Spc110 multimerization *in*

vitro could account for the inability of Spc110 to enhance MT nucleation from purified γ-TuSCs (Kollman et al., 2010; Vinh et al., 2002). Perhaps, multimerization of purified Mto1-bonsai by Mto2 will be sufficient for generating a potent activator of the γ-TuC.

Ultimately, confirming that Mto1/2 is a γ-TuC activator will require reconstitution of a complex that is capable of robust MT nucleation *in vitro*. We suspect that complexes composed of Mto1/2-bonsai and the γ-TuSC proteins may be sufficient for nucleating MTs. Towards the long-term objective of demonstrating this, I purified Mto1/2-bonsai complex using the MultiBac insect cell expression system. Features of the Mto1/2-bonsai complex that were observed *in vivo* appeared to be conserved in the recombinant complex. Purified Mto1/2-bonsai complex had a 1:1 stoichiometry of Mto1-bonsai:Mto2. Further, SEC-MALS revealed that Mto1/2-bonsai assembled into multimers with a range of sizes, the largest of which were consistent with ~9 copies each of Mto1-bonsai and Mto2. Therefore, these complexes are comparable to the nucleating puncta observed by fluorescence microscopy, which contained 13 copies each of Mto1-bonsai and Mto2. Importantly, only actively nucleating Mto1/2-bonsai puncta were included in fluorescence quantification. This likely explains why the Mto1/2-bonsai complex appeared to have a relatively defined size *in vivo*, while recombinant Mto1/2-bonsai complex showed a much wider range of sizes *in vitro*.

The precise oligomeric states of Mto2 and Mto1-bonsai purified on their own remain unknown. Gel filtration experiments revealed that the elution volume of Mto2 was increased upon dilution, indicating that Mto2 must be multimerized to some degree. Similar experiments suggested that Mto1-bonsai is monodisperse, although based on its elution volume I argued that Mto1-bonsai is unlikely to be monomeric. Because it contains coiled-coil sequences, we suspect that Mto1-bonsai is at least dimerized. SEC-MALS would be ideal for confirming the multimerization states of Mto1-bonsai and Mto2, although additional techniques such as analytical ultracentrifugation could also be used. If it is

indeed monodisperse, Mto1-bonsai could be amenable to structural analysis by X-ray crystallography.

Given its large size (ie. 100s of kDa) the Mto1/2-bonsai complex is a good candidate for structural studies by single particle electron microscopy. It would be interesting to see if Mto1/2-bonsai forms ring-like or helical structures — the sorts of structures one might predict to template γ-TuSC multimerization. However, the polydispersity of recombinant Mto1/2-bonsai complex could complicate this analysis. Gel filtration and SEC-MALS experiments demonstrate that Mto1/2-bonsai is in a dynamic equilibrium of complexes with a large distribution of molecular weights (~75-800 kDa). Perhaps, varying buffer conditions, such as salt or pH, could increased the homogeneity of the complex by promoting assembly or disassembly. Also, it is possible that the full-length Mto1/2 complex would show reduced polydispersity. The additional coiled-coils in full-length Mto1 (compared to truncated Mto1-bonsai) could promote more stable, robust multimerization into higher-order complexes. However, purification of full-length Mto1 could be complicated by the fact that it appears to be extensively degraded. Given that Mto1/2 forms multimers, degraded products of Mto1 would likely co-purify with full-length, undegraded Mto1. Still, purification and characterization of recombinant wild-type Mto1/2 is certainly worth pursuing.

Ultimately, our greatest interest lies in reconstitution of complexes composed of Mto1/2-bonsai and γ-TuSCs. Given the versatility of the MultiBac system, viruses for the co-expression of Mto1-bonsai, Mto2, Alp4, Alp6, and γ-tubulin could certainly be constructed. MultiBac has been successfully used to express many different protein subunits from a single virus genome. For example, the entire 13-protein anaphase promoting complex (APC/C) was reconstituted by co-infecting insect cells with 2 MultiBac viruses, one encoding 8 proteins and the other encoding 5 proteins (Schreiber et al., 2011).

Alternatively, Mto1/2-bonsai and γ-TuSCs could be expressed and purified separately, and later combined *in vitro*. This latter approach would likely be preferable, as it would allow both sub-complexes to be characterized individually and in combination. One could address, for example, whether or not Mto1/2-bonsai is capable of promoting γ-TuSC multimerization. Most importantly, reconstitution of these complexes would allow us to directly address whether or not Mto1/2-bonsai is sufficient for activating MT nucleation from the γ-TuC. The identification and characterization of Mto1/2-bonsai as a γ-TuC activator could provide insight into the mechanism of γ-TuC activation in other systems.

References

Aldaz, H., L.M. Rice, T. Stearns, and D.A. Agard. 2005. Insights into microtubule nucleation from the crystal structure of human gamma-tubulin. *Nature*. 435:523-527.

Anders, A., P.C. Lourenco, and K.E. Sawin. 2006. Noncore components of the fission yeast gamma-tubulin complex. *Mol Biol Cell*. 17:5075-5093.

Anders, A., and K.E. Sawin. 2011. Microtubule stabilization in vivo by nucleation-incompetent gamma-tubulin complex. *J Cell Sci*. 124:1207-1213.

Arnal, I., E. Karsenti, and A.A. Hyman. 2000. Structural transitions at microtubule ends correlate with their dynamic properties in Xenopus egg extracts. *J Cell Biol*. 149:767-774.

Azimzadeh, J., and M. Bornens. 2007. Structure and duplication of the centrosome. *J Cell Sci*. 120:2139-2142.

Bahler, J., J.Q. Wu, M.S. Longtine, N.G. Shah, A. McKenzie, 3rd, A.B. Steever, A. Wach, P. Philippsen, and J.R. Pringle. 1998. Heterologous modules for efficient and versatile PCR-based gene targeting in Schizosaccharomyces pombe. *Yeast*. 14:943-951.

Beisson, J., and M. Wright. 2003. Basal body/centriole assembly and continuity. *Curr Opin Cell Biol*. 15:96-104.

Berger, B., D.B. Wilson, E. Wolf, T. Tonchev, M. Milla, and P.S. Kim. 1995. Predicting coiled coils by use of pairwise residue correlations. *Proc Natl Acad Sci U S A*. 92:8259-8263.

Berger, I., D.J. Fitzgerald, and T.J. Richmond. 2004. Baculovirus expression system for heterologous multiprotein complexes. *Nature biotechnology*. 22:1583-1587.

Bettencourt-Dias, M., and D.M. Glover. 2007. Centrosome biogenesis and function: centrosomics brings new understanding. *Nature reviews. Molecular cell biology*. 8:451-463.

Bezanilla, M., S.L. Forsburg, and T.D. Pollard. 1997. Identification of a second myosin-II in Schizosaccharomyces pombe: Myp2p is conditionally required for cytokinesis. *Mol Biol Cell*. 8:2693-2705.

Bieniossek, C., and I. Berger. 2009. Towards eukaryotic structural complexomics. *Journal of structural and functional genomics*. 10:37-46.

Bond, J., E. Roberts, K. Springell, S.B. Lizarraga, S. Scott, J. Higgins, D.J. Hampshire, E.E. Morrison, G.F. Leal, E.O. Silva, S.M. Costa, D. Baralle, M. Raponi, G. Karbani, Y. Rashid, H. Jafri, C. Bennett, P. Corry, C.A. Walsh, and C.G. Woods. 2005. A centrosomal mechanism involving CDK5RAP2 and CENPJ controls brain size. *Nat Genet*. 37:353-355.

Braun, M., Z. Lansky, G. Fink, F. Ruhnow, S. Diez, and M.E. Janson. 2011. Adaptive braking by Ase1 prevents overlapping microtubules from sliding completely apart. *Nat Cell Biol*. 13:1259-1264.

Bugnard, E., K.J. Zaal, and E. Ralston. 2005. Reorganization of microtubule nucleation during muscle differentiation. *Cell Motil Cytoskeleton*. 60:1-13.

Burns, R.G. 1991. Alpha-, beta-, and gamma-tubulins: sequence comparisons and structural constraints. *Cell Motil Cytoskeleton*. 20:181-189.

Busch, K.E., and D. Brunner. 2004. The microtubule plus end-tracking proteins mal3p and tip1p cooperate for cell-end targeting of interphase microtubules. *Curr Biol*. 14:548-559.

Caplow, M., and J. Shanks. 1996. Evidence that a single monolayer tubulin-GTP cap is both necessary and sufficient to stabilize microtubules. *Mol Biol Cell*. 7:663-675.

Carazo-Salas, R.E., and P. Nurse. 2006. Self-organization of interphase microtubule arrays in fission yeast. *Nat Cell Biol*. 8:1102-1107.

Caviston, J.P., and E.L. Holzbaur. 2006. Microtubule motors at the intersection of trafficking and transport. *Trends Cell Biol*. 16:530-537.

Choi, Y.K., P. Liu, S.K. Sze, C. Dai, and R.Z. Qi. 2010. CDK5RAP2 stimulates microtubule nucleation by the gamma-tubulin ring complex. *J Cell Biol*. 191:1089-1095.

Choy, R.M., J.M. Kollman, A. Zelter, T.N. Davis, and D.A. Agard. 2009. Localization and orientation of the gamma-tubulin small complex components using protein tags as labels for single particle EM. *J Struct Biol*. 168:571-574.

Chretien, D., S.D. Fuller, and E. Karsenti. 1995. Structure of growing microtubule ends: two-dimensional sheets close into tubes at variable rates. *J Cell Biol*. 129:1311-1328.

Chretien, D., and R.H. Wade. 1991. New data on the microtubule surface lattice. *Biology of the cell / under the auspices of the European Cell Biology Organization*. 71:161-174.

Daga, R.R., and F. Chang. 2005. Dynamic positioning of the fission yeast cell division plane. *Proc Natl Acad Sci U S A*. 102:8228-8232.

Daga, R.R., K.G. Lee, S. Bratman, S. Salas-Pino, and F. Chang. 2006. Self-organization of microtubule bundles in anucleate fission yeast cells. *Nat Cell Biol*. 8:1108-1113.

DeLuca, J.G., and A. Musacchio. 2012. Structural organization of the kinetochore-microtubule interface. *Curr Opin Cell Biol*. 24:48-56.

Dictenberg, J.B., W. Zimmerman, C.A. Sparks, A. Young, C. Vidair, Y. Zheng, W. Carrington, F.S. Fay, and S.J. Doxsey. 1998. Pericentrin and gamma-tubulin form a protein complex and are organized into a novel lattice at the centrosome. *J Cell Biol*. 141:163-174.

Ehrhardt, D.W., and S.L. Shaw. 2006. Microtubule dynamics and organization in the plant cortical array. *Annual review of plant biology*. 57:859-875.

Erickson, H.P. 2000. Gamma-tubulin nucleation: template or protofilament? *Nat Cell Biol*. 2:E93-96.

Erickson, H.P., and D. Stoffler. 1996. Protofilaments and rings, two conformations of the tubulin family conserved from bacterial FtsZ to alpha/beta and gamma tubulin. *J Cell Biol*. 135:5-8.

Erlemann, S., A. Neuner, L. Gombos, R. Gibeaux, C. Antony, and E. Schiebel. 2012. An extended gamma-tubulin ring functions as a stable platform in microtubule nucleation. *J Cell Biol*. 197:59-74.

Evans, L., T. Mitchison, and M. Kirschner. 1985. Influence of the centrosome on the structure of nucleated microtubules. *J Cell Biol*. 100:1185-1191.

Feierbach, B., and F. Chang. 2001. Cytokinesis and the contractile ring in fission yeast. *Current opinion in microbiology*. 4:713-719.

Fitzgerald, D.J., P. Berger, C. Schaffitzel, K. Yamada, T.J. Richmond, and I. Berger. 2006. Protein complex expression by using multigene baculoviral vectors. *Nature methods*. 3:1021-1032.

Fitzgerald, D.J., C. Schaffitzel, P. Berger, R. Wellinger, C. Bieniossek, T.J. Richmond, and I. Berger. 2007. Multiprotein expression strategy for structural biology of eukaryotic complexes. *Structure*. 15:275-279.

Flory, M.R., M. Morphew, J.D. Joseph, A.R. Means, and T.N. Davis. 2002. Pcp1p, an Spc110p-related calmodulin target at the centrosome of the fission yeast Schizosaccharomyces pombe. *Cell Growth Differ*. 13:47-58.

Fong, C.S., M. Sato, and T. Toda. 2010. Fission yeast Pcp1 links polo kinase-mediated mitotic entry to gamma-tubulin-dependent spindle formation. *EMBO J*. 29:120-130.

Fong, K.W., Y.K. Choi, J.B. Rattner, and R.Z. Qi. 2008. CDK5RAP2 is a pericentriolar protein that functions in centrosomal attachment of the gamma-tubulin ring complex. *Mol Biol Cell*. 19:115-125.

Gaglio, T., A. Saredi, J.B. Bingham, M.J. Hasbani, S.R. Gill, T.A. Schroer, and D.A. Compton. 1996. Opposing motor activities are required for the organization of the mammalian mitotic spindle pole. *J Cell Biol*. 135:399-414.

Gardner, M.K., B.D. Charlebois, I.M. Janosi, J. Howard, A.J. Hunt, and D.J. Odde. 2011. Rapid microtubule self-assembly kinetics. *Cell*. 146:582-592.

Goldstein, L.S., and Z. Yang. 2000. Microtubule-based transport systems in neurons: the roles of kinesins and dyneins. *Annual review of neuroscience*. 23:39-71.

Goshima, G., M. Mayer, N. Zhang, N. Stuurman, and R.D. Vale. 2008. Augmin: a protein complex required for centrosome-independent microtubule generation within the spindle. *J Cell Biol*. 181:421-429.

Guillet, V., M. Knibiehler, L. Gregory-Pauron, M.H. Remy, C. Chemin, B. Raynaud-Messina, C. Bon, J.M. Kollman, D.A. Agard, A. Merdes, and L. Mourey. 2011. Crystal structure of gamma-tubulin complex protein GCP4 provides insight into microtubule nucleation. *Nature structural & molecular biology*. 18:915-919.

Gunawardane, R.N., O.C. Martin, K. Cao, L. Zhang, K. Dej, A. Iwamatsu, and Y. Zheng. 2000. Characterization and reconstitution of Drosophila gamma-tubulin ring complex subunits. *J Cell Biol*. 151:1513-1524.

Gunawardane, R.N., O.C. Martin, and Y. Zheng. 2003. Characterization of a new gammaTuRC subunit with WD repeats. *Mol Biol Cell*. 14:1017-1026.

Hagan, I., and M. Yanagida. 1997. Evidence for cell cycle-specific, spindle pole body-mediated, nuclear positioning in the fission yeast Schizosaccharomyces pombe. *J Cell Sci*. 110 (Pt 16):1851-1866.

Hagan, I.M. 1998. The fission yeast microtubule cytoskeleton. *J Cell Sci*. 111 (Pt 12):1603-1612.

Hagan, I.M., and J.S. Hyams. 1988. The use of cell division cycle mutants to investigate the control of microtubule distribution in the fission yeast Schizosaccharomyces pombe. *J Cell Sci*. 89 (Pt 3):343-357.

Haren, L., M.H. Remy, I. Bazin, I. Callebaut, M. Wright, and A. Merdes. 2006. NEDD1-dependent recruitment of the gamma-tubulin ring complex to the centrosome is necessary for centriole duplication and spindle assembly. *J Cell Biol*. 172:505-515.

Hutchins, J.R., Y. Toyoda, B. Hegemann, I. Poser, J.K. Heriche, M.M. Sykora, M. Augsburg, O. Hudecz, B.A. Buschhorn, J. Bulkescher, C. Conrad, D. Comartin, A. Schleiffer, M. Sarov, A. Pozniakovsky, M.M. Slabicki, S. Schloissnig, I. Steinmacher, M. Leuschner,

A. Ssykor, S. Lawo, L. Pelletier, H. Stark, K. Nasmyth, J. Ellenberg, R. Durbin, F. Buchholz, K. Mechtler, A.A. Hyman, and J.M. Peters. 2010. Systematic analysis of human protein complexes identifies chromosome segregation proteins. *Science*. 328:593-599.

Hyman, A.A., S. Salser, D.N. Drechsel, N. Unwin, and T.J. Mitchison. 1992. Role of GTP hydrolysis in microtubule dynamics: information from a slowly hydrolyzable analogue, GMPCPP. *Mol Biol Cell*. 3:1155-1167.

Jaspersen, S.L., and M. Winey. 2004. The budding yeast spindle pole body: structure, duplication, and function. *Annual review of cell and developmental biology*. 20:1-28.

Kalil, K., and E.W. Dent. 2004. Hot +TIPS: guidance cues signal directly to microtubules. *Neuron*. 42:877-879.

Khodjakov, A., R.W. Cole, B.R. Oakley, and C.L. Rieder. 2000. Centrosome-independent mitotic spindle formation in vertebrates. *Curr Biol*. 10:59-67.

Khodjakov, A., and C.L. Rieder. 1999. The sudden recruitment of gamma-tubulin to the centrosome at the onset of mitosis and its dynamic exchange throughout the cell cycle, do not require microtubules. *J Cell Biol*. 146:585-596.

Knop, M., G. Pereira, S. Geissler, K. Grein, and E. Schiebel. 1997. The spindle pole body component Spc97p interacts with the gamma-tubulin of Saccharomyces cerevisiae and functions in microtubule organization and spindle pole body duplication. *EMBO J*. 16:1550-1564.

Knop, M., G. Pereira, and E. Schiebel. 1999. Microtubule organization by the budding yeast spindle pole body. *Biology of the cell / under the auspices of the European Cell Biology Organization*. 91:291-304.

Knop, M., and E. Schiebel. 1997. Spc98p and Spc97p of the yeast gamma-tubulin complex mediate binding to the spindle pole body via their interaction with Spc110p. *EMBO J*. 16:6985-6995.

Knop, M., and E. Schiebel. 1998. Receptors determine the cellular localization of a gamma-tubulin complex and thereby the site of microtubule formation. *EMBO J*. 17:3952-3967.

Kollman, J.M., A. Merdes, L. Mourey, and D.A. Agard. 2011. Microtubule nucleation by gamma-tubulin complexes. *Nature reviews. Molecular cell biology*. 12:709-721.

Kollman, J.M., J.K. Polka, A. Zelter, T.N. Davis, and D.A. Agard. 2010. Microtubule nucleating gamma-TuSC assembles structures with 13-fold microtubule-like symmetry. *Nature*. 466:879-882.

Kollman, J.M., A. Zelter, E.G. Muller, B. Fox, L.M. Rice, T.N. Davis, and D.A. Agard. 2008. The structure of the gamma-tubulin small complex: implications of its architecture and flexibility for microtubule nucleation. *Mol Biol Cell*. 19:207-215.

Kuchnir Fygenson, D., H. Flyvbjerg, K. Sneppen, A. Libchaber, and S. Leibler. 1995. Spontaneous nucleation of microtubules. *Physical review. E, Statistical physics, plasmas, fluids, and related interdisciplinary topics*. 51:5058-5063.

Laporte, D., V.C. Coffman, I.J. Lee, and J.Q. Wu. 2011. Assembly and architecture of precursor nodes during fission yeast cytokinesis. *J Cell Biol*. 192:1005-1021.

Li, H., D.J. DeRosier, W.V. Nicholson, E. Nogales, and K.H. Downing. 2002. Microtubule structure at 8 A resolution. *Structure*. 10:1317-1328.

Li, R., and G.G. Gundersen. 2008. Beyond polymer polarity: how the cytoskeleton builds a polarized cell. *Nature reviews. Molecular cell biology*. 9:860-873.

Lowe, J., H. Li, K.H. Downing, and E. Nogales. 2001. Refined structure of alpha beta-tubulin at 3.5 A resolution. *Journal of molecular biology*. 313:1045-1057.

Luders, J., U.K. Patel, and T. Stearns. 2006. GCP-WD is a gamma-tubulin targeting factor required for centrosomal and chromatin-mediated microtubule nucleation. *Nat Cell Biol*. 8:137-147.

Mandelkow, E.M., R. Schultheiss, R. Rapp, M. Muller, and E. Mandelkow. 1986. On the surface lattice of microtubules: helix starts, protofilament number, seam, and handedness. *J Cell Biol*. 102:1067-1073.

Manning, J.A., S. Shalini, J.M. Risk, C.L. Day, and S. Kumar. 2010. A direct interaction with NEDD1 regulates gamma-tubulin recruitment to the centrosome. *PloS one*. 5:e9618.

Margolis, R.L., and L. Wilson. 1978. Opposite end assembly and disassembly of microtubules at steady state in vitro. *Cell*. 13:1-8.

McDonnell, A.V., T. Jiang, A.E. Keating, and B. Berger. 2006. Paircoil2: improved prediction of coiled coils from sequence. *Bioinformatics*. 22:356-358.

McIntosh, J.R., and E.T. O'Toole. 1999. Life cycles of yeast spindle pole bodies: getting microtubules into a closed nucleus. *Biology of the cell / under the auspices of the European Cell Biology Organization*. 91:305-312.

Megraw, T.L., K. Li, L.R. Kao, and T.C. Kaufman. 1999. The centrosomin protein is required for centrosome assembly and function during cleavage in Drosophila. *Development*. 126:2829-2839.

Miller, P.M., A.W. Folkmann, A.R. Maia, N. Efimova, A. Efimov, and I. Kaverina. 2009. Golgi-derived CLASP-dependent microtubules control Golgi organization and polarized trafficking in motile cells. *Nat Cell Biol*. 11:1069-1080.

Mitchison, T., and M. Kirschner. 1984a. Dynamic instability of microtubule growth. *Nature*. 312:237-242.

Mitchison, T., and M. Kirschner. 1984b. Microtubule assembly nucleated by isolated centrosomes. *Nature*. 312:232-237.

Mitchison, T.J. 1993. Localization of an exchangeable GTP binding site at the plus end of microtubules. *Science*. 261:1044-1047.

Mitchison, T.J. 2005. Mechanism and function of poleward flux in Xenopus extract meiotic spindles. *Philosophical transactions of the Royal Society of London. Series B, Biological sciences*. 360:623-629.

Mogensen, M.M. 1999. Microtubule release and capture in epithelial cells. *Biology of the cell / under the auspices of the European Cell Biology Organization*. 91:331-341.

Mogensen, M.M., A. Malik, M. Piel, V. Bouckson-Castaing, and M. Bornens. 2000. Microtubule minus-end anchorage at centrosomal and non-centrosomal sites: the role of ninein. *J Cell Sci*. 113 (Pt 17):3013-3023.

Moritz, M., M.B. Braunfeld, V. Guenebaut, J. Heuser, and D.A. Agard. 2000. Structure of the gamma-tubulin ring complex: a template for microtubule nucleation. *Nat Cell Biol*. 2:365-370.

Morris, N.R. 2003. Nuclear positioning: the means is at the ends. *Curr Opin Cell Biol*. 15:54-59.

Motegi, F., K. Nakano, C. Kitayama, M. Yamamoto, and I. Mabuchi. 1997. Identification of Myo3, a second type-II myosin heavy chain in the fission yeast Schizosaccharomyces pombe. *FEBS Lett*. 420:161-166.

Moudjou, M., N. Bordes, M. Paintrand, and M. Bornens. 1996. gamma-Tubulin in mammalian cells: the centrosomal and the cytosolic forms. *J Cell Sci*. 109 (Pt 4):875-887.

Muller-Reichert, T., D. Chretien, F. Severin, and A.A. Hyman. 1998. Structural changes at microtubule ends accompanying GTP hydrolysis: information from a slowly hydrolyzable analogue of GTP, guanylyl (alpha,beta)methylenediphosphonate. *Proc Natl Acad Sci U S A*. 95:3661-3666.

Murata, T., S. Sonobe, T.I. Baskin, S. Hyodo, S. Hasezawa, T. Nagata, T. Horio, and M. Hasebe. 2005. Microtubule-dependent microtubule nucleation based on recruitment of gamma-tubulin in higher plants. *Nat Cell Biol*. 7:961-968.

Nogales, E., M. Whittaker, R.A. Milligan, and K.H. Downing. 1999. High-resolution model of the microtubule. *Cell*. 96:79-88.

Nogales, E., S.G. Wolf, and K.H. Downing. 1998. Structure of the alpha beta tubulin dimer by electron crystallography. *Nature*. 391:199-203.

O'Toole, E.T., M. Winey, and J.R. McIntosh. 1999. High-voltage electron tomography of spindle pole bodies and early mitotic spindles in the yeast Saccharomyces cerevisiae. *Mol Biol Cell*. 10:2017-2031.

Oakley, C.E., and B.R. Oakley. 1989. Identification of gamma-tubulin, a new member of the tubulin superfamily encoded by mipA gene of Aspergillus nidulans. *Nature*. 338:662-664.

Oegema, K., C. Wiese, O.C. Martin, R.A. Milligan, A. Iwamatsu, T.J. Mitchison, and Y. Zheng. 1999. Characterization of two related Drosophila gamma-tubulin complexes that differ in their ability to nucleate microtubules. *J Cell Biol*. 144:721-733.

Ohkura, H., I.M. Hagan, and D.M. Glover. 1995. The conserved Schizosaccharomyces pombe kinase plo1, required to form a bipolar spindle, the actin ring, and septum, can drive septum formation in G1 and G2 cells. *Genes Dev*. 9:1059-1073.

Oliferenko, S., and M.K. Balasubramanian. 2002. Astral microtubules monitor metaphase spindle alignment in fission yeast. *Nat Cell Biol*. 4:816-820.

Pardo, M., and P. Nurse. 2003. Equatorial retention of the contractile actin ring by microtubules during cytokinesis. *Science*. 300:1569-1574.

Reilein, A., and W.J. Nelson. 2005. APC is a component of an organizing template for cortical microtubule networks. *Nat Cell Biol*. 7:463-473.

Reilein, A., S. Yamada, and W.J. Nelson. 2005. Self-organization of an acentrosomal microtubule network at the basal cortex of polarized epithelial cells. *J Cell Biol*. 171:845-855.

Reinsch, S., and P. Gonczy. 1998. Mechanisms of nuclear positioning. *J Cell Sci*. 111 (Pt 16):2283-2295.

Rice, L.M., E.A. Montabana, and D.A. Agard. 2008. The lattice as allosteric effector: structural studies of alphabeta- and gamma-tubulin clarify the role of GTP in microtubule assembly. *Proc Natl Acad Sci U S A*. 105:5378-5383.

Roque, H., J.J. Ward, L. Murrells, D. Brunner, and C. Antony. 2010. The fission yeast XMAP215 homolog Dis1p is involved in microtubule bundle organization. *PloS one*. 5:e14201.

Samejima, I., P.C. Lourenco, H.A. Snaith, and K.E. Sawin. 2005. Fission yeast mto2p regulates microtubule nucleation by the centrosomin-related protein mto1p. *Mol Biol Cell*. 16:3040-3051.

Samejima, I., V.J. Miller, L.M. Groocock, and K.E. Sawin. 2008. Two distinct regions of Mto1 are required for normal microtubule nucleation and efficient association with the gamma-tubulin complex in vivo. *J Cell Sci*. 121:3971-3980.

Samejima, I., V.J. Miller, S.A. Rincon, and K.E. Sawin. 2010. Fission yeast Mto1 regulates diversity of cytoplasmic microtubule organizing centers. *Curr Biol*. 20:1959-1965.

Sawin, K.E., K. LeGuellec, M. Philippe, and T.J. Mitchison. 1992. Mitotic spindle organization by a plus-end-directed microtubule motor. *Nature*. 359:540-543.

Sawin, K.E., P.C. Lourenco, and H.A. Snaith. 2004. Microtubule nucleation at non-spindle pole body microtubule-organizing centers requires fission yeast centrosomin-related protein mod20p. *Curr Biol*. 14:763-775.

Sawin, K.E., and H.A. Snaith. 2004. Role of microtubules and tea1p in establishment and maintenance of fission yeast cell polarity. *J Cell Sci*. 117:689-700.

Sawin, K.E., and P.T. Tran. 2006. Cytoplasmic microtubule organization in fission yeast. *Yeast*. 23:1001-1014.

Schreiber, A., F. Stengel, Z. Zhang, R.I. Enchev, E.H. Kong, E.P. Morris, C.V. Robinson, P.C. da Fonseca, and D. Barford. 2011. Structural basis for the subunit assembly of the anaphase-promoting complex. *Nature*. 470:227-232.

Seltzer, V., N. Janski, J. Canaday, E. Herzog, M. Erhardt, J.L. Evrard, and A.C. Schmit. 2007. Arabidopsis GCP2 and GCP3 are part of a soluble gamma-tubulin complex and have nuclear envelope targeting domains. *The Plant journal : for cell and molecular biology*. 52:322-331.

Small, J.V., and I. Kaverina. 2003. Microtubules meet substrate adhesions to arrange cell polarity. *Curr Opin Cell Biol*. 15:40-47.

Snaith, H.A., and K.E. Sawin. 2005. Tea for three: control of fission yeast polarity. *Nat Cell Biol*. 7:450-451.

Stearns, T., L. Evans, and M. Kirschner. 1991. Gamma-tubulin is a highly conserved component of the centrosome. *Cell*. 65:825-836.

Stiess, M., N. Maghelli, L.C. Kapitein, S. Gomis-Ruth, M. Wilsch-Brauninger, C.C. Hoogenraad, I.M. Tolic-Norrelykke, and F. Bradke. 2010. Axon extension occurs independently of centrosomal microtubule nucleation. *Science*. 327:704-707.

Stoppin, V., M. Vantard, A.C. Schmit, and A.M. Lambert. 1994. Isolated Plant Nuclei Nucleate Microtubule Assembly: The Nuclear Surface in Higher Plants Has Centrosome-like Activity. *The Plant cell*. 6:1099-1106.

Takahashi, M., A. Yamagiwa, T. Nishimura, H. Mukai, and Y. Ono. 2002. Centrosomal proteins CG-NAP and kendrin provide microtubule nucleation sites by anchoring gamma-tubulin ring complex. *Mol Biol Cell*. 13:3235-3245.

Tanaka, K., J. Petersen, F. MacIver, D.P. Mulvihill, D.M. Glover, and I.M. Hagan. 2001. The role of Plo1 kinase in mitotic commitment and septation in Schizosaccharomyces pombe. *EMBO J*. 20:1259-1270.

Tassin, A.M., B. Maro, and M. Bornens. 1985. Fate of microtubule-organizing centers during myogenesis in vitro. *J Cell Biol*. 100:35-46.

Teixido-Travesa, N., J. Villen, C. Lacasa, M.T. Bertran, M. Archinti, S.P. Gygi, C. Caelles, J. Roig, and J. Luders. 2010. The gammaTuRC revisited: a comparative analysis of interphase and mitotic human gammaTuRC redefines the set of core components and identifies the novel subunit GCP8. *Mol Biol Cell*. 21:3963-3972.

Tilney, L.G., J. Bryan, D.J. Bush, K. Fujiwara, M.S. Mooseker, D.B. Murphy, and D.H. Snyder. 1973. Microtubules: evidence for 13 protofilaments. *J Cell Biol*. 59:267-275.

Tolic-Norrelykke, I.M., L. Sacconi, G. Thon, and F.S. Pavone. 2004. Positioning and elongation of the fission yeast spindle by microtubule-based pushing. *Curr Biol*. 14:1181-1186.

Tournebize, R., A. Popov, K. Kinoshita, A.J. Ashford, S. Rybina, A. Pozniakovsky, T.U. Mayer, C.E. Walczak, E. Karsenti, and A.A. Hyman. 2000. Control of microtubule dynamics by the antagonistic activities of XMAP215 and XKCM1 in Xenopus egg extracts. *Nat Cell Biol*. 2:13-19.

Tran, P.T., L. Marsh, V. Doye, S. Inoue, and F. Chang. 2001. A mechanism for nuclear positioning in fission yeast based on microtubule pushing. *J Cell Biol*. 153:397-411.

Trowitzsch, S., C. Bieniossek, Y. Nie, F. Garzoni, and I. Berger. 2010. New baculovirus expression tools for recombinant protein complex production. *J Struct Biol*. 172:45-54.

Uehara, R., R.S. Nozawa, A. Tomioka, S. Petry, R.D. Vale, C. Obuse, and G. Goshima. 2009. The augmin complex plays a critical role in spindle microtubule generation for mitotic progression and cytokinesis in human cells. *Proc Natl Acad Sci U S A*. 106:6998-7003.

Vale, R.D., T.S. Reese, and M.P. Sheetz. 1985a. Identification of a novel force-generating protein, kinesin, involved in microtubule-based motility. *Cell*. 42:39-50.

Vale, R.D., B.J. Schnapp, T.S. Reese, and M.P. Sheetz. 1985b. Movement of organelles along filaments dissociated from the axoplasm of the squid giant axon. *Cell*. 40:449-454.

Venkatram, S., J.L. Jennings, A. Link, and K.L. Gould. 2005. Mto2p, a novel fission yeast protein required for cytoplasmic microtubule organization and anchoring of the cytokinetic actin ring. *Mol Biol Cell*. 16:3052-3063.

Venkatram, S., J.J. Tasto, A. Feoktistova, J.L. Jennings, A.J. Link, and K.L. Gould. 2004. Identification and characterization of two novel proteins affecting fission yeast gamma-tubulin complex function. *Mol Biol Cell*. 15:2287-2301.

Verde, I., G. Pahlke, M. Salanova, G. Zhang, S. Wang, D. Coletti, J. Onuffer, S.L. Jin, and M. Conti. 2001. Myomegalin is a novel protein of the golgi/centrosome that interacts with a cyclic nucleotide phosphodiesterase. *J Biol Chem*. 276:11189-11198.

Verollet, C., N. Colombie, T. Daubon, H.M. Bourbon, M. Wright, and B. Raynaud-Messina. 2006. Drosophila melanogaster gamma-TuRC is dispensable for targeting gamma-tubulin to the centrosome and microtubule nucleation. *J Cell Biol*. 172:517-528.

Vinh, D.B., J.W. Kern, W.O. Hancock, J. Howard, and T.N. Davis. 2002. Reconstitution and characterization of budding yeast gamma-tubulin complex. *Mol Biol Cell*. 13:1144-1157.

Waschke, J., and D. Drenckhahn. 2000. Uniform apicobasal polarity of microtubules and apical location of gamma-tubulin in polarized intestinal epithelium in situ. *European journal of cell biology*. 79:317-326.

Weisenberg, R.C. 1972. Microtubule formation in vitro in solutions containing low calcium concentrations. *Science*. 177:1104-1105.

Wiese, C., and Y. Zheng. 2006. Microtubule nucleation: gamma-tubulin and beyond. *J Cell Sci*. 119:4143-4153.

Wu, J.Q., J.R. Kuhn, D.R. Kovar, and T.D. Pollard. 2003. Spatial and temporal pathway for assembly and constriction of the contractile ring in fission yeast cytokinesis. *Developmental cell*. 5:723-734.

Wu, J.Q., and T.D. Pollard. 2005. Counting cytokinesis proteins globally and locally in fission yeast. *Science*. 310:310-314.

Xiong, Y., and B.R. Oakley. 2009. In vivo analysis of the functions of gamma-tubulin-complex proteins. *J Cell Sci*. 122:4218-4227.

Yaffe, M.P., D. Harata, F. Verde, M. Eddison, T. Toda, and P. Nurse. 1996. Microtubules mediate mitochondrial distribution in fission yeast. *Proc Natl Acad Sci U S A*. 93:11664-11668.

Yamashita, A., M. Sato, A. Fujita, M. Yamamoto, and T. Toda. 2005. The roles of fission yeast ase1 in mitotic cell division, meiotic nuclear oscillation, and cytokinesis checkpoint signaling. *Mol Biol Cell*. 16:1378-1395.

Zeng, C.J., Y.R. Lee, and B. Liu. 2009. The WD40 repeat protein NEDD1 functions in microtubule organization during cell division in Arabidopsis thaliana. *The Plant cell*. 21:1129-1140.

Zhai, Y., P.J. Kronebusch, and G.G. Borisy. 1995. Kinetochore microtubule dynamics and the metaphase-anaphase transition. *J Cell Biol*. 131:721-734.

Zhang, J., and T.L. Megraw. 2007. Proper recruitment of gamma-tubulin and D-TACC/Msps to embryonic Drosophila centrosomes requires Centrosomin Motif 1. *Mol Biol Cell*. 18:4037-4049.

Zheng, Y., M.K. Jung, and B.R. Oakley. 1991. Gamma-tubulin is present in Drosophila melanogaster and Homo sapiens and is associated with the centrosome. *Cell*. 65:817-823.

Zheng, Y., M.L. Wong, B. Alberts, and T. Mitchison. 1995. Nucleation of microtubule assembly by a gamma-tubulin-containing ring complex. *Nature*. 378:578-583.

Zimmerman, W.C., J. Sillibourne, J. Rosa, and S.J. Doxsey. 2004. Mitosis-specific anchoring of gamma tubulin complexes by pericentrin controls spindle organization and mitotic entry. *Mol Biol Cell*. 15:3642-3657.